MODELING DAMAGE IN COMPOSITES USING THE ELEMENT-FAILURE METHOD

TAN HWEE NAH SERENA

(*B.Eng. (Hons), NUS*)

A THESIS SUBMITTED FOR THE DEGREE OF DOCTOR OF PHILOSOPHY

DEPARTMENT OF MECHANICAL ENGINEERING
NATIONAL UNIVERSITY OF SINGAPORE
2005

Acknowledgment

This research project has been a very interesting and challenging experience for me, especially the thesis-writing phase which has taken up a lot of my after-work hours and involves tons of self-discipline in the process. It would not have been completed without the assistance, encouragement and understanding from the following people:

My supervisors: *Dr Tay Tong Earn* and *Dr Vincent Tan Beng Chye*, for letting me seek financial employment before completing the thesis. I also enjoyed our weekly project discussions and the occasional chit-chatting sessions. Especially to *Dr Tay*, for being so honestly critical of my work - this is most probably the only way I am going to improve! ☺

Staff of NUS: *Peter, Malik, Chiam* and *Joe*, for assisting me in my experiments.

Postgraduate students in my NUS lab: *Liu Guangyan*, *Arief Yudhanto, Zahid Hossain, Naing Tun, Cheewei* and *Kar Tien*, for making the research environment a livelier place.

And above all, to *feichu*, who kept encouraging me to finish my thesis, whose idealism often challenges my pragmatic realism, yet at the same time exposing me to a different point of view and best of all, whose humor brightens up my many days.

Table of Contents

List of articles by the author

1. Tay T E, Tan S H N, Tan T L and Tan V B C (2003). Progressive damage and delamination in composites by the element-failure approach and Strain Invariant Failure Theory (SIFT), *14th International Conference on Composite Materials, ICCM-14*, San Diego, US, 14-18 July 2003.

2. Tay T E, Tan S H N, Tan V B C and Gosse J H (2005). Damage progression by the element-failure method (EFM) and strain invariant failure theory (SIFT), *Composites Science and Technology,* vol. 65, no. 6, pp. 935-944.

3. Tay T E, Tan V B C and Tan S H N (2005). Element-failure: an alternative to material property degradation method for progressive damage in composite structures, *Journal of Composite Materials*, vol. 39, no. 18, pp. 1659-1675.

Summary

Traditionally, progressive damage in composites is mostly modeled using the material property degradation method (MPDM), which assumes that damaged material can be replaced with an equivalent material with degraded properties. Unfortunately, MPDM often employs rather restrictive degradation schemes, which in some cases, leads to computational problems. In this thesis, a new **Element-failure method** (EFM) is proposed for the finite element modeling of damage in composites under quasi-static load. It is based on the idea that the nodal forces of an element of a damaged composite material can be modified to reflect the general state of damage and loading. Because the material properties of the element are not modified, there is no ill-conditioning of stiffness matrix in EFM and convergence to a solution is always assured. There is also no need to reformulate the global stiffness matrix during the damage progression process, resulting in savings in computational effort.

The EFM is used with a micromechanics-based strain-invariant failure theory (SIFT) for the first time to predict the initiation and progression of in composite laminate under quasi-static load. A two dimensional finite element code is developed for that purpose. When applied to the problem of a composite laminate under a quasi-static three-point bend load, the predicted damage pattern obtained from the use of the EFM with SIFT is found to be in good agreement with experimental observations. Parametric studies on SIFT also shows the damage prediction by SIFT to be robust within ± 18% of the critical SIFT strain invariant values, with the changes in the

damage pattern being the most significant when J_{1Crit} is increased by 19%, while ε^{f}_{vmCrit} is least sensitive.

Using SIFT as the common failure criterion, the results obtained with the EFM are compared with those generated by the traditional MPDM. It was observed that the damage pattern generated from the use of the EFM with SIFT correlate well with experimental observations while those generated from the use of the MPDM with SIFT correlate poorly. Thus, for the three-point bend problem studied herein, the use of the EFM with SIFT is found to be a more suitable combination for mapping damage initiation and propagation in composite laminates. Finite element formulations of the EFM and the MPDM further reveal the EFM to be a more general and versatile method than the MPDM for accounting local damage in composite laminates. This is because the EFM can be reformulated to produce the results by MPDM whereas the converse is not true in general.

List of Figures

List of Tables

List of Symbols

J_1	Volumetric strain invariant
J_{1Crit}	Critical volumetric strain invariant
ε_{vm}^{m}	von Mises strain invariant at matrix phase
ε_{vmCrit}^{m}	Critical von Mises strain invariant at matrix phase
ε_{vm}^{f}	von Mises strain invariant at fiber phase
ε_{vmCrit}^{f}	Critical von Mises strain invariant at fiber phase
$\{\varepsilon\}_i^{phase}$	Local mechanical strain vector at position i within a representing unit volume (RUV). i can be either IF1, IF2, IS (for matrix phase) or any of the F1 to F9 (for fiber phase)
$\{\varepsilon\}^{mech}$	Homogenized mechanical strain vector obtained from the macro-finite element analysis of the composite laminates
$[MF]_i^{phase}$	Column matrix of mechanical strain amplification factors at position i within each phase
$\{TF\}_i^{phase}$	Column vector of thermal-mechanical strain amplification factors at position i within each phase
ΔT	Temperature differential

Subscripts 1,2,3	Directions of material coordinate system where 1 refers to direction of fiber
Subscripts x, y, z	Directions of global coordinate system
E_1, E_2, E_3	Young's modulus along the $1, 2, 3$ directions respectively
E_x, E_y, E_z	Young's modulus along the (x, y, z) global coordinate axes
v_{12}, v_{13}, v_{23}	Poisson ratios defined using material axes
v_{xy}, v_{xz}, v_{yz}	Poisson ratios defined using (x, y, z) global coordinate axes
G_{12}, G_{13}, G_{23}	Shear modulus defined using material axes
G_{xy}, G_{xz}, G_{yz}	Shear modulus defined using (x, y, z) global coordinate axes
D_1, D_2, D_6	Degradation factors in the fiber direction, transverse to fiber direction and shear direction respectively.
F_{v1}, F_{v2}, F_{v3}	Damage variables representing matrix failure, fiber-matrix shearing failure and fiber failure respectively.
V_f	Fiber volume fraction
$\mathbf{K}$	Elemental stiffness matrix
$\mathbf{K}_{MPDM}$	Elemental stiffness matrix in MPDM
$\mathbf{K}_{EFM}$	Elemental stiffness matrix in EFM

$\mathbf{K}^d$	Degraded elemental stiffness matrix
$\mathbf{C}$	Material stiffness matrix
$\mathbf{C}^d$	Degraded material stiffness matrix
C_{ij}	Material stiffness coefficients
Ω	Domain of integration
$\mathbf{B}$	Strain operator
$\mathbf{u}$	Nodal displacement vector of an element
$\mathbf{u}^*$	Unique solution of nodal displacement vector
$\mathbf{u}_{MPDM}$	Nodal displacement vector of a damaged element in MPDM
$\mathbf{u}_{EFM}$	Nodal displacement vector of a failed element in EFM
u_x, u_y	x and y components of displacement
$\mathbf{f}$	Nodal force vector of an element
$\mathbf{f}_{MPDM}$	Nodal force vector of a damaged element in MPDM
$\mathbf{f}_{applied}$	Nodal force vector that is applied to the nodes of a failed element in EFM
f_x, f_y	x and y components of nodal force

$\sum_{j=1}^{m} f_j^0$	Nett internal nodal force at node i belonging to non-fail elements j. For a 2-D 8-noded failed element B, node i takes values from $i = 1, 2, \ldots, 8$
m	the maximum number of non-fail elements j that share a common node i. For example, in Figure 2-2b, $m = 3$
f_B^N	Internal nodal force at node i belonging to failed element B at Nth iteration
f_{app}^N	External applied force on node i at Nth iteration
$\sum_{j=1}^{m} f_{j,D}$	Desired value of nett internal nodal force of non-fail elements A
R^N	The difference between the desired and current nett internal nodal force of non-fail elements j at Nth iteration.
$f(\sigma_i)$	Scalar function
F_i, F_{ij}	Experimentally determined strength tensors of the second and fourth rank respectively
X_T, X_C	Tensile strength and compression strength of the composite in its fiber direction respectively
Y_T, Y_C	Tensile strength and compression strength in the transverse to fiber direction
S	Shear strength
δ	Prescribed displacement

$\varepsilon_{xx}, \varepsilon_{yy}, \varepsilon_{zz}, \gamma_{xy}, \gamma_{yz}, \gamma_{xz}$	Six components of the mechanical strain vector in general Cartesian coordinates
$\sigma_{xx}, \sigma_{yy}, \sigma_{zz}, \tau_{xy}, \tau_{yz}, \tau_{xz}$	Six components of the mechanical strain vector in general Cartesian coordinates

List of Abbreviations

EFM	Element-Failure method
FE	Finite element
MPDM	Material property degradation method
RUV	Repeating unit volume
SIFT	Strain invariant failure theory
SRC	Stiffness reduction coefficient
2-D	Two-dimensional
3-D	Three-dimensional
IF1, IF2	Inter-fiber positions 1 and 2
IS	Interstitial position

1. Introduction to the Modeling of Damage in Composites

Composite materials are now widely used in a variety of components for automotive, aerospace, marine, defense, petrol-chemical and architectural structures. Especially in aerospace industries, the use of composite materials has improved the performance of aircraft because of their higher strength-to-weight and higher stiffness-to-weight ratios compared to other classes of engineering materials.

However, laminated composite structures may develop local failure modes such as matrix cracks, fiber breakage, fiber/matrix debonds and delaminations (Figure 1-1), all of which have strong interactions with one another. The failure mechanisms involve different length scales [*Ochoa and Reddy, 1992*]: at the micro level, the focus is on failure of matrix, fiber and fiber/matrix interface; at the macro level, the focus is on the laminae such as delamination between the layers of the laminate. These failure modes cause a permanent loss in structural integrity within the laminate and result in a loss of strength and stiffness of the composite material. Hence, accurate determination of failure modes and their progression while the composite structure is loaded is essential for assessing the performance of the composite structures and for designing them safely.

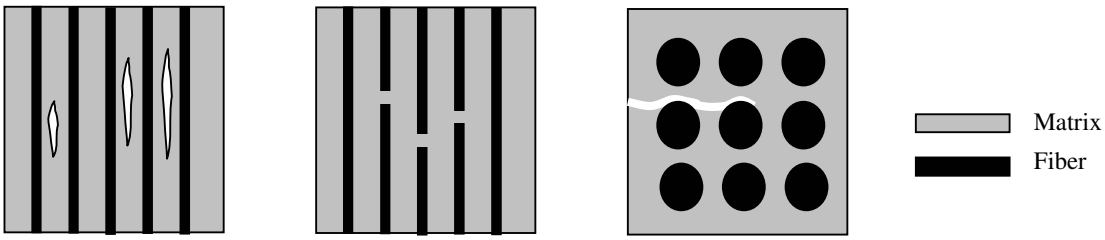

(a) Matrix cracking (b) Fiber fracture (c) Fiber/matrix debonding

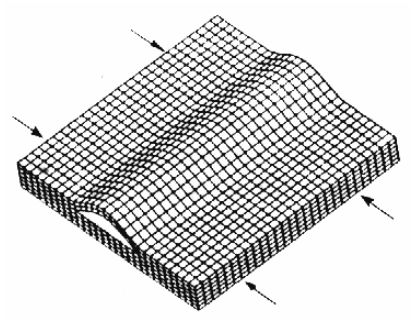

(d) Delamination

Figure 1-1: Damage modes in fibrous composites at different length scales

Progressive failure analysis of composite structures is usually performed to understand the initiation and progression of damage in the composite structures subjected to either single or multiple loading conditions [*Petit and Waddoups, 1969; Chang and Chang, 1987b; Tan, 1991; Reddy et al., 1995; Lessard and Shokrieh, 1995*]. A typical progressive failure analysis comprises the following three steps: stress analysis, failure analysis and the use of a stiffness-reduction technique. The stress analysis studies the response of a material due to prescribed loading and boundary condition and computes the stress and strain distributions within the

material. Failure analysis involves assessing one or more failure models to determine whether a strength allowable as in the Maximum Stress Criterion [*Jenkins, 1920*], strain allowable as in the Maximum Strain Criterion [*Waddoups, 1967*] or some interacting stress-based failure criteria [*Tsai and Wu, 1971; Hashin, 1980; Tan, 1991*] has been exceeded, thereby denoting the failure at that material point. When damage is detected in a finite element, a stiffness-reduction technique is applied to simulate a loss in the load-carrying capability of that element.

1.1. Review of the Finite Element Modeling of Damage

Considerable research has been performed on the use of progressive failure models to understand the failure behavior of composite laminates subjected to in-plane loading conditions such as tension, compression and shear. Usually, these models use the finite element method (FEM) to perform the stress analysis for problems of composite laminates under quasi-static loading [*Tan, 1994; Reddy et al., 1995; Lessard and Shokrieh, 1995; Sandhu et al., 1982; Camanho and Matthews, 1999; Tserpes et al., 2002; Sleight et al., 1997; Knight et al., 2002; Ambur et al., 2004a and 2004b*]. Analytical methods are seldom preferred to solve the stress analysis because the failure mechanisms of composites are usually so complicated that analytical methods are impractical. Furthermore, progressive failure analysis of laminated composites entails some three-dimensional stresses and effects along free-edges and along delamination fronts in multidirectional laminates. Such problems require tremendous amount of computational effort. Therefore, this research project

will only focus on the use of the finite element method for the modeling of damage progression in composites.

A two-dimensional (2-D) finite element (FE) method based on the Classical Laminate Plate Theory (CLPT) was used by Sandhu *et al.* [*1982*] to model the failure behavior of composite laminates. Following the approach similar to Petit and Waddoups [*1969*], experiments were first performed to obtain the stress-strain curves of unidirectional composite specimens under in-plane loads. These curves were later represented as piecewise continuous cubic spline interpolation functions for the finite element analysis. A total strain energy failure criterion was developed by Sandhu *et al.* [*1982*] to determine lamina failure and the ply-discount method [*Tsai and Azzi, 1966*] was used for stiffness-reduction of the damaged lamina.

Another use of 2-D finite element method based on the Classical Laminate Plate Theory (CPLT) was also reported in the works of Chang et al. [*Chang et al., 1984; Chang and Chang, 1987b*]. They performed progressive failure analysis of notched composite laminates in tension and compression. A non-linear stress-strain relation proposed by Hahn and Tsai [*1973*] was used for in-plane shear. The resulting non-linear finite element equations were solved by the modified Netwon-Raphson iterative technique.

A 2-D FE code was also developed by Averill and Reddy [*1992*] to study failure behavior of laminated shell structures. A third-order expansion of displacement through the thickness of the shell laminate was assumed for the finite element method. A micromechanical elasticity solution for predicting the failure and

effective composite properties was used. Another 2-D FE-based progressive failure model for the study of composite plate was found in the work of Tolson and Zabaras [*1991*]. In their FE formulations, a seven degree-of-freedom (DOF) plate element based on a higher order shear deformation plate theory was used, where the seven DOF consist of three displacements, two rotations of normals about the plane midplane and two rotations of the normals to the datum surfaces.

A full three-dimensional (3-D) finite element method was used by Lee [*1980*] to perform stress analysis for a biaxially loaded composite laminates with a central hole. He later developed a 3-D FE code [*Lee, 1982*] to analyze damage accumulation and progressive failure for the same problem. Stiffness-reduction was carried out at the element level and a stress-based failure criterion was used to identify three modes of failure: fiber breakage, transverse matrix cracking and delamination. However, it was observed that his code has never detected any delamination. According to investigations of free-edge effects in composite laminates [*Spilker and Chou, 1980 and Atlus et al., 1980*], delamination should happen because both the normal and shear stresses between two composite layers have singularities near the free edge. Lee attributed the reason to the coarseness of the FE mesh near the edge of the hole. Unfortunately, further refinement of the FE mesh to the required level at that stage is impossible at his time (i.e. year 1982) as the amount of computational resources required is unavailable. An incremental formulation for stiffness matrix is later proposed by Hwang and Sun [*1989*] to improve computational efficiency of 3-D progressive failure analysis.

Other progressive failure models using the finite element method were developed to study the failure behavior of composite laminates containing stress concentrations such as open-holes [*Chang and Chang, 1987b; Chang and Lessard, 1991; Tan, 1991*] and bolted joints [*Lessard and Shokrieh, 1995; Hung and Chang, 1996; Tserpes et al., 2002; Camanho and Matthews, 1999; Shokrieh and Lessard, 2000a*]. Despite the progress made in the application of these progressive damage models, many issues regarding the choice of the damage-modeling technique and failure criterion are still open for research. A discussion of them is given in the following sections.

1.2. Review of Failure Criteria of Laminated Composites

With the wide use of laminated composite materials in structural design, it is important to understand the conditions under which the composite structure fails. The initial failure of a ply in laminated composite, also known as *first-ply failure*, can be predicted by applying an appropriate failure criterion [*Reddy and Pandey, 1987; Turvey and Osman, 1989; Reddy and Reddy, 1992*]. The subsequent failure prediction requires an understanding of damage modes and damage accumulation and their effect on the mechanical behavior. Many such failure criteria have been proposed to predict the onset of failures and their progression [*Petit and Waddoups, 1969; Tsai, 1984; Hashin, 1980, Hinton et al., 1998, 2002a and 2002b, 2004a and 2004b; Hinton and Soden, 1998; Soden et al., 1998a and 1998b; Rousseau, 2003; Kaddour et al., 2004*].

One of the earliest and most widely used failure criteria is the Maximum Stress Criterion [*Jenkins, 1920*] for orthotropic materials. It is an extension of the Maximum Normal Stress Theory (or Rankine's Theory) for isotropic materials and failure is assumed to occur when any one of the stress components along the principal material axes reaches, or is greater than, its individual strength value. An alternative is the Maximum Strain Criterion [*Waddoups, 1967*] for orthotropic materials where the failure conditions are based on strain components instead. However, these two criteria fail to represent interactions of different stress or strain components in failure mechanisms. Despite these shortcomings, these two criteria are still being used as they are simple and easy to apply [*Hart-Smith, 1998a and 1998b*].

Polynomial failure criteria similar to the von Mises criterion were proposed to account for the interaction of stress or strain components. Hill [*1948*] proposed an extension of the von Mises yield criterion for isotropic materials [*Chen and Han, 1988*] to anisotropic plastic materials with equal strengths in tension and compression. Tsai [*1968*] extended Hill's criterion to orthotropic fibrous composites by relating some coefficients of Hill's polynomial failure criterion to the longitudinal, transverse and shear failure strengths of composites. The latter was generally referred as Tsai-Hill criterion. Hill's criterion was also generalized by Hoffman [*1967*] to account for different tensile and compressive strengths of composites.

An assumption of the above-mentioned failure criteria is that hydrostatic stresses do not contribute to failure. Terms other than the deviatoric components are included by

Tsai and Wu [*1971*]. By simplifying a tensor polynomial failure theory for anisotropic materials suggested by Gol'denblat and Kopnov [*1965*], Tsai and Wu developed a general form of quadratic failure criterion to represent failure of any anisotropic material. It was observed that Hill's criterion, Hoffman's criterion and maximum stress (strain) criterion are degenerate cases of the more general Tsai-Wu failure theory.

Micromechanical-based failure criteria were also developed to account for specific modes of failure at the micro-scale. Matrix and fiber failure of composites were accounted through the use of a separate failure criterion [*Hashin and Rotem, 1973; Rotem and Hashin, 1975; Hahin, 1980; Hashin, 1983; Rotem, 1998*]. Subsequent failure criteria by Shahid and Chang [*1993b, 1995*] based on Hashin's criteria, consider three modes of micro failure: matrix failure, fiber breakage and fiber-matrix shear-out. Phenomenological-based failure criteria were developed by Puck et al [*Puck and Schneider, 1969; Puck and Schürmann; 1998 and 2002*] and applied to fracture analysis of composite laminates to distinguish between fiber failure and inter-fiber failure.

Apart from the use of stress components to predict failure in composites, other failure criteria report the use of dissipated energy [*Huang et al, 2003*], strain energy [*Sandhu, 1974; Wolfe and Butalia, 1998; Butalia and Wolfe, 2002*] or the use of strains [*Christensen, 1988; Feng, 1991; Gosse et al., 2001 and 2002*]. Christensen [*1988*] developed a three-dimensional failure criterion from the consideration of tensor transformation of strains while Feng [*1991*] developed a three-dimensional failure criterion in terms of strain invariants.

Gosse [*Gosse, 2002; Gosse et al., 2001, 2002, submitted for publication*] developed a micromechanistic strain-based failure criterion that predicts constituent-level damage in composite. Also known as the Strain Invariant Failure Theory (SIFT), failure modes of composites are associated with three strain invariants and thermal residual stresses and microstructural geometric effects are accounted for. A simplified form of SIFT (whereby only the first strain invariant is used to predict failure) was applied by Li *et al.* [*2002, 2003*] to successfully predict matrix-dominated failure in I-beams, curved beams and T-cleats. As the results from the use of SIFT are promising, SIFT is adopted in this thesis to predict damage in composites materials.

1.3. Review of Damage-modeling Techniques of Laminated Composites

In the event of damage, the effect of damage on the load-carrying capability of the material is described by the use of a suitable damage-modeling technique. Two approaches are commonly adopted in the modeling of damage in composite laminates. The first approach, known as the *Material-property degradation method (MPDM)*, assumes that a damaged material can be replaced with an equivalent material with degraded properties. When used for the finite element modeling of damage, finite elements containing damage are considered "damaged" and the stiffness reduction is simulated by degrading the material properties of these damaged elements. The second approach is an *element-delete approach*, in which finite elements containing damage are totally removed from the FE model. No

consideration is given to the damage status of the deleted elements. A brief review of these approaches is given below.

1.3.1. Material Property Degradation Method, MPDM

The Material property degradation method (MPDM) is a common and practical approach to modeling damage in composite laminates [*Chang and Chang, 1987a and 1987b; Chang and Lessard, 1991; Camanho and Matthews, 1999; Hyer and Wolford, 2003; Hallet and Wisnom, 2003*]. In the event a damage mode is detected, degradation of the material stiffness can be applied either at (a) ply-level or (b) element-level:

(a) <u>Ply-level Approach</u>

In this approach, the material properties of damaged plies of the composite laminates are modified when ply-level damage is predicted. Attention is focused on ply-level damage because it is difficult and computationally expensive to model the damage events taking place at the micro-level. Among the various failure modes, the problem of stiffness reduction due to matrix cracking has received the most attention in the past. This is because matrix cracking is among the most common failure modes and is also usually the first sign of damage observed in general angle-ply laminates loaded in tension [*Tsai 1965; Parvizi et al., 1978; Highsmith and Reifsnider 1982; Hashin, 1990*].

An immediate consequence of matrix cracking is the loss of load-carrying capability in the direction normal to the cracks and a reduced structural stiffness in that direction [*Tsai, 1965; Tsai and Hahn, 1975; Petit and Waddoups, 1969*]. Several material property degradation approaches to model stiffness reduction have been proposed and these include the ply-discount methods [*Tsai, 1965; Petit and Waddoups, 1969; Chou et al., 1976*] and continuum damage mechanics models [*Allen et al., 1987a, 1987b and 1988; Lee et al., 1989; Lim and Tay, 1994 and 1996; Talreja, 1985a, 1985b, 1986a, 1986b, 1987, 1990a and 1990b; Tay and Lim, 1996*].

In the ply-discount method, the stiffness matrix of the damaged ply is modified at the onset of the first transverse crack [*Tsai, 1965; Tsai and Azzi, 1966; Petit and Waddoups, 1969; Chou et al., 1979*]. A stress analysis of the composite laminate is first performed to identify the first ply that contains the first transverse crack. The Young's modulus in the transverse to fiber direction E_2 and the shear modulus G_{12} of the damaged ply were then reduced to zero (the subscripts 1 and 2 refer to the fiber and transverse to fiber directions respectively). A new stress analysis of the laminate using the reduced stiffness of the damaged ply was carried out and the next ply containing transverse crack is identified and its material properties are similarly reduced. This procedure is stopped when the first fiber failure in the 0° ply (i.e. ply whose direction is aligned with the tensile loading direction) is predicted.

The advantage of the ply-discount method is that it is simple to use. However, the amount of stiffness reduction to the damaged ply is applied without any physical basis, as the mechanism of transverse crack damage is not accounted for. This leads

to an underestimation of the laminate strength because the damaged ply is still capable of retaining a considerable amount of its initial load-bearing capability despite the presence of cracks. Hence, the ply-discount method is over-conservative.

In continuum damage models, a constitutive model of the damage states of composites is used with a damage evolution criterion to predict progressive damage in composite laminates due to matrix cracking [*Talreja, 1985a, 1985b, 1986a, 1986b, 1990a and 1990b; Allen et al., 1987a, 1987b and 1988; Allen and Lo, 1991; Lee et al, 1989; Lim and Tay, 1994 and 1996; Tay and Lim, 1996; Coats and Harris, 1995 and 1998; Lo et al., 1996*]. The state of damage in constitutive relations of composite is described by a set of internal state variables, which contains information on the crack geometry and fracture modes.

A first order tensor of internal state variables was first introduced by Talreja [*1987*] to characterize the internal damage in composites. By assuming the energy density in a cracked volume to be a function of the strain tensor and a damage vector, a set of constitutive equations with observable strains and an effective stress tensor can be constructed. However, this method requires the determination of ten constants for a general laminate containing matrix cracks. The number of constants is reduced to four in the case of cross-ply laminates. The predictions of the change in longitudinal stiffness with cycles of loading for a glass/epoxy $[0°/90°_3]_S$ laminate under tensile fatigue load agreed reasonably well with experiments.

Allen and co-workers [*Allen et al., 1987a and 1987b*] used a second order tensor of internal state variables that are originally proposed by Kachanov [*1972*] in their

continuum damage model. This model requires fewer constants and explicitly incorporates the crack kinematic features into the formulation for the internal state variables. The internal state variables for matrix cracks are related to the energy release rate due to cracking, using the concept of linear elastic fracture mechanics. Predictions from the damage model compared well with experiments.

An upper bound on stiffness based on the internal state approach was proposed by Lee *et al.* [*1989*]. The internal state variables were solved by assuming the displacement field in the presence of cracks to be in terms of trigonometric function series. Tay and Lim [*1993*] used the damage model proposed by Kachanov [*1972*] and Allen et al. [*Allen et al., 1987a and 1987b; Lee et al., 1989*] in conjunction with a simple kinematic representation of transverse crack profile to predict the stress-strain behavior of damaged cross-ply laminates. The predicted stress-strain curves compare reasonable well with the experimental curves obtained from Daniel and Lee [*1990*] and Laws and Dvorak [*1988*]. A series of parametric finite element analysis was also performed to establish the effects of crack opening profiles, relative ply thickness of the longitudinal and the transverse plies and crack density on the stiffness of the laminate.

The above continuum damage models were proposed to model the stiffness reduction due to matrix cracking only. Unfortunately, they often lacked detailed information on the extent of transverse crack interactions. They are basically phenomenological in nature. Clearly, more refined methodologies that account for all the identified damage mechanisms in composites are needed.

Subsequent degradation models were developed to include other ply-level damage modes such as fiber breakage and fiber-matrix shearing failure. Different failure criteria are considered for various failure modes of composites, and there exists an appropriate material property degradation rule for each failure mode predicted [*Chang and Lessard, 1991; Shahid and Chang, 1995; Tan, 1991; Tan, 1994; Shokrieh and Lessard, 2000a and 2000b; Tserpes et al., 2001 and 2002*].

Tan [*1994*] proposed a 2-D FE progressive failure model for laminated composites containing stress concentrations subjected to tensile loading and used a modified Tsai-Wu failure criterion [*Tan, 1988*] to distinguish the failure modes by matrix failure or fiber breakage. When failure is predicted, material properties of the damaged lamina is applied as follows:

$$E_1^d = D_1 E_1$$

$$E_2^d = D_2 E_2$$

$$G_{12}^d = D_6 G_{12} \qquad (1\text{-}1)$$

where stiffness degradation factors D_1, D_2 and D_6 represent the damaged state of a lamina, E_1, E_2 and G_{12} are the material properties of the undamaged lamina, the superscript d refers to the material properties of the damaged lamina and the subscripts 1 and 2 refers to the fiber direction and transverse to fiber direction respectively. Here, D_1 is the stiffness degradation factor of a lamina along the fiber direction caused by fiber breakage while D_2 and D_6 are the degradation factors transverse to the fiber direction and shear component respectively, due to matrix

failure. The degradation factors D_1, D_2 and D_6 in equation (1-1) have values less than unity if damage occurs in a lamina or an element. Estimates of their values are given in Tan's earlier works [*Tan and Nuismer, 1989; Nuismer and Tan, 1988*] where an approach based on an elasticity solution of a micromechanical model of a cracked lamina is used. For a given crack density, the equilibrium equations and appropriate boundary and continuity conditions are solved to obtain the damaged lamina constitutive equations (and hence the degradation factors).

Damage accumulation was addressed in the works of Chang and Lessard [*1991*] and Shahid and Chang [*1993a, 1995*]. Chang and Lessard's degradation model [*1991*] was later used in the analysis of Ambur *et al.* [*2004a and 2004b*] to study composite curved panels subjected to axial compression loading and in-plane shear loading well into their postbuckling regime. In their analysis, the elastic properties are made to be linearly dependent on three damage variables F_{v1}, F_{v2} and F_{v3}. The first damage variable represents matrix failure, the second represents fiber-matrix shearing failure and the third represents fiber failure. The values of the three damage variables are set to zero in the undamaged state. If any of the three ply damage mode is predicted, the value of the associated damage variable are set to 1.0 and the material property is then degraded accordingly to the property degradation model defined in Table 1-1 (the subscript 1 refers to the fiber direction while subscripts 1 and 3 are transverse to fiber direction).

Table 1-1: Dependence of material elastic properties on the damage variables (referenced from Ambur *et al.* [*2004a and 2004b*])

No failure	**Matrix cracking**	**Fiber-matrix shear**	**Fiber failure**
E_1	E_1	E_1	$E_1 \to 0$
E_2	$E_2 \to 0$	E_2	$E_2 \to 0$
v_{12}	$v_{12} \to 0$	$v_{12} \to 0$	$v_{12} \to 0$
G_{12}	G_{12}	$G_{12} \to 0$	$G_{12} \to 0$
G_{13}	G_{13}	$G_{13} \to 0$	$G_{13} \to 0$
G_{23}	G_{23}	G_{23}	$G_{23} \to 0$
$F_{v1} = 0$	$F_{v1} = 1$	$F_{v1} = 0$	$F_{v1} = 0$
$F_{v2} = 0$	$F_{v2} = 0$	$F_{v2} = 1$	$F_{v2} = 0$
$F_{v3} = 0$	$F_{v3} = 0$	$F_{v3} = 0$	$F_{v3} = 1$

A three-dimensional material degradation model was developed by Tserpes *et al.* [*2001*] to simulate damage accumulation of bolted composite joints under in-plane tensile loading. The Hashin-type failure criteria [*Hashin, 1980*] reported in the work of Shokrieh *et al.* [*1996*] were used to predict various distinct damage modes in composites: matrix tensile and compressive cracking, fiber tensile and compressive failure, fiber-matrix shear-out and delamination in tension and compression. If matrix tensile and compressive cracking is detected in a ply, it is assumed that the matrix cannot carry any load. Therefore, material properties of the failed ply in the matrix direction such as Young modulus in the transverse-to-fiber direction E_y and Poisson's ratio υ_{xy} are reduced to zero. In the case of delamination failure, it is

assumed that the material loses its ability to carry shear loads and load in the z-direction and therefore, $E_z = G_{xz} = G_{yz} = 0$ and $v_{xz} = v_{yz} = 0$ for compatibility.

In another three-dimensional problem of progressive fatigue damage in a pin/bolt-loaded composite laminate studied by Shokrieh and Lessard [*2000a*], seven different failure modes for the unidirectional ply are considered, which are: fiber tension, fiber compression, fiber-matrix shearing, matrix tension, matrix compression, normal tension and normal compression failure modes. Suitable stress-based failure criteria for detecting these failure modes under multiaxial state of stress are derived and there exists an appropriate set of material property degradation rule for these failure modes. For example, when either fiber tension or fiber compression failure modes are detected in a ply, all material properties of the damaged ply i.e. E_x, E_y, E_z, v_{xy}, v_{xz}, v_{yz}, G_{xy}, G_{xz} and G_{yz} are reduced to zero (the subscripts x, y and z refers to the global x-, y- and z- axes respectively). This is because fiber failure modes are catastrophic and therefore it is assumed that the ply with fiber breaks cannot sustain any stress. In the case of matrix tension failure mode, it is assumed that since matrix mode is not catastrophic, this failure mode only affects the matrix direction properties and therefore other material properties are left unchanged. In this case, only the transverse modulus E_y and Poisson's ratios v_{xy} and v_{yz} are reduced to zero. The progressive fatigue damage model is later validated with experiments [*Shokrieh and Lessard, 2000b*].

(b) Element-level approach

In this approach, it is assumed that damage within an element has an effect on the material properties of that element only. Therefore, degradation was done on an element-basis.

In the 2-D progressive failure analysis of notched composite laminates in tension and compression studied by Chang et al. [*Chang et al., 1984; Chang and Chang, 1987b*], stiffness-reduction was carried out at element level and a failure criterion proposed by Yamada and Sun [*1978*] was used. If matrix cracking is predicted in an element, all material properties except E_x of the damaged element are reduced to zero (the subscript x refers to the fiber direction). In the case of fiber and/or fiber/matrix shear failure, E_x and G_{xy} of the damaged element are reduced according to a Weibull distribution, while the other two parameters in-plane properties E_y and ν_{xy} are reduced to zero.

It may be noted that size of actual damage in the form of cracks is very small compared to the size of elements used in the mesh. Hence, it appears unjustified to reduce the material properties of damaged elements to zero. A gradual stiffness reduction was proposed by Reddy *et al.* [*1995*] in which the degraded material properties of the damaged element are assumed to be a constant multiple of the properties before degradation. The constant, called the stiffness reduction coefficient (SRC), is given a value between 0 and 1 where 1 refers to an undamaged element. When an element is considered failed by a failure criterion, the SRC of that element

is determined by gradually reducing the stiffness properties of that element until the failure criterion is not satisfied. Results indicate that the gradual stiffness reduction scheme of Reddy *et al.* [*1995*] provides a more accurate ultimate load estimation compared to those stiffness reduction schemes which reduce the material properties of damaged elements to zero [*Lee, 1982; Hwang and Sun, 1989; Tolson and Zabaras, 1991*].

A 3-D material property degradation model was developed by Camanho and Matthews [*1999*] to predict damage progression and strength of mechanically fastened joints in carbon fiber-reinforced composites in the bearing, tension and shear-out modes. Based on the approach of Tan [*Tan, 1991; Tan and Perez, 1993; Tan and Nuismer, 1989; Nuismer and Tan, 1988*], a set of internal state variables for various damage mechanisms is used to describe the effect of damage on the stiffness of the material. Four types of damage modes are considered: (1) matrix tensile or shear cracking, (2) fiber tensile fracture, (3) matrix compressive or shear cracking and (4) fiber compressive fracture. Selected elastic material properties of a damaged element are degraded according to the damage mode predicted. The progressive damage model is able to accurately predict failure modes, joint strength and stiffness.

1.3.2. Element-delete Approach

Another approach used in the finite element modeling of damage in composite is known as the *element-delete* approach. The concept of element-delete is first formulated by Mahishi and Adams [*1982*] to predict the initiation and propagation

of cracks in a model of a single broken fiber embedded in an annular sheath of aluminum matrix. In their analysis, a finite element loaded beyond its maximum strain energy capacity is removed from the FE mesh and omitted from further computations. The stiffness associated with the element is also reduced to zero. Load that was sustained by the element prior to failure is transferred to surrounding undeleted elements.

However, this analysis by Mahishi and Adams is at the micromechanics level; element deletion is too conservative when applied at the macroscopic continuum scale. In addition, the element-delete approach becomes inadequate if the loading experienced by the material is compressive in nature, as the element containing the crack is still capable of resisting volumetric compression. This problem is addressed by Beissel *et al.* [*1998*] in the analysis of dynamic crack propagation in isotropic materials. Extending the concepts of nodal release [*Rousselier, 1979*] and nodal splitting [*Bakuckas et al., 1995a and 1995b*], Beissel proposed an element-failure algorithm to model crack propagation within elements of an FE mesh. In his algorithm, an element containing a propagating crack is considered partially failed and is not removed from FE computations. Instead, a fraction of the stresses that were computed before the crack tip entered the element contribute to the nodal forces of the element. This fraction is dependent on the crack length of the element. When the crack propagates through the element, the element is considered to have completely failed element and can only resist volumetric compression. The advantage of this treatment of dynamic crack propagation is that it allows crack growth in any arbitrary direction without the need of remeshing. In addition, there is

no need to redefine new crack surfaces or use any contact algorithm to prevent interpenetration of the crack surfaces.

Recently, the element-failure approach was extended to composite structures by Tay *et al.* [*2003*] to analyze damage and delamination propagation in low-velocity impact of composite laminates. An advantage of this analysis is that it eliminates the need to use contact algorithms to ensure that the interpenetration of delamination surfaces does not occur, because the failed elements are not removed from the mesh. Good agreement with experimental results was reported.

1.4. Problem Statement

In view of the previous studies, there are still many aspects of the finite element modeling of damage progression of composite laminates that can be improved. With regard to damage-modeling technique, the element-delete approach underestimates the stiffness of composite laminate. This is because elements containing damage are removed from the FE mesh, although they are still capable of sustaining compressive loads. For the material-property degradation method (MPDM), it employs rather restrictive degradation schemes which in some cases, leads to computational problems. In addition, the reformulation of the stiffness matrix with damage progression is a computationally intensive process, especially with fine meshes. There is also a possibility that by reducing the material properties, the stiffness matrix of the damaged finite element become ill-conditioned and convergence to a solution is not assured.

Hence, our main objective here is to propose a damage-modeling technique that will overcome the above limitations of the element-delete approach and the MPDM and at the same time, is able to account well for local damage in composite structures. Since the element-failure concept is found to be particularly suited for dynamic fracture and delamination in low-velocity impact of composites [*Tay et al., 2003*], we proposed an **Element-failure method (EFM)** for the modeling of damage in composites under quasi-static loading. As the failed element is not removed from the mesh and its stiffness matrix is not modified, the above-mentioned drawbacks associated with the element-delete approach and the MPDM are not present in the EFM. There will also be savings in computational efforts since there is no reformulation of stiffness matrix.

1.5. Scope of Study

The use of the EFM is illustrated in the case of progressive damage analysis of a composite laminate under quasi-static three-point bend. To achieve this, we develop a FORTRAN code which uses the finite element method to perform the stress analysis. The effects of damage are described by the EFM while a recently proposed micromechanics-based *strain invariant failure theory (SIFT)* is used for damage initiation and progression. Damage progression patterns predicted by the use of the EFM and SIFT is compared with the experimental observations.

As EFM and SIFT are both relatively new methods, a secondary objective of this project is to assess both methods. Because SIFT only identifies the location of damage and not actual failure modes, local failure modes are interpreted by correlating the data from SIFT with experimental observations. In addition, parametric studies based on a variation of critical strain invariants values of SIFT are conducted to assess the robustness of damage pattern predictions.

Another set of damage pattern prediction, using material property degradation method (MPDM) with SIFT, is generated for the three-point bend problem and compared with experimental observations. The difference between these patterns is investigated by examining the finite element formulations of MPDM and EFM. The relationship between nodal forces and element stiffness properties is discussed. Finally, the force-stiffness equation of the EFM is reformulated to show that the EFM can yield identical results with MPDM.

2. Introduction to the EFM and SIFT

This chapter describes the principles of element-failure method (EFM) and strain-invariant failure theory (SIFT) that are used in our in-house code[1]. The EFM is a new concept that is proposed herein to model the effects of damage on the load-bearing capability of an element while SIFT is a micro-mechanically based failure criterion that was recently developed by Gosse [*Gosse et al., 2001; Gosse, 2002*].

2.1. The Element-Failure Method, EFM

Traditionally, progressive damage in composites is mostly modeled using material property degradation method (MPDM), which assumes that a damaged material can be replaced with an equivalent material with degraded properties. Unfortunately, MPDM often employs rather restrictive degradation schemes which in some cases, leads to computational problems. In this section, we proposed a new **element-failure method** to overcome the associated disadvantages of the MPDM. This shall be used for modeling damage in composite laminates under quasi-static loading in Chapter 4.

[1] An in-house finite element (FE) code has been developed to study the initiation and progression of damage in composites. Details regarding the development of the code and how the EFM and SIFT are implemented are given in Chapter 3.

2.1.1. Principles of EFM

An element-failure algorithm was originally proposed by Beissel *et al.* [*1998*] to model crack propagation with finite elements in the analysis of dynamic crack propagation in isotropic materials. In their approach, an element is in one of three states – undamaged, partially failed and completely failed. When a crack is propagating *within* an element, the element is considered to have partially failed and is not removed from the FE computations. However, only a fraction of stresses that were computed before the crack tip entered the element contribute to the nodal forces of that element. This fraction is dependent on the crack length within the element. When the crack has propagated *through* the element, the element is deemed as completely failed and can only resist volumetric compression. The T^* energy integral [*Atluri, 1982; Atluri et al., 1984*] is employed as the dynamic fracture parameter, guiding the crack tip through the mesh. The advantage of the element-failure algorithm is that it allows crack growth in any arbitrary direction without the need for remeshing.

Recently, the element-failure concept was extended to composite structures by Tay *et al.* [*2003*] to analyze damage and delamination propagation in low-velocity impact of composite laminates. The delamination crack surfaces are not explicitly modeled, but are simulated by a series of partially-failed elements. This avoids the difficult task of identifying crack tips for the application of traditional fracture mechanics. Another advantage of element-failure algorithm is that the analysis does not require any contact algorithm to ensure that interpenetration of delamination

surfaces does not occur, because the failed elements are not removed from the finite element computations.

In our proposed new element-failure method here, a different definition for a failed element is used. Here, a failed element is defined as one with damage, where damage can be a single or multiple matrix cracks, fiber breakage, fiber matrix debonding or even delamination. A failure theory is used to predict damage in the element. The nodal forces of the failed element are modified to reflect the general state of damage and loading. This is achieved by applying external forces on the nodes of the failed element in succession until the nett internal nodal forces of the surrounding non-fail elements are reduced to an appropriate value (Figure 2-1). The implementation of the EFM is given in the next section. For this reason, EFM is also known as *nodal force reduction method.*

The *magnitude* and *direction* of external nodal forces to be applied depends on the *mode* and *extent* of local damage predicted in the element. Suppose damage in the form of matrix cracks occur in an element, an immediate consequence is the loss of load-carrying capability in the direction normal to the cracks and a reduced structural stiffness in that direction [*Tsai, 1965; Tsai and Hahn, 1975; Petit and Waddoups, 1969*]. This is simulated by applying external nodal forces in the direction transverse to the fiber.

The magnitude of external nodal forces to be applied depends on the extent of damage modeled. If the element is partially-failed, external nodal forces are added until the nett internal nodal forces of the surrounding non-fail elements are reduced to just a fraction of their initial values, whereas a completely failed element is represented by reducing these internal nodal forces to zero.

Similarly, for a completely failed element that no longer sustain any load in both its fiber and transverse directions, we apply external nodal forces in these two directions until the nett internal nodal forces of surrounding non-fail elements are reduced to zero. This models effectively traction-free edges within the structure. Figure 2-1 shows the various states of damage in a failed element of a composite material and their respective direction of external forces to be applied.

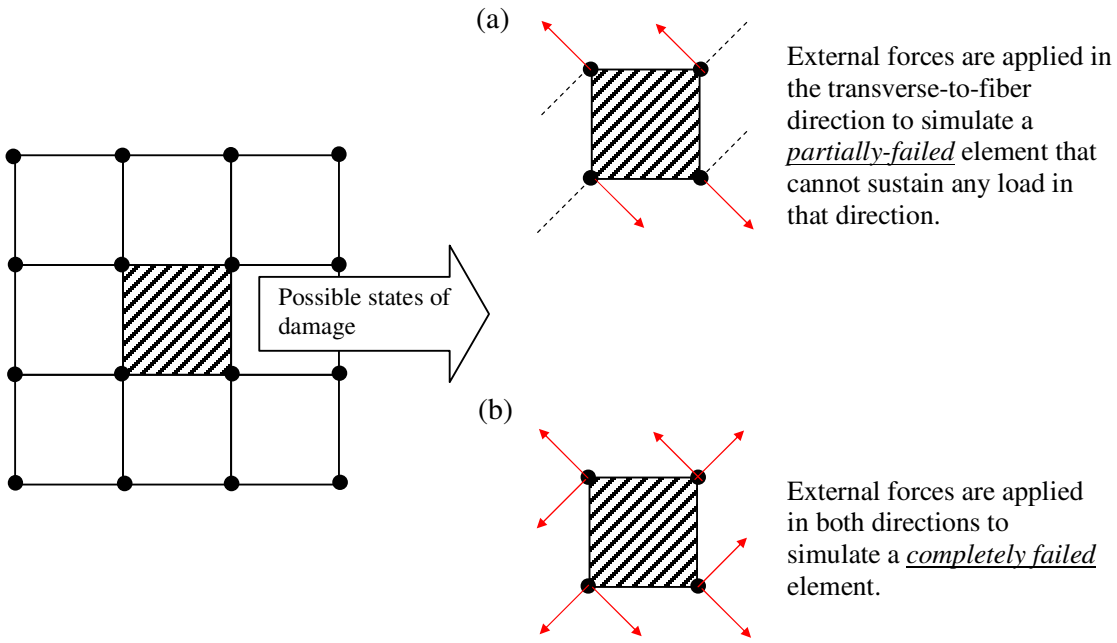

Figure 2-1(a) to (c): How the element-failure method is applied to simulate a *partially* or *completely* failed element.

2.1.2. Force Convergence Criterion of EFM

The "correct" magnitude of external forces to be applied is unknown at the start of the force-modification process. This magnitude is determined through a series of iterations whereby external loads are added per iteration step until the nett internal nodal forces of the surrounding non-fail elements converge to a desired force value (zero for complete failure).

The above concept is illustrated in Figure 2-2. Let us suppose a crack or some damage occurs in element B which compromises its load-carrying capability in the vertical *y*-direction. Here, element B is determined to have failed by an application of an appropriate failure criterion. The non-failed elements surrounding element B are denoted as j where $j = 1, 2, \ldots, etc$.

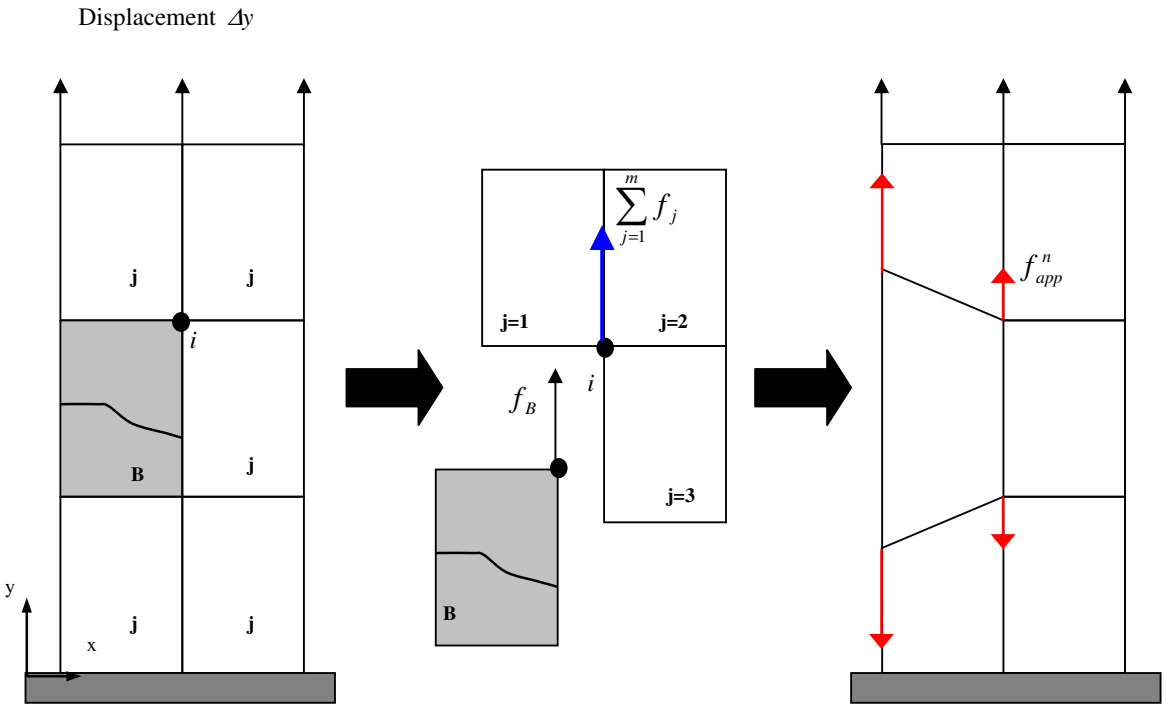

(a) Failed element **B** cannot sustain any load in y-direction

(b) Internal nodal forces of non-fail elements j at node *i* (blue arrow) in the *y*-direction are modified

(c) External nodal forces (red arrows) in the y-direction is applied to modify the internal nodal forces

Figure 2-2(a) to (c): Application of element-failure method to node i of failed element B. Elements j are the non-fail elements surrounding element B.

At iteration 0 (i.e. before any external force is applied), force equilibrium at node i of failed element B requires

$$\sum_{j=1}^{m} f_j^0 + f_B^0 = f_{app}^0 = 0 \qquad (2\text{-}1)$$

where

$\sum_{j=1}^{m} f_j^0$ is the nett internal nodal force at node i belonging to surrounding non-fail elements j. For a 2-D 8-noded failed element B, node i takes the value from $i = 1, 2, \ldots, 8$.

m is the maximum number of non-fail elements j that share a common node i. For example, in Figure 2-2b, m=3.

f_B^0 is the internal nodal force at node i belonging to failed element B,

f_{app}^0 is the external applied force on node i,

and the superscript refers to the iteration number.

It is noted that $f_{app}^0 = 0$ because at the beginning of the series of iterations, there is no applied external nodal force on the node i.

Suppose at node i, the desired nett internal nodal force of non-fail elements j is $\sum_{j=1}^{m} f_{j,D}$, we define the residual R^0 of non-fail elements j (i.e. the difference between the desired and current nett internal nodal force of non-fail elements j at node i) as:

$$R^0 = \sum_{j=1}^{m} f_{j,D} - \sum_{j=1}^{m} f_j^0 \qquad (2\text{-}2)$$

Substituting equation (2-1) into equation (2-2), equation (2-2) can be written in terms of the internal nodal forces of failed element B, f_B^0, as:

$$R^0 = \sum_{j=1}^{m} f_{j,D} + f_B^0 - f_{app}^0 \tag{2-3}$$

The first externally applied nodal force f_{app}^1 becomes:

$$\begin{aligned} f_{app}^1 &= f_{app}^0 + R^0 \\ &= R^0 \\ &= \sum_{j=1}^{m} f_{j,D} + f_B^0 \end{aligned} \tag{2-4}$$

The application of f_{app}^1 at node i for the next iteration (i.e. iteration 1) results in the following force equilibrium equation:

$$\sum_{j=1}^{m} f_j^1 + f_B^1 = f_{app}^1 \tag{2-5}$$

The resulting residual is:

$$R^1 = \sum_{j=1}^{m} f_{j,D} - \sum_{j=1}^{m} f_j^1$$

$$= \sum_{j=1}^{m} f_{j,D} + f_B^1 - f_{app}^1 \qquad (2\text{-}6)$$

In the same fashion, the expression of residual for the nth iteration takes the form:

$$R^n = \sum_{j=1}^{m} f_{j,D} + f_B^n - f_{app}^n \qquad (2\text{-}7)$$

while the expression for the converged external forces is:

$$f_{app}^n = f_{app}^{n-1} + R^{n-1}$$

$$= \sum_{j=1}^{m} f_{j,D} + f_B^{n-1} \qquad (2\text{-}8)$$

The force modification process is stopped at the *nth* iteration when the "correct" amount of external forces f_{app}^n is attained. In this case, the nett internal nodal forces for all the nodes of elements j have reached their desired values. The nodal forces at node i of non-fail elements j is:

$$\sum_{j=1}^{m} f_j^n \rightarrow \sum_{j=1}^{m} f_{j,D} \tag{2-9}$$

The residual is zero when convergence is reached:

$$R^n = \sum_{j=1}^{m} f_{j,D} + f_B^n - f_{app}^n \rightarrow 0 \tag{2-10}$$

i.e. we iterate until the residual R^n of non-fail elements j at node i becomes zero, or a very small pre-set number.

We call equation (2-10) the **force convergence criterion of EFM**, which is to be satisfied for every node i of failed element B for any force component of interest (in this case, it is the *y*-component that is modified). As such, equation (2-10) is equally applicable for three-dimensional conditions.

2.1.3. Validation of EFM

To demonstrate the technique of EFM, we apply equations (2-1) to (2-10) to an analysis of a 2-D orthotropic plate containing a central "crack-like slit" and subjected to uniform tensile displacement $\Delta y = 0.1$ mm prescribed at its top and bottom edges (Figure 2-3a). Dimensions of the plate are 100mm by 200mm in the *x*- and *y*- direction respectively and the plate is modeled with 2-D eight-noded plane-

strain finite elements using material properties $E_1 = 161.3GPa$, $E_2 = E_3 = 8.3GPa$, $G_{12} = G_{13} = 5.16GPa$, $G_{23} = 3.38GPa$, and $\upsilon_{12} = \upsilon_{13} = \upsilon_{23} = 0.3$. The refined FE mesh is shown in Figure 2-3b.

A crack in this problem is expected to grow in the direction perpendicular to the loading direction, i.e. in the x-direction. Hence, the crack is modeled as a "crack-like slit" with a thickness (Figure 2-3b) so that the crack-tip can propagate along the row of elements ahead. We consider the case where the crack has propagated in such a way that two elements ahead of it (denoted as B1 and B2) have failed (Figure 2-4). In this case, the load-carrying capability of failed elements B1 and B2 are mainly compromised in the y-direction. To represent this effect of damage within the failed elements, EFM is employed by applying external nodal forces in the y-direction on the nodes of these failed elements (i.e. nodes n1 to n12). These external forces are added over a series of iterations until the y-component of the internal nodal forces (at nodes n1 to n12) of surrounding non-fail elements is reduced to zero to simulate traction-free crack surfaces. In this way, the force convergence in equation (2-10) is satisfied.

As the size of failed elements is very small (0.025mm by 0.025mm) compared to the crack length (50mm), it is expected that the failure of two elements ahead of the crack will yield σ_{yy} stress contour and crack-opening displacement profiles that are very similar to those prior to element failure. Comparison of the stress contours and crack-opening displacement profiles confirmed this (Figure 2-5 to Figure 2-6).

We find that 15 iterations are required to fail the two elements. The number of iterations is expected to increase as more elements are failed but typically, less than 200 iterations are required to fail an element (for all the problems analyzed in this thesis).

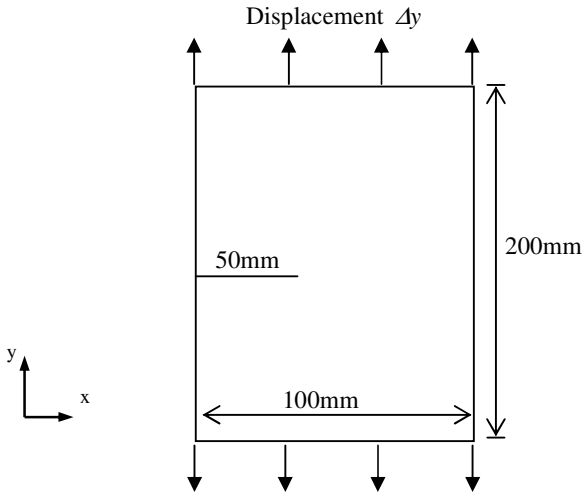

(a) Schematic of tensile problem

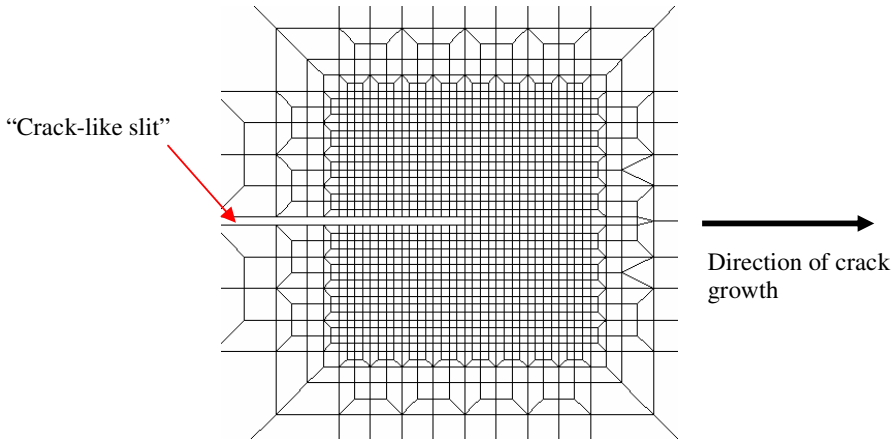

(b) Refined FE mesh in crack tip region

Figure 2-3: FE model of a plate containing a central crack-like slit subjected to tensile loading.

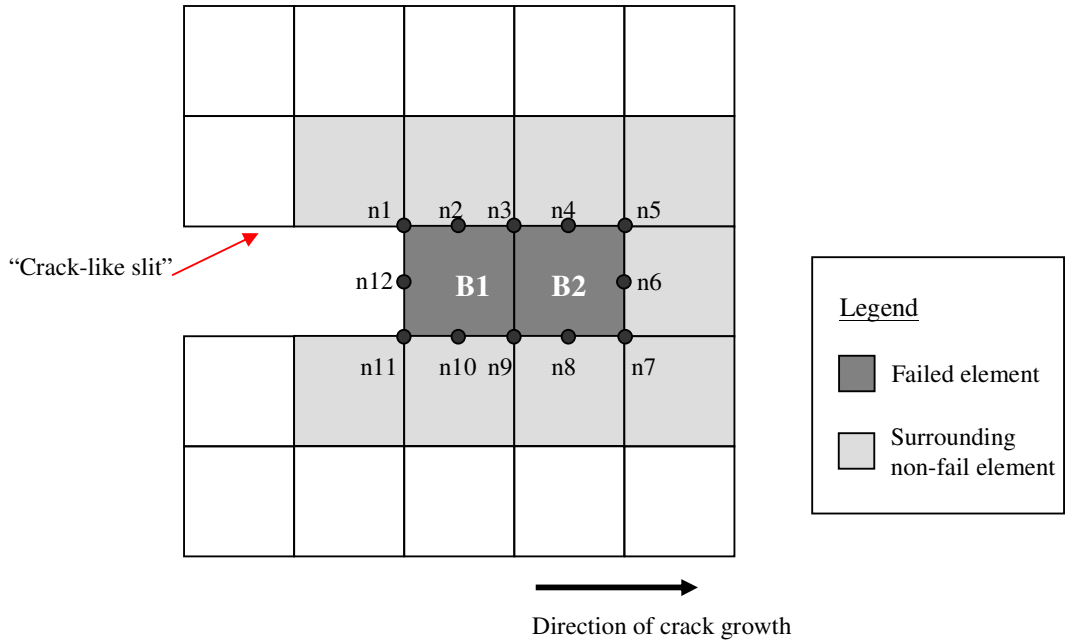

Figure 2-4: Locations of elements and nodes that are involved in the element-failure method.

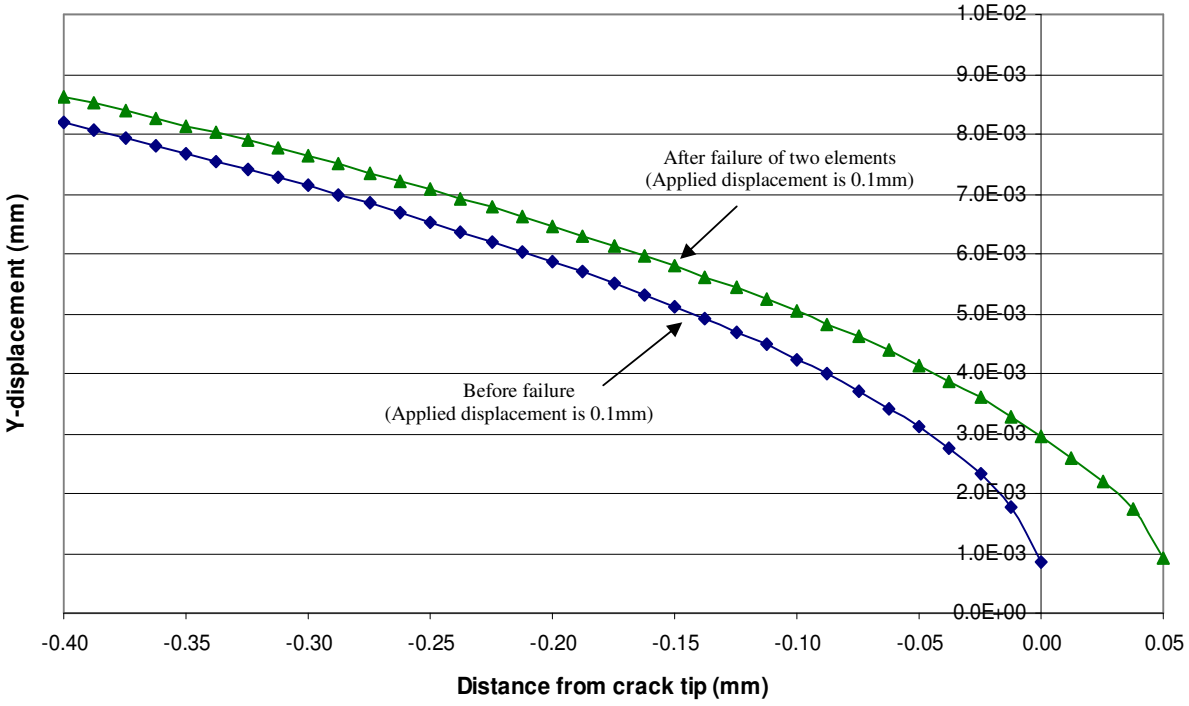

Figure 2-5: Crack-opening displacement profiles before and after failure of two elements.

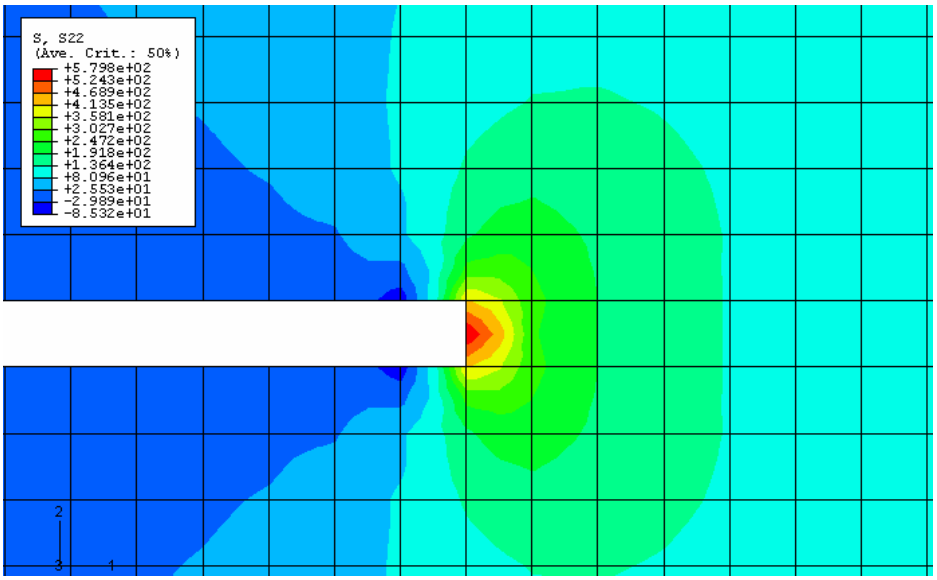

(a): Initial σ_{yy} contour plot without any failure.

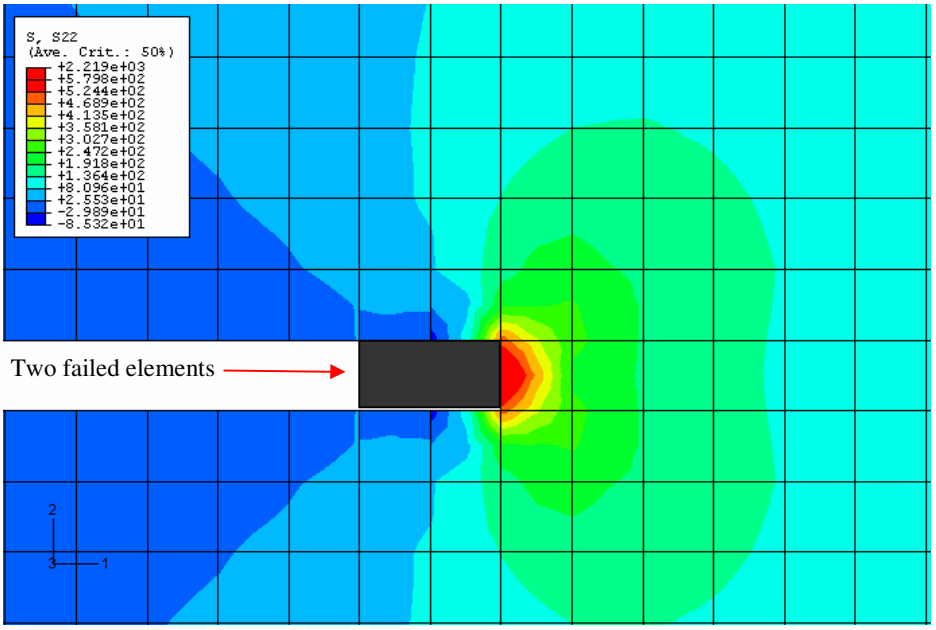

(b): Final σ_{yy} contour plot (after failure of two elements using the element-failure method).

Figure 2-6(a) and (b): σ_{yy} contour plots before and after the failure of two elements

2.1.4. Conclusions

In the element-failure method, we assume that damage in a failed element affects only the internal nodal forces of that element and its surrounding non-fail elements. The addition of external nodal forces at each iteration step only reduces the nett internal nodal forces of non-fail elements whereas those belonging to the damaged element increases. Compatibility is preserved but "stresses" within failed elements are not physical because of the fictitious applied nodal forces.

In addition, as the material properties of the failed element are not modified, there is no ill-conditioning of stiffness matrix in EFM and convergence of a solution is always assured. There is also no need to reformulate the global stiffness matrix during the damage progression process, thereby resulting in savings in computational effort.

Hence, **the EFM does not contain any of the drawbacks associated with the MPDM** (refer to the summary in Table 2-1). A detailed comparative study between the two methods is performed in Chapter 5.

Table 2-1: Differences between the MPDM and the EFM

	Material property degradation method (MPDM)	**Element-failure method (EFM)**
Main feature	Effects of damage are described using material properties	Effects of damage are described using nodal forces
Drawback	As stiffness matrix **C** is degraded, there is a possible problem of ill-conditioning of stiffness matrix. Hence, to ensure its determinant is positive, there are limitations to the amount of degradation that can be applied to the material properties.	As stiffness matrix **C** is not modified, its determinant is always positive. Convergence of a solution is always assured.
Requires iteration?	No	Yes, external nodal forces are added until the internal nodal forces converge to the force convergence criterion in equation (2-9). Iterations are required only for implicit FE.

2.2. Failure Criteria

In this section, we briefly review two failure criteria used in this project. The first is the well-known and established Tsai-Wu failure theory [*Tsai, 1992*], and the second is the strain invariant failure theory (SIFT), a micromechanics-based failure theory that is very recently proposed by Gosse [*Gosse et al., 2001; Gosse, 2002; Gosse et al., submitted for publication*].

2.2.1. Tsai-Wu Failure Theory

The Tsai-Wu failure theory [*Tsai, 1992*] is a tensor polynomial failure theory for anisotropic materials. In this quadratic failure theory for orthotropic materials, the failure surface in stress space is described by a scalar function $f(\sigma_i)$ as

$$f(\sigma_i) = F_i \sigma_i + F_{ij} \sigma_i \sigma_j = 1 \qquad i, j = 1,2,\ldots,6 \qquad (2\text{-}11)$$

where F_i and F_{ij} are experimentally determined strength parameters and a vector notation for stress tensor is adopted as follows: $\sigma_1 = \sigma_{11}$, $\sigma_2 = \sigma_{22}$, $\sigma_3 = \sigma_{33}$, $\sigma_4 = \tau_{23}$, $\sigma_5 = \tau_{31}$ and $\sigma_6 = \tau_{12}$.

In the case of plane stress where $\sigma_3 = \sigma_4 = \sigma_5 = 0$, failure occurs when equation (2-11) becomes

$$F_1 \sigma_1 + F_2 \sigma_2 + F_{11} \sigma_1^2 + F_{22} \sigma_2^2 + 2F_{12} \sigma_1 \sigma_2 + F_{66} \sigma_6^2 \geq 1 \qquad \text{(2-12a)}$$

Or

$$F_1 \sigma_1 + F_2 \sigma_2 + F_{11} \sigma_1^2 + F_{22} \sigma_2^2 + 2F_{12} \sigma_1 \sigma_2 + F_{66} \tau_{12}^2 \geq 1 \qquad \text{(2-12b)}$$

where equation (2-12b) is more commonly used.

The linear terms in shear stress σ_6 have been dropped because the shear strength along the principal material axes is not affected by the sign of the shear stress. Thus, only a quadratic term in shear stress σ_6 remains. However, the linear term in the normal stresses σ_1 and σ_2 are retained because they take into account the different strengths in tension and compression. In addition, the term $2F_{12} \sigma_1 \sigma_2$ takes into account the interaction between the normal stresses.

With the exception of F_{12}, all the other strength parameters in equation (2-12) can be expressed in terms of uniaxial and shear strengths. For example, for the tension and compression tests with uniaxial stresses $\sigma_1 = X_T$ and $\sigma_1 = X_C$ respectively, the simultaneous solution of these two equations resulting from equation (2-12) yields

$$F_1 = \frac{1}{X_T} + \frac{1}{X_C}, \qquad F_{11} = -\frac{1}{X_T X_C} \qquad \text{(2-13)}$$

Similarly, it can be shown from uniaxial and shear tests that

$$F_2 = \frac{1}{Y_T} + \frac{1}{Y_C}, \qquad F_{22} = -\frac{1}{Y_T Y_C}, \qquad F_{66} = \frac{1}{S^2} \tag{2-14}$$

In the case of a composite material, subscript 1 refers to the fiber direction while subscript 2 refers to the transverse to fiber direction, X_T and X_C represents the tensile strength and compression strength of the composite in its fiber direction respectively, Y_T and Y_C represent the tensile strength and compression strength in the transverse to fiber direction and S is the shear strength.

The determination of interaction parameter F_{12} requires a biaxial test involving both σ_1 and σ_2. However, F_{12} can have four different values because there are four different failure pairs σ_1, σ_2 [*Hashin, 1983*]. Wu [*Wu, 1972, 1974*] has suggested that in order to determine F_{12} accurately, the biaxial ratio $B = \sigma_1 / \sigma_2$ must be optimized to account for the sensitivity of F_{12} to experimental scatter in the applied stresses. The optimization procedure is complicated and the reader is referred to articles by Wu [*Wu, 1972, 1974*] for more details.

Subsequently, Tsai and Hahn [*Tsai and Hahn, 1980*] proposed:

$$F_{12} = -\frac{(F_{11}F_{22})^{1/2}}{2}$$

$$= \frac{-1}{2\sqrt{X_T X_C Y_T Y_C}} \tag{2-15}$$

which means equation (2-12) may be interpreted as a generalized von Mises equation. It is interesting to note that equation (2-12) reduces to Tsai-Hill criterion [*Tsai, 1968*] when the tensile and compressive strengths are assumed to be equal and

$$F_{12} = -\frac{1}{2X_T^2}. \tag{2-16}$$

The Tsai-Wu failure criterion is appropriate for fiber-reinforced composite materials because the compressive strength in the fiber direction is usually greater than its corresponding tensile strength.

Comments

The single-valued scalar equation in equation (2-12) makes Tsai-Wu failure theory easy to use. It accounts for the interaction of stresses by using interaction coefficient F_{ij}. It also correlates well with experimental data as it uses homogenized material strengths X_T, X_C, Y_T, Y_C and S that are measured from experiments. In this aspect, Tsai-Wu failure theory is used to predict macroscopic failure. However, Tsai-Wu failure theory does not explicitly distinguish between the failure modes of

composites. In addition, it is not a micromechanics-based criterion, which means that failure mechanisms at their microstructural scale cannot be directly and easily related to the various strength values.

2.2.2. Strain Invariant Failure Theory, SIFT

Since the strain invariant failure theory is relatively new, its essential features are briefly described here. Proposed by Gosse [*Gosse et al., 2001; Gosse, 2002; Gosse et al., submitted for publication*], failure is determined in SIFT by considering the criticality of three strain invariants. These invariants were calculated using strains that have been "amplified" through a separate micromechanical analysis, which is described in the next section.

The first of the invariants is J_1 and is defined as:

$$J_1 = \varepsilon_{xx} + \varepsilon_{yy} + \varepsilon_{zz} \tag{2-17}$$

where $\varepsilon_{xx}, \varepsilon_{yy}, \varepsilon_{zz}, \gamma_{xy}, \gamma_{yz}, \gamma_{xz}$ are the six components of the strain vector in general Cartesian coordinates. The subscripts could also represent the directions of any orthogonal coordinate system such as material coordinate system 1-2-3 since J_1 is an invariant.

Where distortional deformation is significant, SIFT employs the von Mises (or equivalent) strain ε_{vm} that is defined by:

$$\varepsilon_{vm} = \sqrt{\frac{1}{2}[(\varepsilon_{xx} - \varepsilon_{yy})^2 + (\varepsilon_{xx} - \varepsilon_{zz})^2 + (\varepsilon_{yy} - \varepsilon_{zz})^2 + \frac{3}{2}(\gamma_{xy}^2 + \gamma_{xz}^2 + \gamma_{yz}^2)]} \qquad (2\text{-}18)$$

A simplified form of SIFT (where only the first strain invariant J_1 is considered) has been recently used by Li *et al.* [*2003*] to successfully predict matrix-dominated failure in I-beams, curved beams and T-cleats. Their findings also suggest that the J_1 criterion is most appropriate for interlaminar failure of composite structures subjected to quasi-static tension-tension load cases where the failure is dominated by volume increase of the matrix. On the other hand, von Mises strain invariant ε_{vm} is more suitable for other load cases where the failure is dominated by distortion.

2.2.2.1. Micromechanical Enhancement of Strains

The strains ε_{xx}, ε_{yy}, ε_{zz}, γ_{xy}, γ_{yz}, γ_{xz} used in equations (2-17) and (2-18) are obtained from the "amplification" of macro strains. The amplification factors involved have been determined earlier through a separate micromechanical analysis, where a repeating unit volume (RUV) consisting of individual matrix and fibers have been modeled by three-dimensional finite elements. Three types of fiber packing patterns

with a fiber volume V_f of 60% are considered: square, hexagonal and diamond (Figure 2-7).

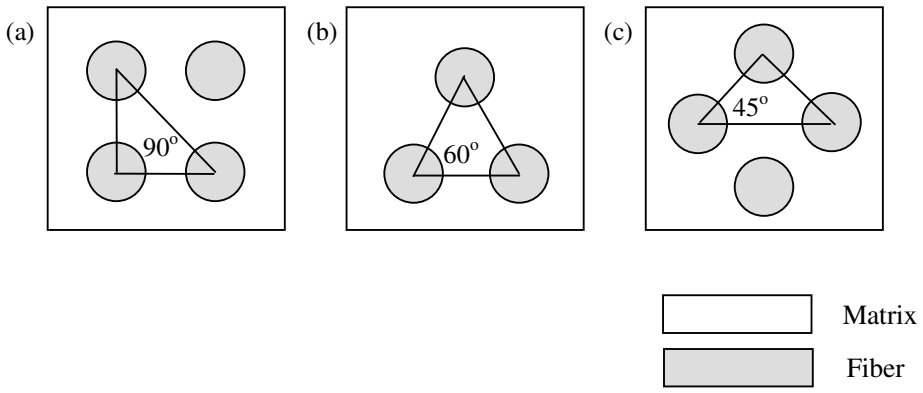

Figure 2-7: Fiber packing patterns: (a) Square (b) Hexagonal and (c) Diamond

For each fiber packing pattern, unit strains in three cases of normal and three cases of shear deformations (defined as boundary conditions BC1 through BC6 in Table 2-2) are separately prescribed to the RUV to extract the mechanical strain amplification factors (Figure 2-8). For example, in order to obtain the mechanical strain amplification factor for prescribed strain $\bar{\varepsilon}_{11} = 1$ in the fiber-direction, the other faces of the RUV are constrained (Figure 2-8a). The local mechanical strains are extracted from various locations within the RUV (Figure 2-9) and normalized with respect to the prescribed strains. In addition to the mechanical amplification factors, the thermal-mechanical amplification factor is obtained by constraining all the faces of the RUV from expansion and performing a thermo-mechanical analysis by prescribing a unit temperature differential ΔT above the stress-free temperature.

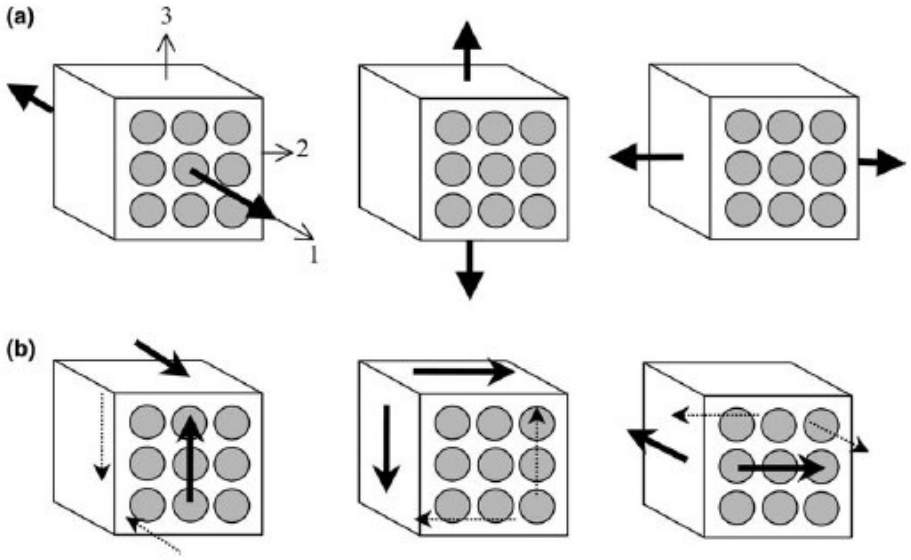

Figure 2-8: (a) Prescribed normal displacements, (b) prescribed shear deformations.

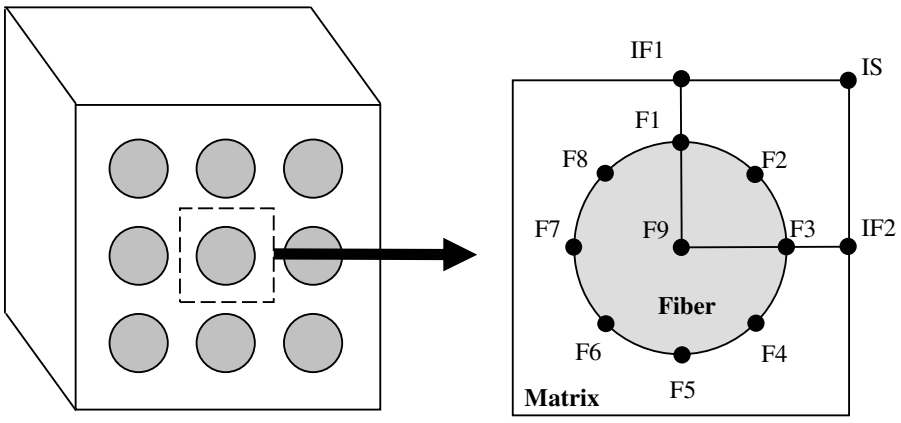

Figure 2-9: Locations for extraction of mechanical strain and thermal-mechanical strain amplification factors.

Table 2-2: Definition of boundary conditions BC1 to BC6 used in the extraction of mechanical strain amplification factors.

Boundary	**Prescribed Constraints**
BC1	$\bar{\varepsilon}_{11}=1,\ \bar{\varepsilon}_{22}=\bar{\varepsilon}_{33}=\bar{\gamma}_{12}=\bar{\gamma}_{13}=\bar{\gamma}_{23}=0,\ \Delta T=0$
BC2	$\varepsilon_{22}=1,\ \varepsilon_{11}=\varepsilon_{33}=\gamma_{12}=\gamma_{13}=\gamma_{23}=0,\ \Delta T=0$
BC3	$\varepsilon_{33}=1,\ \varepsilon_{11}=\varepsilon_{22}=\gamma_{12}=\gamma_{13}=\gamma_{23}=0,\ \Delta T=0$
BC4	$\gamma_{12}=1,\ \varepsilon_{11}=\varepsilon_{22}=\varepsilon_{33}=\gamma_{13}=\gamma_{23}=0,\ \Delta T=0$
BC5	$\gamma_{23}=1,\ \varepsilon_{11}=\varepsilon_{22}=\varepsilon_{33}=\gamma_{12}=\gamma_{13}=0,\ \Delta T=0$
BC6	$\gamma_{13}=1,\ \varepsilon_{11}=\varepsilon_{22}=\varepsilon_{33}=\gamma_{12}=\gamma_{23}=0,\ \Delta T=0$

For each fiber-packing pattern, Gosse [*Gosse, 2002*] has chosen twelve locations for the extraction of amplification factors (Figure 2-9). Three are related to the matrix phase (IF1, IF2, IS) and 9 related to the fiber phase (F1 to F9). Points F1 through F8 are located at the fiber-matrix interface, F9 is located at the center of the (assumed circular) fiber, IF1 and IF2 are inter-fiber positions, and IS corresponds to the interstitial position. Therefore, there are 6 mechanical amplification factors and 6 thermo-mechanical amplification factors for each position. Since there are 12 positions per RUV and 3 fiber-packing pattern, the total number of amplification factors is 432 (i.e. $12\times12\times3$).

It is noted that the above micromechanical analysis needs only be performed once, for a given matrix and fiber material system. For this project, the set of amplification factors are referenced from Gosse [*Gosse, 2002*] based on a carbon-fiber/epoxy IM7/977-3 system with a fiber volume V_f of 60%. These factors are coded in a

subroutine so that strains from the macro-finite element analysis can be efficiently amplified.

The expression for the amplification of macro strains is given as:

$$\{\varepsilon\}_i^{phase} = [MF]_i^{phase}\{\varepsilon\}^{mech} + (\Delta T)\{TF\}_i^{phase} \tag{2-19}$$

where

$\{\varepsilon\}_i^{phase}$ is the local mechanical strain vector at position i within RUV. i can be either IF1, IF2, IS (for matrix phase) or any of the F1 to F9 (for fiber phase).

$\{\varepsilon\}^{mech}$ is the homogenized mechanical strain vector obtained from the macro-finite element analysis of the composite laminates,

$[MF]_i^{phase}$ is the column matrix of mechanical strain amplification factors at location i within each phase,

$\{TF\}_i^{phase}$ is the column vector of thermal-mechanical strain amplification factors at location i within each phase ,

(ΔT) is the temperature differential.

The first invariant J_1 in equation (2-17) is calculated with strains amplified only at IF1, IF2 and IS locations within the matrix material in the RUV. It is generally believed that J_1 -driven failure is dominated by volumetric changes in the matrix

material. On the other hand, the von Mises strain ε_{vm} in equation (2-18) may be amplified with factors within the matrix material (IF1, IF2 and IS) and also with the fiber and fiber-matrix interface (F1 through F9). Thus, we designate the superscript m to denote "matrix" (i.e. ε_{vm}^{m}) and the superscript f to denote "fiber" (i.e. ε_{vm}^{f}). This corresponds to 3 sets of J_1, 3 sets of ε_{vm}^{m} and 9 sets of ε_{vm}^{f} for one fiber-packing pattern.

Hence, an element from the macro FE model will own a total of 9 (i.e. 3 matrix locations ×3 packing patterns) sets of J_1, and 9 (i.e. 3 matrix locations ×3 packing patterns) sets of ε_{vm}^{m} and 27 (i.e. 9 fiber locations ×3 packing patterns) sets of ε_{vm}^{f}. Failure is said to have occurred when *either* of the three strain invariants at any of the twelve locations in the RUV reaches its respective critical value (i.e. J_{1Crit}, ε_{vmCrit}^{m} and ε_{vmCrit}^{f}):

$$J_1 \geq J_{1Crit}; \quad \varepsilon_{vm}^{m} \geq \varepsilon_{vmCrit}^{m}; \quad \text{or} \quad \varepsilon_{vm}^{f} \geq \varepsilon_{vmCrit}^{f} \tag{2-20a}$$

or

$$\frac{J_1}{J_{1Crit}} \geq 1; \quad \frac{\varepsilon_{vm}^{m}}{\varepsilon_{vmCrit}^{m}} \geq 1; \quad \text{or} \quad \frac{\varepsilon_{vm}^{f}}{\varepsilon_{vmCrit}^{f}} \geq 1 \tag{2-20b}$$

It is noted that the critical values of the strain invariants J_{1Crit} and ε^{m}_{vmCrit} are obtained by Gosse [*Gosse, 2002*] from tensile testing of several un-notched uniformly strained IM7/977-3 laminae with a fiber volume ratio of 60%, whose fiber orientations varied between 15° and 90°, relative to the loading axis. The third critical SIFT criterion ε^{f}_{vmCrit} is an effective property because it is obtained through the testing of unnotched 0° unidirectional and $[10°/-10°]_{ns}$ laminates in tension [*Gosse et al., 2001; Gosse et al., submitted for publication*].

A pictorial summary of how SIFT is used to predict the failure of an element is given in Figure 2-10. Suppose we are studying the damage progression of a composite laminate under a three-point bend load, a finite element analysis is first performed to obtain the macro strains (Step 1 of Figure 2-10). For each element, the macro strains are amplified according to equation (2-10) using the set of amplification factors derived from the micromechanical analysis (Step 2 of Figure 2-10). Since the amplification factors were extracted from various locations of a RUV (Figure 2-9) of three fiber-packing patterns (Figure 2-7), the macro strains are effectively "amplified" to represent the micro strains at those locations. These micro strains are subsequently used to calculate the strain invariants defined in equations (2-17) and (2-18)). An element is considered "failed" if one of its strain invariants becomes critical according to equation (2-20) (Step 3 of Figure 2-10).

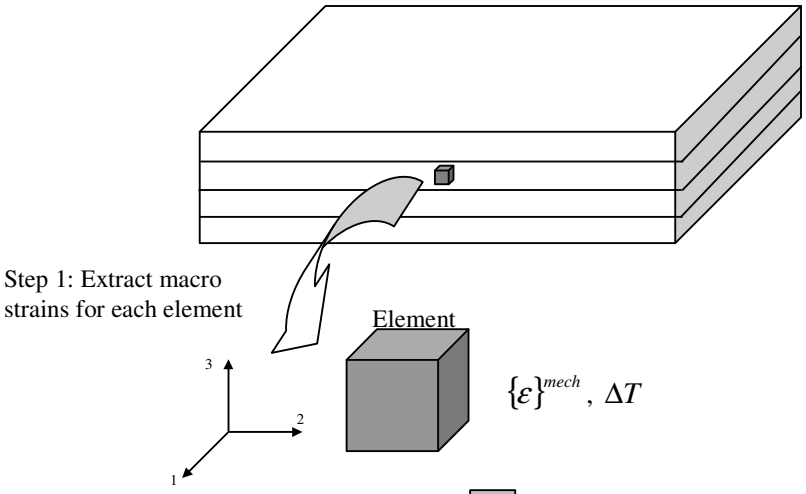

Step 2: Amplify macro strains $\{\varepsilon\}^{mech}$ according to Eq. (2-19). The "amplified" strains are used to calculate the strain invariants J_1 , ε_{vm}^m and ε_{vm}^f defined in Eqs (2-17) and (2-18).

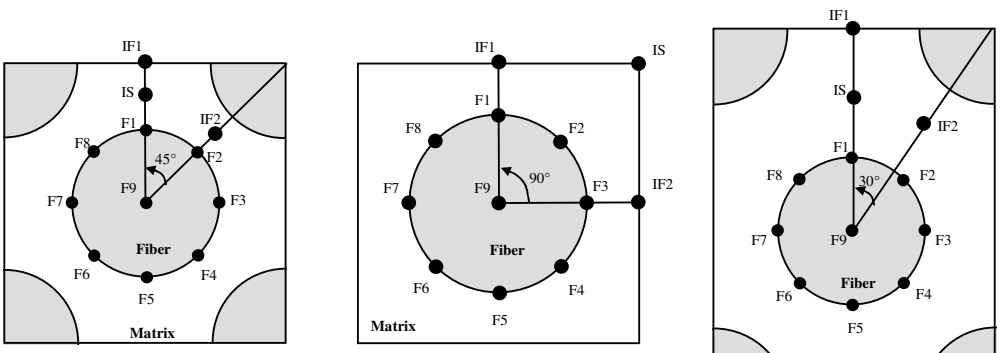

(i) Diamond RUV

3 sets of J_1 ;
3 sets of ε_{vm}^m ;
9 sets of ε_{vm}^f

(ii) Square RUV

3 sets of J_1 ;
3 sets of ε_{vm}^m ;
9 sets of ε_{vm}^f

(iii) Hexagonal RUV

3 sets of J_1 ; 3 sets of ε_{vm}^m ;
9 sets of ε_{vm}^f

Total 9 sets of J_1 , 9 sets of ε_{vm}^m and 27 sets of ε_{vm}^f

Step 3: Determine the most critical invariant: $J_1 \geq J_{1Crit}$? $\varepsilon_{vm}^m \geq \varepsilon_{vmCrit}^m$? $\varepsilon_{vm}^f \geq \varepsilon_{vmCrit}^f$?

Figure 2-10: Sequence of micromechanical enhancement of macro strains.

2.2.3. Conclusions

For each failure prediction, it is possible not only to determine the invariant that has become critical, but also the position within the RUV where this has occurred. It remains to be seen whether the information extracted from the micromechanics analysis may be correlated to the observed local failure mechanisms. This is because like Tsai-Wu failure theory, SIFT does not explicitly distinguish failure modes as each critical strain invariant is not associated with a particular damage mode.

However, an advantage of SIFT over Tsai-Wu failure theory is that it offers information occurring at the micro-mechanical level. This is because failure can be traced at either the matrix or fiber phase. For example, if the largest normalized strain invariant is due to J_1 , it means that the matrix has undergone some irreversibility locally and damage in the form of matrix cracks, fiber/matrix debonding or delamination are possible. And if the largest normalized strain invariant is due to ε_{vm}^{f}, the damage can occur at either the fiber phase (F9) or matrix-fiber interface (F1 to F8) depending on the location within the fiber phase where the largest normalized invariant occurs. In this case, fiber fracture or fiber/matrix debonding are possible damage modes.

The basic features and differences between Tsai-Wu Theory and SIFT are tabulated in Table 2-3. A detailed comparative study between the two methods applied to the three-point bend test is given in Chapter 4.

Table 2-3: Differences between Tsai-Wu failure theory and SIFT

	Tsai-Wu failure theory	**Strain invariant failure theory (SIFT)**
Basic features	Macromechanical-based equation usually expressed in stress space. There is also a strain-based formulation but less commonly used.	Micromechanical based method. Equations expressed in strain space.
Identify failure modes?	Does not explicitly distinguish between failure modes	Failure can be traced at either the matrix or fiber phase. But it still does not explicitly identify local failure mechanisms.
Ease of use	Simple to use as failure criterion is described using one equation.	Not as straightforward as Tsai-Wu theory. Micromechanical amplification factors must be obtained from a set of separate 3-D analysis. But once obtained, the factors can be readily used.

3. Implementation of the EFM and SIFT into an FE Code

In this chapter, we develop a finite element (FE) code to implement the element-failure method (EFM). The code is to be used to model the initiation and progression of damage in composite laminates under quasi-static load in Chapter 4. Two-dimensional (2-D) plane-strain finite element method is used to perform the stress analysis and failure of the elements is predicted using strain invariant failure theory (SIFT). The principles of the finite element method are not mentioned here, as there are already many excellent texts on it [*Bathe, 1996; Rao, 1989; Cook et al., 1989; Strang and Fix, 1973; Zienkiewicz, 1991*]. A description of the development of our code and its algorithms are covered in the following sections.

3.1. Development of Our Code

We prefer to develop our own code here instead of using commercial implicit FE codes such as ABAQUS because the former will be more computationally efficient. This is because ABAQUS reformulates the global stiffness matrix at every iteration step. On the other hand, our code only formulates the global stiffness once at the beginning of the computation. No reformulation of global matrix is necessary because the EFM does not modify the material properties of failed element and

hence, the initial global stiffness matrix remains unchanged throughout the computations.

Our FE code is built upon a simple 2D plane strain FE code by Smith and Griffiths [*2004*]. The extension to a 3-D code is similar and straightforward since a basic 3-D FE code is also available [*Smith and Griffiths, 2004*]. The original 2-D code uses 8-noded quadrilateral elements in their FE mesh and is used to perform only stress analysis of isotropic material. It uses very simple geometry and does not have complex mesh-generating routines. Available outputs from the code are nodal displacements and elemental stresses.

We modify the original code and extend it to predict damage initiation and progression in composite laminates. Written in FORTRAN language, our code performs stress analysis for orthotropic composite materials subjected to quasi-static prescribed displacements. It is able to read in a FE mesh created by commercial modeling software such as Msc/PATRAN. The advantage of this is that a FE mesh needs not be restricted to rectangular shape and can have finer mesh in areas of interest.

In addition, the effect of thermal residual strains from fabrication process is accounted for and the code provides output for nodal forces and elemental strains. The nodal forces are needed for the application of EFM while strains are needed for the application of SIFT in order to predict the next element to fail. Subroutines implementing EFM and SIFT are also written. A summary of the functions of the code is tabulated in Table 3-1.

Table 3-1: Summary of the functions of the developed code.

Function	Description
Purpose	• Predicts damage progression pattern in a composite
Mesh	• Reads in mesh that is created using Msc/Patran • Mesh can be of any shape as long as quadrilateral elements are used.
Material	• Material is linear elastic and can be orthotropic, transversely isotropic or isotropic • Elements can be assigned with material properties that are different from one another
Load	• Can be applied in the form of nodal forces or as prescribed displacement
Thermal effects	• Accounts for thermal residual stresses from fabrication
Outputs	• Nodal displacements • Nodal forces • Elemental thermal residual strains and mechanical strains • Elemental stresses
Add-ons	• Includes damage-modeling techniques such as EFM and MPDM • Includes failure criteria like SIFT and Tsai-Wu • Lookup tables for amplification factors • Residual force calculations for EFM

3.2. Flowchart

A flowchart of our 2-D implicit finite element (FE) code (where EFM and SIFT are implemented) is illustrated in Figure 3-1. The 2-D finite element mesh consisting of eight-noded plane strain elements is first generated using a commercial modeling software MSC/Patran and later read by our code. The algorithm performs the following steps:

Step 1. Reads in mesh information such as dimensions, element and node numbers, element-node connectivity, nodal coordinates, boundary conditions and applied load in the form of prescribed displacement δ_0.

Step 2. Reads in user-specified material properties, laminate layup and temperature change from the stress-free state.

Step 3. Performs finite element analysis to solve for nodal displacements and elemental strains due to the prescribed displacement δ_0. The elemental strains are obtained by averaging the strains evaluated at 2×2 Gaussian points.

Step 4. Apply SIFT to determine the next element to fail. This is done by first amplifying the elemental strains from Step 3 with the set of amplification factors stored in a look-up subroutine on SIFT. The amplified strains are subsequently used to calculate the strain invariants J_1, ε_{vm}^m and ε_{vm}^f. An element is considered failed if any of its normalized strain invariant values exceeds 1.0 (Refer to Chapter 2 for more details on SIFT).

Step 5. If no failed element is found in step 5, increase the prescribed displacement $\delta_0 + \Delta\delta$. Repeat steps 4 and 5 until the first failed element is determined.

Step 6. Apply the element-failure method (EFM) to the failed element. Depending on the nodal force reduction scheme chosen, appropriate external nodal forces are successively applied to the nodes of the failed element until the force convergence of EFM in equation (2-10) is satisfied (Refer to Chapter 2 for more details on EFM).

Step 7. Proceed to fail more elements using steps 3 to 6 until the desired number of failed elements is reached.

Step 8. Plot the damage progression pattern using Matlab.

Our code was later tested by repeating the 2-D stress analysis problem (without any damage) in an example given in the book by Smith and Griffiths [*2004*]. The nodal displacements and stress values computed by our code are identical to the original solutions.

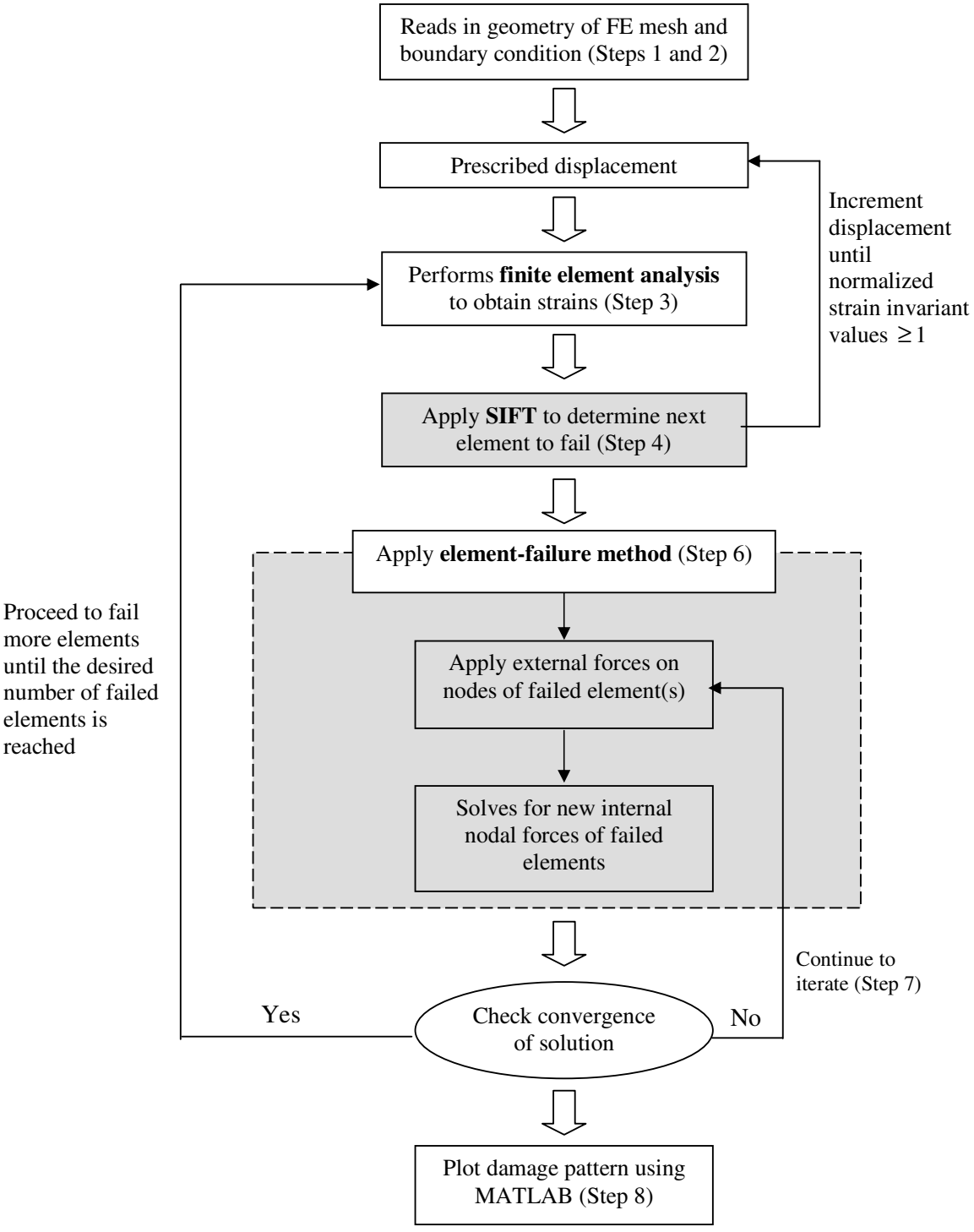

Figure 3-1: Flowchart of our FE code using the EFM and SIFT (Details of steps 1 to 9 are given in Section 3.2)

Our FE code can be made more general by using other failure criterion such as Tsai-Wu failure theory instead of SIFT, by replacing the SIFT subroutines with appropriate Tsai-Wu subroutines. In this case, elemental stresses instead of strains are computed and the Tsai-Wu equation in equation (2-12b) is used to determine an element that has failed. Likewise, the EFM can also be replaced by another damage-modeling technique such as the material property degradation method (MPDM). In this case, selected material properties of failed elements are modified. This affects the elemental stiffness matrix and the global stiffness matrix must be reformulated as the damage progression is modeled.

The flowchart of a more general code is illustrated in Figure 3-2. This general FE code is useful for comparing different failure theory or damage-modeling technique. For example, in Chapter 4, we use the code to generate damage progression patterns for a composite laminate loaded under three-point bend. There, a set of damage pattern is generated using the EFM with SIFT, while a second set is generated using MPDM with SIFT. The two patterns are compared with experimental observations to determine whether EFM or MPDM is a more suitable damage-modeling technique for that problem.

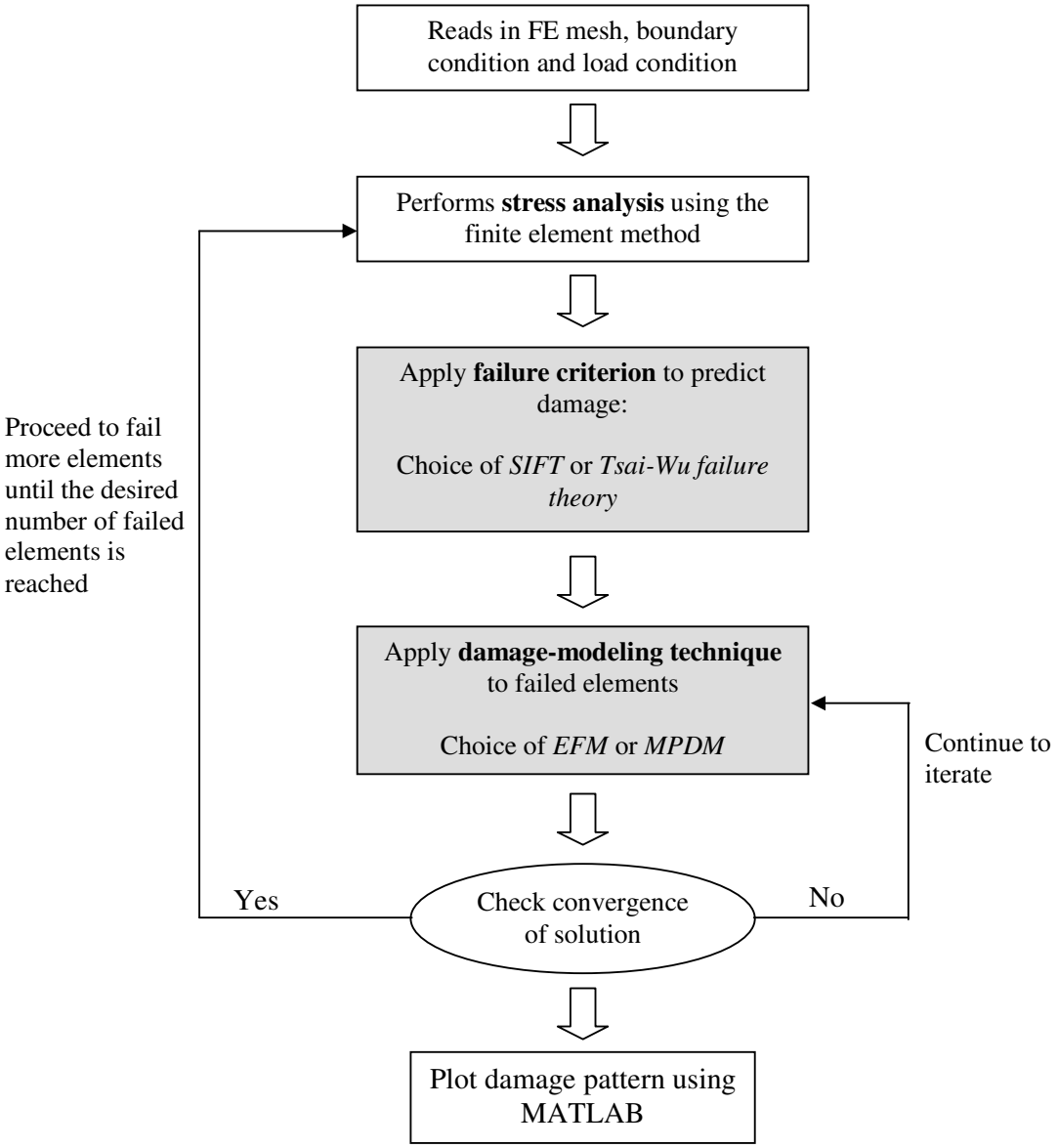

Figure 3-2: Structure of a more general FE code

4. Application of the EFM to a Three-point Bend Analysis

In this chapter, we illustrate the use of the element-failure method (EFM) in the case of progressive damage analysis of a composite laminated beam under quasi-static three-point bend. The EFM has been implemented in an in-house two-dimensional plane strain FE code in Chapter 3. The first section describes the experiments that are performed to obtain the experimental damage progression pattern. The second section discusses the damage patterns generated using the in-house FE code and validation with experimental data.

4.1 Three-point Bend Experiment

4.1.1 Experimental Procedure

Fibredux T800H/924C composite prepreg with fiber volume fraction $V_f = 66\%$ is thawed for 24 hours before being stacked into a lay-up of $[0_3/90_3/0_3/90_3/0_3]$. The laminated plate is then cured in an autoclave at 180° and pressure of 7 bar for 2.5 hours, according to the manufacturer's specifications. Test coupons, each measuring 26 mm wide, 130 mm long and 2.14 mm thick, are cut from the laminate with a diamond circular saw. Their edges are polished with sandpaper and their surfaces are

inspected for defects. Void content and damage due to cutting are found to be negligible.

The set-up of the three-point bend test is shown in Figure 4-1. Each test coupon is simply-supported on two cylindrical rollers placed 120mm apart, while compressive load is applied at its midspan through another cylindrical pin at a constant displacement rate of 5 mm/min using an Instron universal testing machine. Diameters of the loading and support pins are both 8mm for each pin. Rubber pads are placed between the test coupon and the loading pin to prevent premature local crushing of the coupon. The orientation of the fiber in the coupon is such that the 0° fiber direction is along the span wise direction while the 90° direction is in the transverse width direction.

A total of three test coupons have been used and they were loaded to ultimate failure (i.e. the coupon splits into two separate pieces). The entire damage progression of each test is captured on a digital video camera. A close-up view of damage is required at the loading region because of the small thickness of the coupon (Figure 4-1b). The force-displacement curve is recorded and the failed coupons are examined under the microscope to obtain more information on the local damage modes.

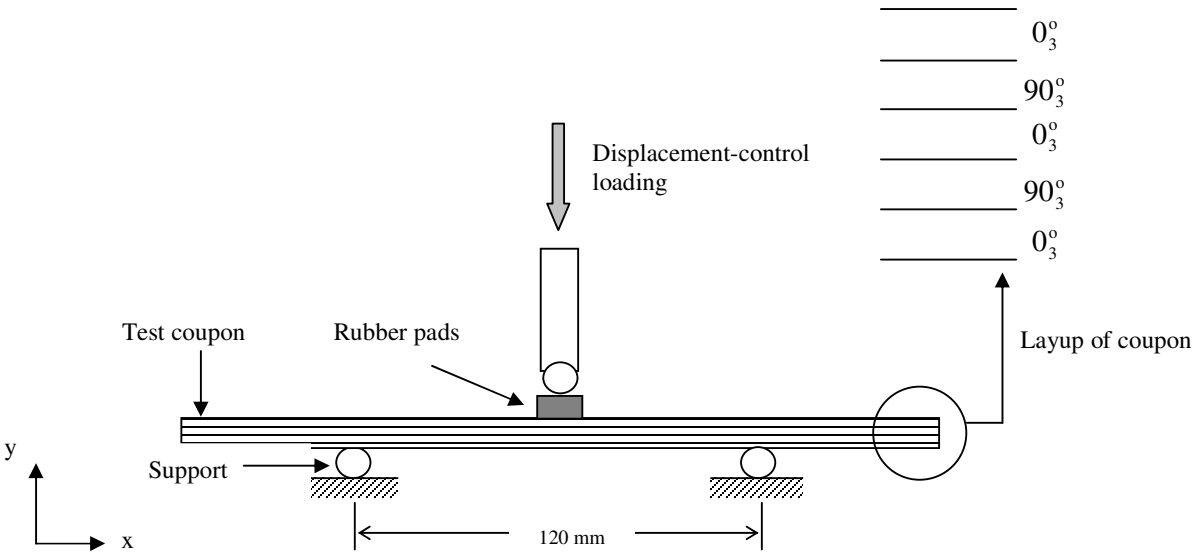

(a) Schematic of set-up

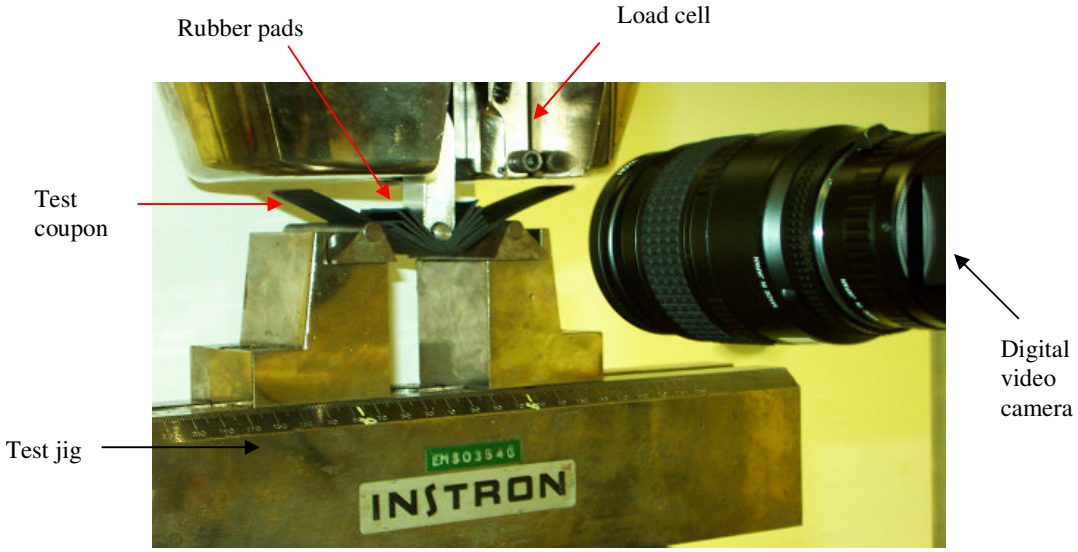

(b) Experimental set-up

Figure 4-1 (a)-(b): Set-up of the three-point bend test.

4.1.2 Experimental Damage Patterns and Observations

Consistent damage patterns were obtained among the three test coupons. The damage pattern is symmetric about the loading axis and the schematic of the damage progression (as seen through the thickness of the specimen) is shown in Figure 4-2a. Here, the layer numbers are referred consecutively from the top surface where each layer consists of three plies of unidirectional tape. The chronological order of damage events can be described in four stages as follows:

Stage 1: The first sign of damage was observed in the form of local matrix-cracking and fiber-breakage of the first 0° plies near the point of load application (Figure 4-2b).

Stage 2: Shortly after the maximum load of 1.94 kN was attained (averaged over three coupons), damage propagated rapidly, corresponding to the onset of the first delamination at the interface between the first (0°) and second (90°) layers (Figure 4-2b). The crushing in the top layer becomes more extensive as the delamination grows.

Stage 3: This was rapidly followed by the initiation and growth of the second delamination at the interface between the third (0°) and fourth (90°) layers. After the second delamination had propagated some distance to the right, it kinked into the fourth (90°) layer and continued along the interface with the fifth (0°) layer (Figure 4-2b).

Stage 4: The coupon was then loaded to ultimate failure when it split into two parts.

A sample of the force-displacement curves is given in Figure 4-3. All the force-displacement curves from the three test coupons demonstrate the same characteristics (refer to Appendix A) i.e. there are two peaks that correspond to the onset of the first and second delaminations respectively.

The load values at the first peak (i.e. the onset of the first delamination) for the three test coupons are:

Test coupon no. 1 = 2.23 kN

Test coupon no. 2 = 1.67 kN

Test coupon no. 3 = 1.92 kN

Hence, the average load that corresponds to the onset of the first delamination is 1.94 kN.

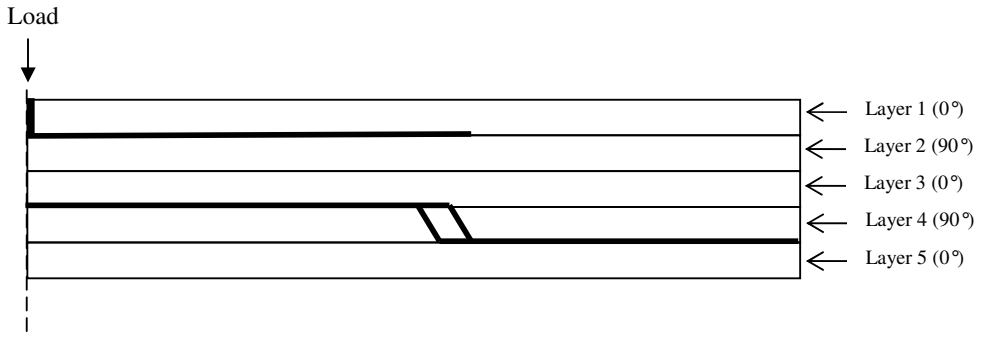

(a) Schematic damage pattern in the loading region. Only half of the specimen is shown as the damage pattern is symmetric about the loading axis.

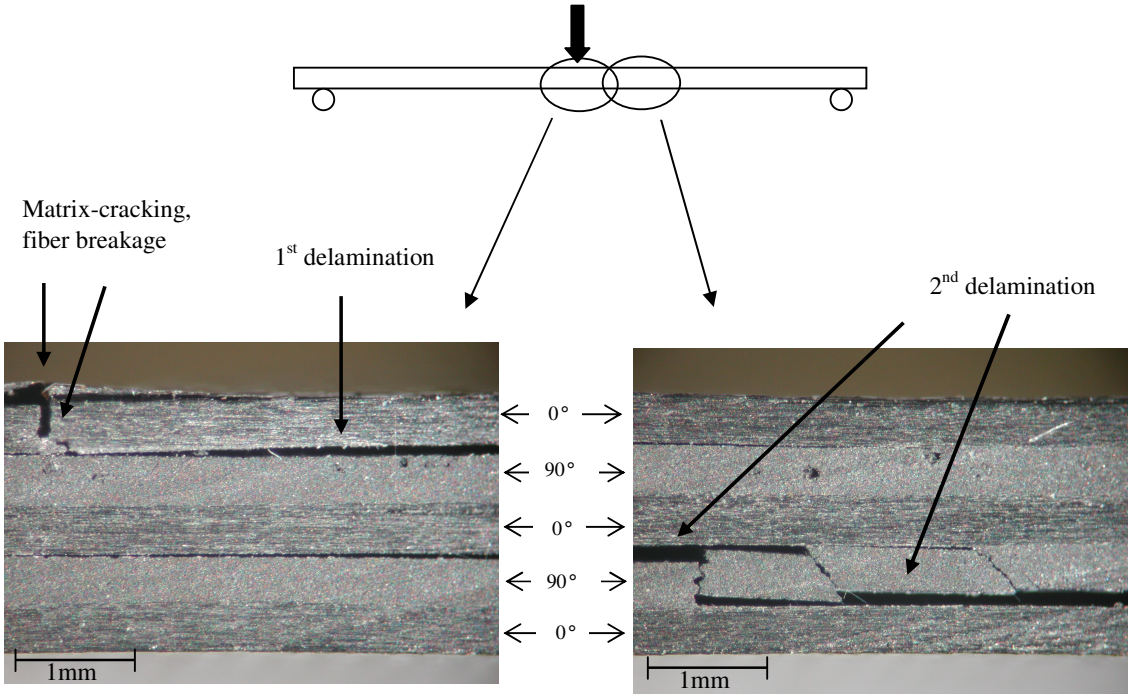

(b) Stage 1 damage (i.e. occurrence of matrix cracks and fiber breakage) and Stage 2 damage (i.e. occurrence of first delamination)

(c) Stage 3 damage (i.e. occurrence of second delamination)

Figure 4-2: Damage pattern of a $[0_3/90_3/0_3/90_3/0_3]$ laminated composite beam under a three-point bend load.

Comment

The observed damage progression pattern described above may be dependent upon the size of the loading roller used (8mm in this case). It is possible that the use of a larger diameter loading roller could prevent the localized crushing failure of the first plies and affect the subsequent development of the delaminations. However, we did not vary the size of the loading roller, and therefore, could not comment on how the damage pattern will differ with the current one.

In addition, post failure examination of the three test coupons show that the failure pattern does not vary significantly from one edge to the other through the width direction. This shows that the transverse component is not that important in the failure process. Hence, we can perform a 2-D analysis for this problem in the next section.

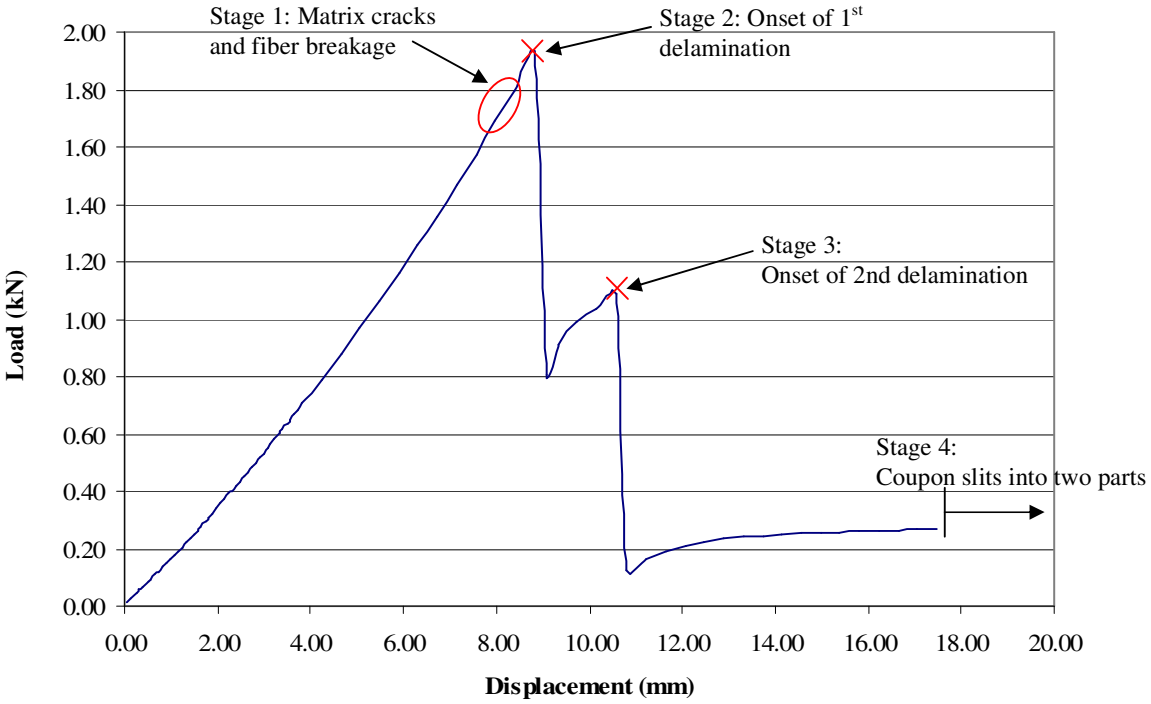

Figure 4-3: Force-displacement curve of a $[0_3/90_3/0_3/90_3/0_3]$ laminated composite beam under a three-point bend load.

4.2 Damage Progression Pattern Predictions from FE Code

In this section, we use our implicit FE code (that is developed in Chapter 3) to generate damage progression patterns for the $[\,0_3/90_3/0_3/90_3/0_3\,]$ laminated composite beam problem. The FE model is shown in Figure 4-4. Due to symmetry in the geometry of the test coupon and applied loading, only half of the test coupon is modeled. Each layer of the laminate (consisting of three unidirectional plies of the same orientation) is modeled with four rows of square eight-node quadrilateral plane-strain elements. The fine mesh is necessary to capture the interlaminar stresses.

The graphite/epoxy composite material properties used in the FE model are given in Table 4-1. These values were obtained from Gosse *et al.* [*submitted for publication*] where subscript 1 of the material properties refers to the fiber direction while subscripts 2 and 3 are along the transverse to fiber directions. The contact (i.e. rubber padding) between the loading pin and composite laminated beam is 5mm thick and is modeled with elastic properties of hard rubber $E = 4MPa$ and $\upsilon = 0.5$ while the pin support is assigned with elastic properties of steel $E = 210GPa$ and $\upsilon = 0.3$. Values of hard rubber and steel were obtained from *Metal Reference Book* [*Smithells C J, 1976*].

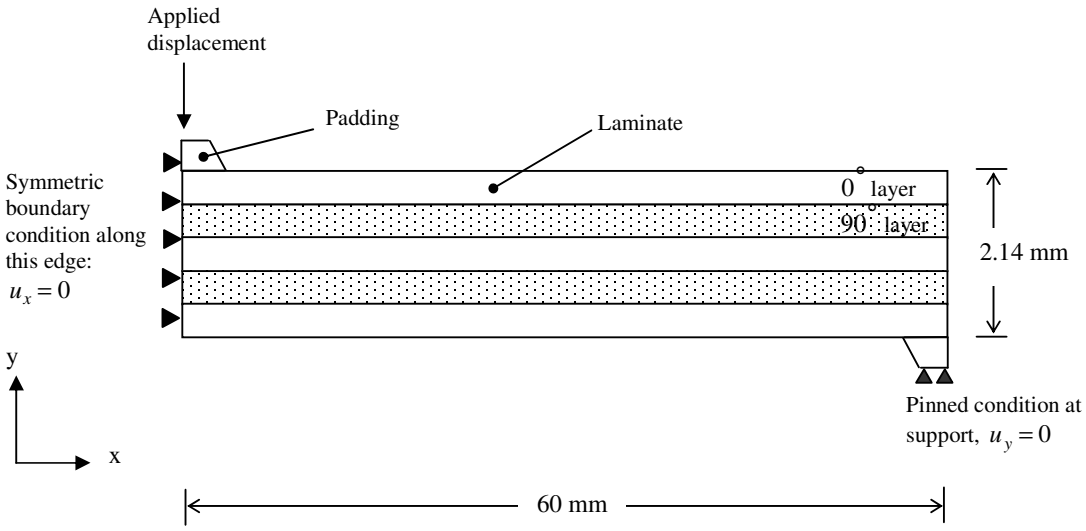

(a) Schematic FE mesh

(b) Full view of the FE mesh

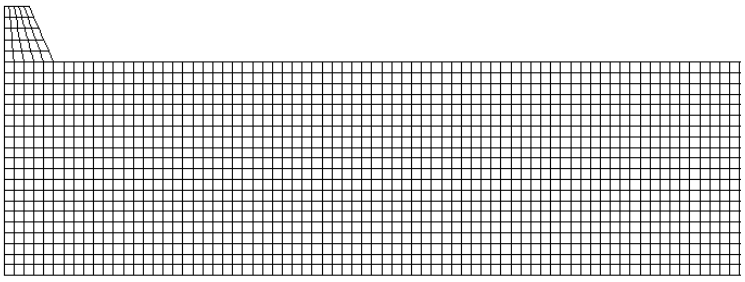

(c) Close-up view of the FE mesh in the loading region

Figure 4-4(a) and (b): Half FE model of $[0_3/90_3/0_3/90_3/0_3]$ laminate

Table 4-1: Material properties of graphite/epoxy composite used in FE model.

Material Properties	**Values**
Modulus in fiber direction, E_1 (GPa)	161.30
Transverse moduli E_2, E_3 (GPa)	8.3
Shear moduli G_{12}, G_{13} (GPa)	5.16
Shear moduli G_{23} (GPa)	3.38
Poisson's ratios $\nu_{12} = \nu_{13}$	0.24
Poisson's ratio ν_{23}	0.3
Thermal expansion coefficient in fiber direction $\alpha_1 (/°C)$	0.01×10^{-6}
Thermal expansion coefficient in transverse directions	32.7×10^{-6}
Fiber volume fraction	60 %

Load in the form of displacement is prescribed at the top left hand corner of the FE mesh. The displacement is incremented slowly until the first element is failed. The thermal-induced strains in the composite laminates due to the fabrication process are accounted in the subroutine on SIFT. The temperature difference between the cure temperature of $180°C$ and room temperature of $25°C$ is $\Delta T = 155°C$.

Five attempts at predicting the damage progression patterns with different combinations of damage-modeling methods and failure theories were made (Table 4-2). The x-direction is defined along the horizontal or spanwise direction, while the y-direction is the out-of-plane direction.

Our main objective here is to evaluate the element-failure method (i.e. case EFX of Table 4-2) and compare it with traditional damage-modeling method – material property degradation method, MPDM. This is achieved by first validating the damage pattern in case EFX with experimental observations and later comparing it with the results obtained using different material degradation schemes of MPDM (i.e. cases MPD_1, MPD_2 and MPD_3). Since SIFT is also relatively new, it is later compared with the well-established Tsai-Wu failure theory by comparing the damage patterns of case EFX with case EFX_TW.

Table 4-2: Damage-modeling methods and failure theories for prediction of damage progression.

Case	**Damage-modeling method**	**Failure theory**
EFX*+	Element-failure with *x*-direction nodal forces zeroed	SIFT
MPD_1*	Material property degradation with E_x reduced to 30% of its original value.	SIFT
MPD_2*	Material property degradation with E_x, G_{xy} and G_{xz} reduced to 30% of their original values.	SIFT
MPD_3*	Material property degradation with E_x, G_{xy} and G_{xz} reduced to 1% of their original values while v_{xy} and v_{xz} are reduced to 0.05.	SIFT
EFX_TW+	EFM where *x*-component of nodal force is reduced to zero	Tsai-Wu

* Cases used to compare damage-modeling methods

+ Cases used to compare failure theories

4.2.1 Case EFX - Damage Pattern Predicted using the EFM with SIFT

4.2.1.1 Modeling Strategy

The EFM is studied where the *x*-direction nodal forces are zeroed. This rather simple nodal force reduction scheme by EFM is acceptable because the primary load-bearing mechanism for this three-point bend problem is bending, where the bending stresses are mainly oriented in the horizontal or spanwise direction. For problem involving more general and complicated composite structures, a more sophisticated nodal force reduction scheme will be necessary. Nevertheless, it would be interesting to see if the use of such simple force-reduction scheme in this simulation is adequate in describing the effects of damage on composite laminates.

Failure is determined using strain-invariant failure theory (SIFT). The critical values of the strain invariants used are J_{1Crit} = 0.0230, ε^{f}_{vmCrit} =0.0182 and ε^{m}_{vmCrit} =0.1030. These values are obtained from Gosse [*Gosse, 2002*] based on experimental testing of unidirectional composite laminates IM7/977-3 with a fiber volume ratio of 60 %. We use the same critical values in our damage predictions although our laminated composites for this three-point bend problem are not strictly the same composition and have a different fiber ratio (our test coupons are manufactured using Fibredux T800H/924C composite prepreg with a fiber volume fraction of 66%). In addition, we have used 3-D SIFT parameters for the 2-D plane strain problem here. This is acceptable because post failure examination of test coupons revealed that the failure pattern does not change much in the width direction, thus justifying the use of a 2-D

analysis. This is also due to the fact that the beam has a cross-ply lay-up. However, in general, most problems would indeed require a full 3-D analysis.

4.2.1.2 Results and Observations

The damage progression pattern predicted by EFM and SIFT is shown in Figure 4-5. A total of 100 elements are failed and the order of failure is numbered in Figure 4-6. When the predicted sequence is compared with that of the experimental damage pattern (Figure 4-2), it is observed that the combination of the EFM and SIFT is able to predict correctly the initial local crushing of the top 0° layer (Figure 4-5a), the occurrence of the first major delamination at the interface between the first (0°) and second (90°) layers, as well as the extensive crushing in the top layer as damage progresses (Figure 4-5c). The onset of the second delamination (Figure 4-5e) is also predicted although the prediction of its location at the interface between the fourth (0°) and fifth (90°) layers is different from experimental observations.

It is observed that the second delamination has initiated at a location unrelated to the rest of the main damage pattern. A look at the strain contours (Figure 4-7) prior to the onset of second delamination reveals that the maximum shear strain γ_{xy} is located at the interface between the fourth (0°) and fifth (90°) layers and this value is about three times and five times higher than the maximum values of the in-plane normal strains ε_{xx} and ε_{yy} respectively. This suggests that the initiation of the second delamination was driven by a dominant shear strain.

In addition, the location of the second delamination is predicted differently from the experimental observations. This may be due to a significant redistribution of stresses as more elements are failed in the damage progression process. In this case, the current nodal force reduction scheme (that zeroes only the x-component of nodal forces) is no longer expected to be adequate in describing the effects of such extensive damage. Nevertheless, the overall agreement with experimental data is remarkable, given the rather simple and conservative nodal force reduction scheme used in EFM.

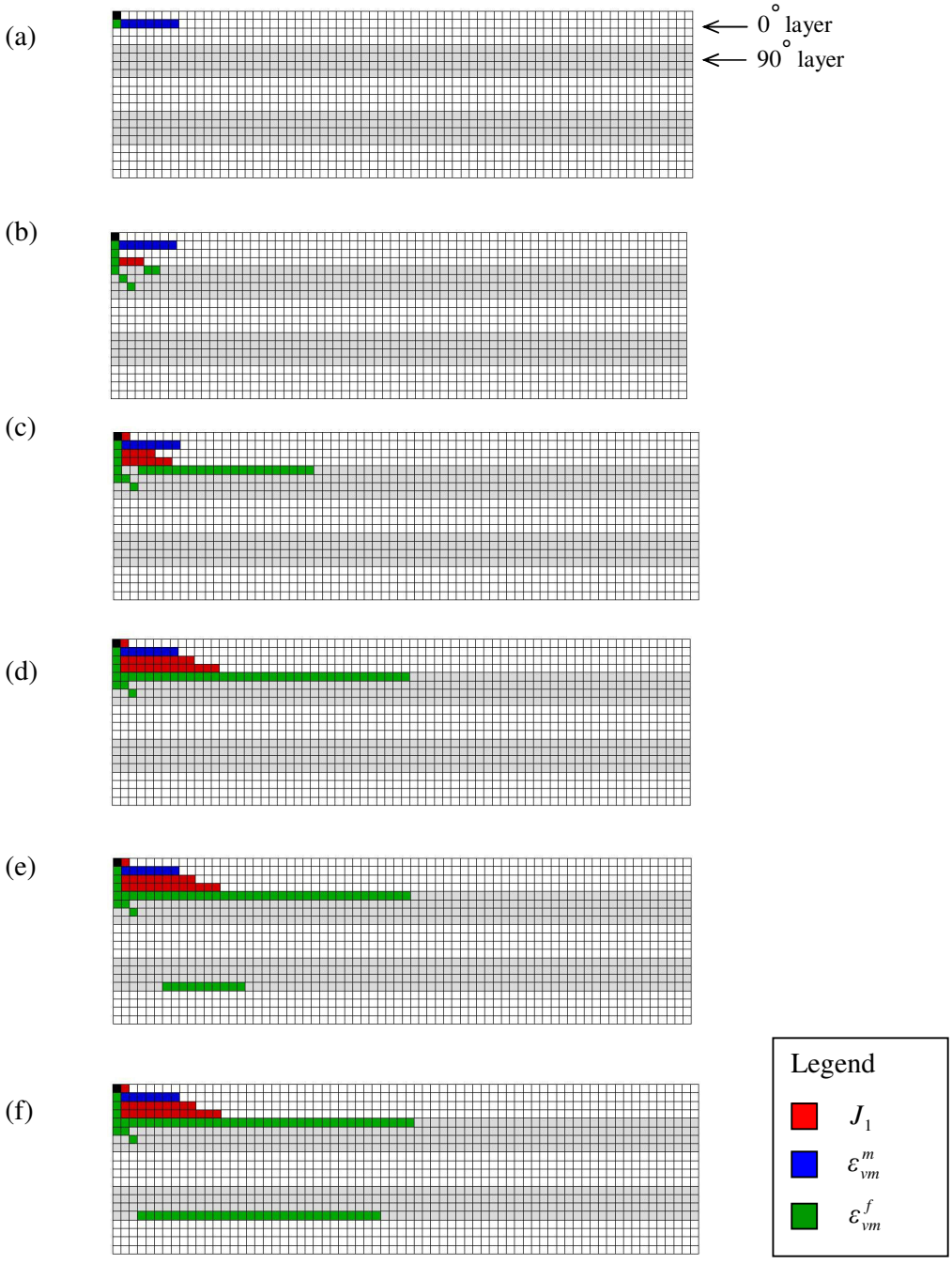

Figure 4-5(a)-(f): Case EFX - EFM predicted damage and delamination progression with J_{1Crit} = 0.0230, ε_{vmCrit}^{f} =0.0182 and ε_{vmCrit}^{m} =0.1030.

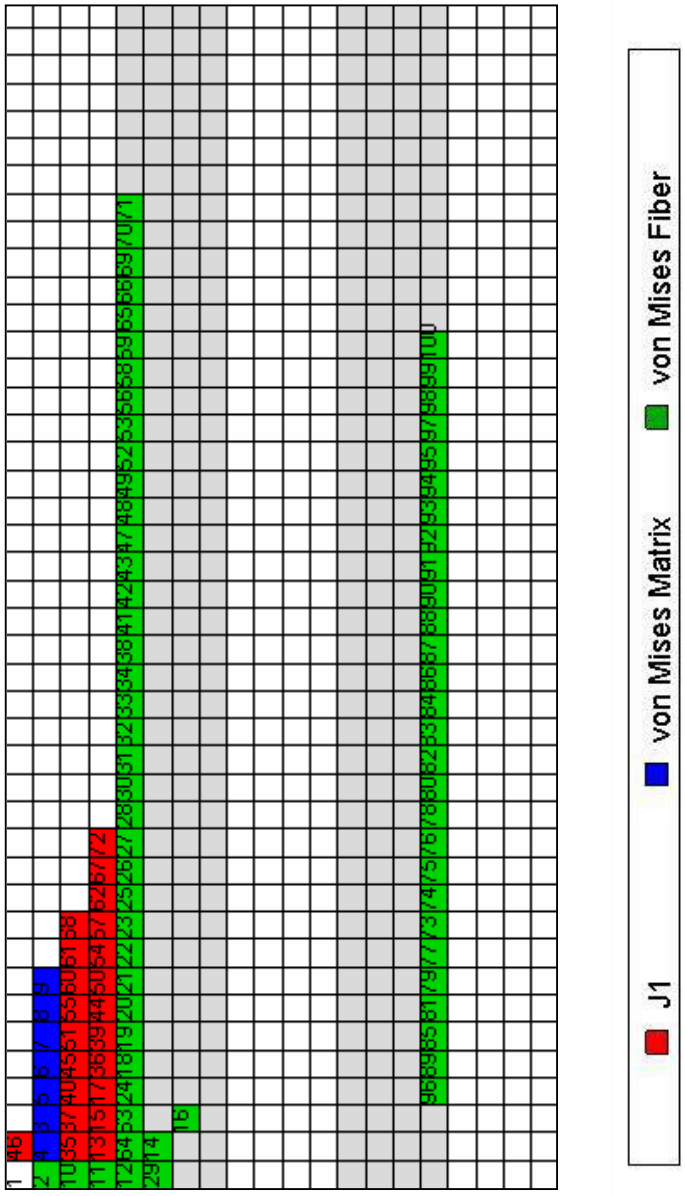

Figure 4-6: EFM numbered sequence of predicted damage and delamination progression with J_{1Crit} = 0.0230, ε^{f}_{vmCrit}=0.0182 and ε^{m}_{vmCrit}=0.1030

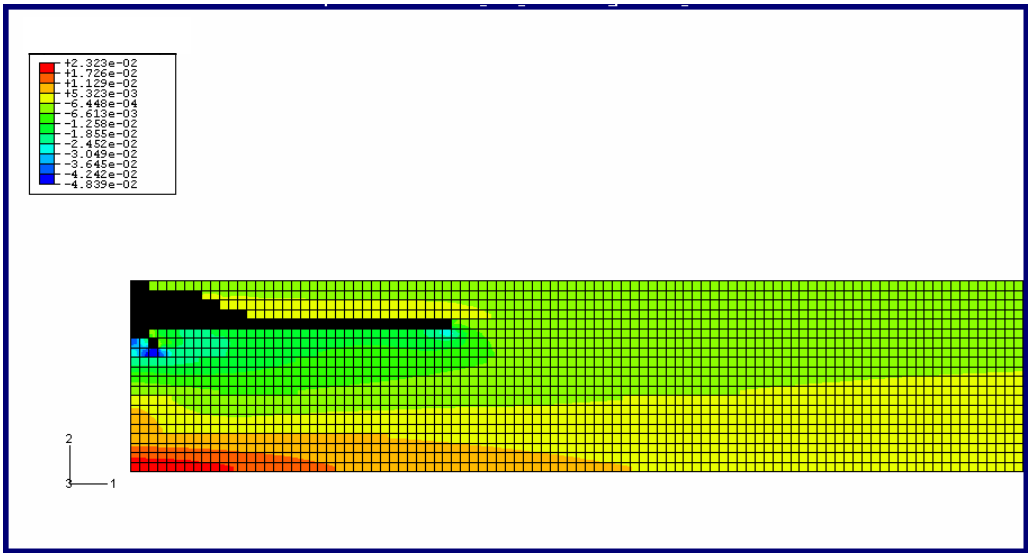

(a) ε_{xx} strain contour plot (the failed elements are shaded in black)

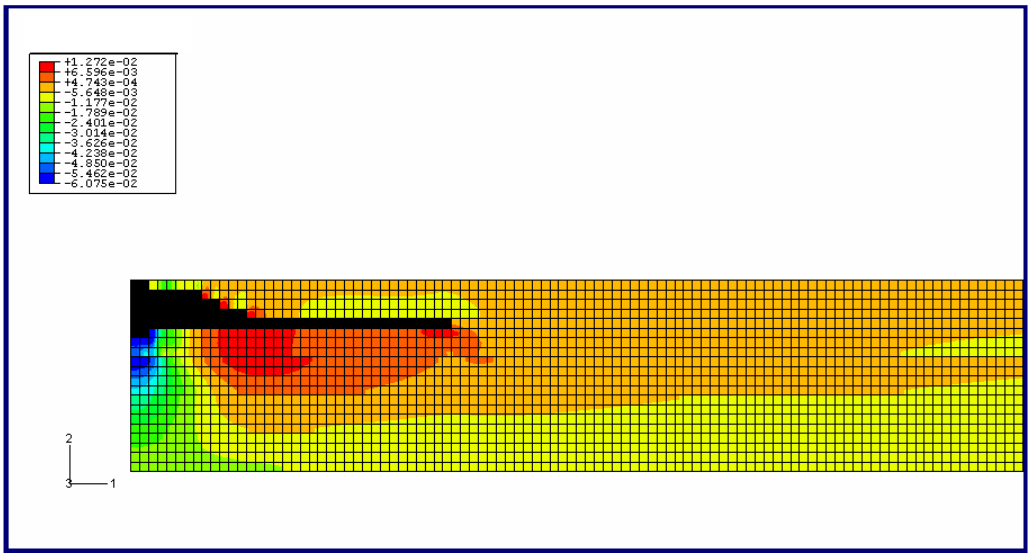

(b) ε_{yy} strain contour plot (the failed elements are shaded in black)

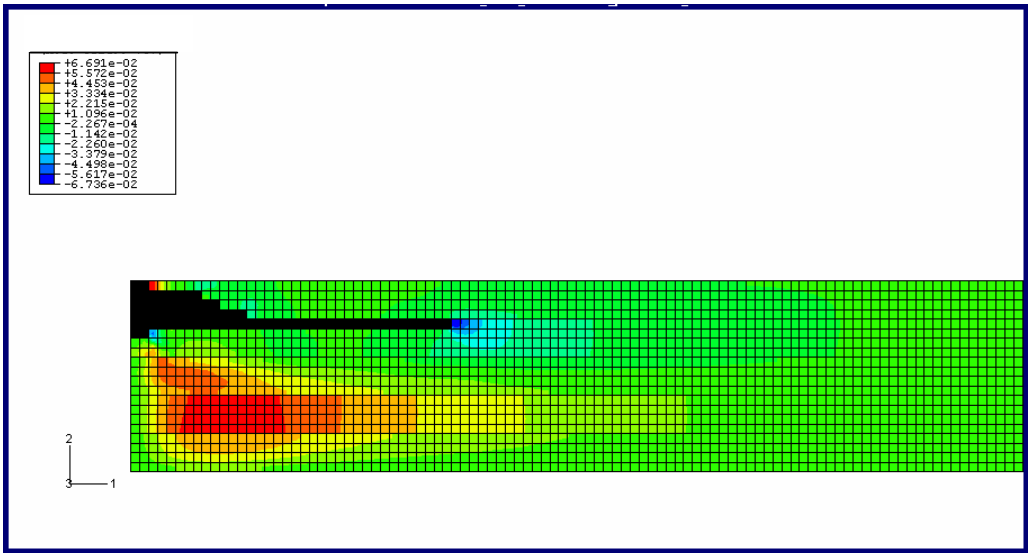

(c) γ_{xy} strain contour plot (the failed elements are shaded in black)

Figure 4-7(a)-(c): Strain contours plots prior to the onset of second delamination.

4.2.1.3 Correlation of Details of Damage Pattern with SIFT Parameters

The first element to fail is determined by SIFT to have occurred when the prescribed displacement is 4.5mm. This corresponds to a predicted load of 2.14kN, compared to the experimental load of 1.95kN. No further increment in displacement is required as the normalized strain invariant values of all the subsequent failed elements are above 1.0 (Figure 4-8). This suggests that failure, once initiated, is unstable and proceeds to final failure. This observation agrees well with experiment.

As failure is predicted by SIFT through the criticality of three strain invariants (refer to the methodology of SIFT in Chapter 3), the failed elements in Figure 4-5 and Figure 4-6 are color-coded to indicate the strain invariant that has become critical. It is observed that much of the local crushing in the first layer is due to J_1 (red) and ε_{vm}^{m} (blue), while the two delaminations are dominated by ε_{vm}^{f} (green). This implies that the initial damage (i.e. the localized crushing of the top plies) of the composite beam is dominated by dilatational and distortional deformation in the matrix phases. Subsequent damage in the form of two major delaminations is mainly dominated by distortional deformation in the fiber phases of their respective plies.

Further information regarding damage at the constituent fiber and matrix phase level can be presented in the form of a chart in Figure 4-9. The vertical axis provides the following information: The first letter (H, S or D) denotes the type of fiber-packing patterns (i.e. Hexagonal, Square or Diamond) where the critical invariant has been

found. The information in brackets denotes the locations at the fiber or matrix phase in the fiber-packing pattern defined according to Figure 2-9 in Chapter 2. The designation xx, xy or yy refers to the component of the local mechanical strain ε_{xx}, ε_{yy} or γ_{xy} (extracted from the micromechanical enhancement of global strains) that provides the largest contribution to the calculated invariant value. The positive or negative sign corresponds to the sign of this dominant strain component. Finally, a color bar just above the horizontal axis indicates the fiber orientation of the layer in which the failed element is located; i.e. grey indicates a 0° layer while black a 90° layer.

The chart in Figure 4-9 can be interpreted together with the numbered damage progression pattern in Figure 4-6 as follows: the initial failure due to local crushing (i.e. for the 3rd to 9th element) is due to ε_{vm}^{m} (Figure 4-6) and is labeled "S(IF2)-xy" in Figure 4-9. This means that the matrix phase of these elements has undergone irreversibility and the damage is localized at inter-fiber location IF2 of the matrix phase within a square fiber-packing array. The critical invariant ε_{vm}^{m} is dominated by shear strain γ_{xy} and the color bar indicates that this occurs in the 0° layer. As the damage progresses, the first delamination at the interface between the first (0°) and second (90°) layers (dominated by ε_{vm}^{f} in Figure 4-6) is labeled "D(F9)-xy" " in Figure 4-9. This means that the fiber phase has suffered some irreversibility and the damage is localized at fiber location F9 within a diamond fiber-packing array. The critical invariant ε_{vm}^{f} is dominated by shear strain γ_{xy}.

The growth of the first delamination is accompanied by extensive matrix-crushing of the top layer. This extensive crushing (e.g. in 35th to 40th element) is dominated by a critical J_1 in Figure 4-6 and is labeled "H(IF1)+yy" in Figure 4-9. This means that the matrix phase of these elements has undergone irreversible dilatational deformation and the damage is localized at inter-fiber location IF1 of the matrix phase within a hexagonal fiber-packing array. Finally, the second delamination that occurs at the interface between the fourth $(0°)$ and fifth $(90°)$ layers is predicted to be due to ε_{vm}^{f} (for the 73th to 100th element in Figure 4-6) and is labeled "D(F9)+xy" in Figure 4-9. Similar to the first delamination, damage has occurred at fiber location F9 in the fiber phase within a diamond fiber-packing array and the critical invariant is dominated by shear strain γ_{xy}. This finding is consistent with the strain contour plots in Figure 4-7 which show that the onset of second delamination is driven by high shear strain. This suggests that the use of SIFT parameters is able to correlate well with damage pattern.

It is noted that the failed elements have been color-coded to indicate the strain invariant that has the biggest value. It is found that some of the failed elements have all their three strain invariants values greater than 1.0. For such elements, both its matrix and fiber phases have suffered an irreversibility and damage is no longer confined to just a single phase as indicated by the critical strain invariant.

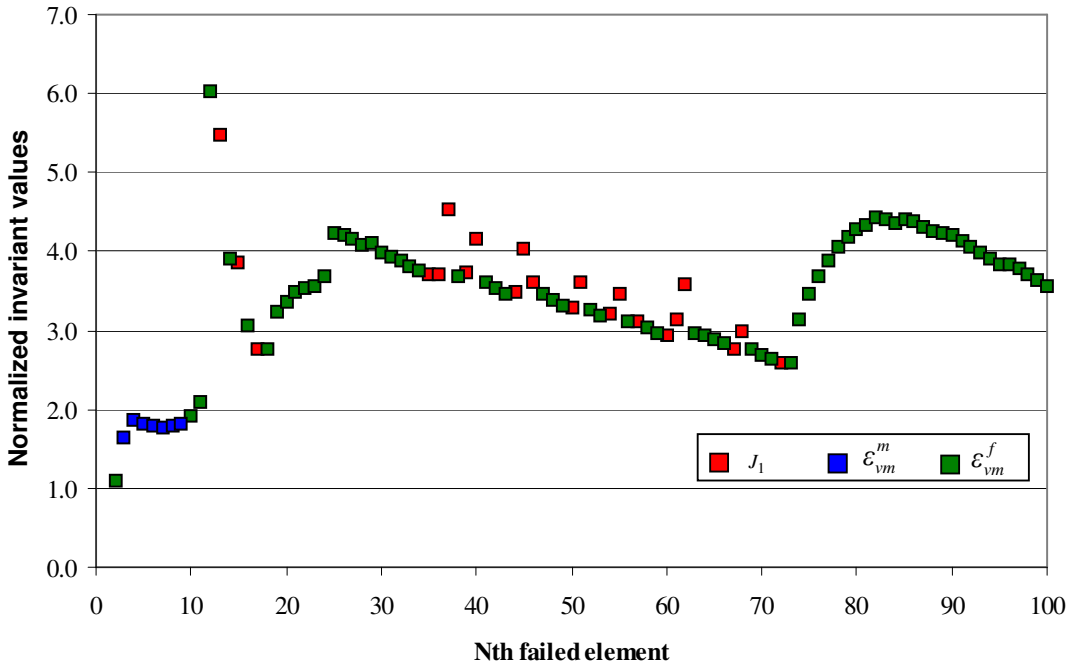

Figure 4-8: Normalized strain invariants and damage progression with J_{1Crit} = 0.0230, ε_{vmCrit}^f =0.0182 and ε_{vmCrit}^m =0.1030

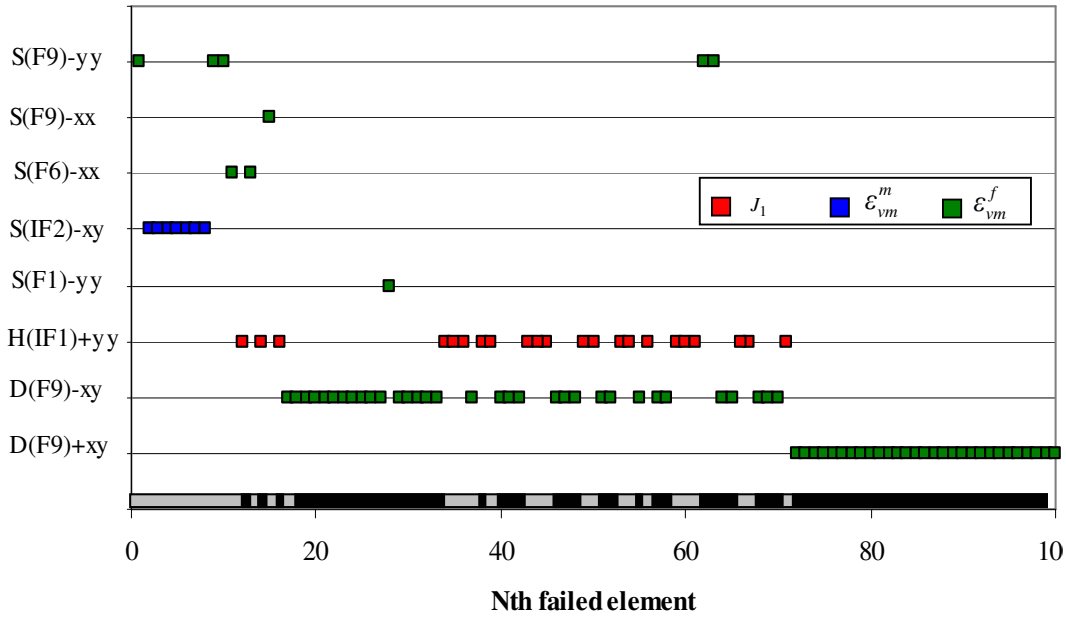

Figure 4-9: SIFT micromechanics-based details and damage progression with J_{1Crit} = 0.0230, ε_{vmCrit}^f =0.0182 and ε_{vmCrit}^m =0.1030.

4.2.1.4 SIFT Parametric Studies

The critical strain invariant values obtained from Gosse [*submitted for publication*] are based on experimental testing of unidirectional composite laminates IM7/977-3 with a fiber volume ratio of 60 %. We use the same critical values in our damage prediction in Figure 4-5 although our laminated composites for this three-point bend problem are not strictly the same composition and have a different fiber ratio (i.e. Fibredux T800H/924C with a fiber volume of 66 % in our case).

Since the critical strain invariants are the effective properties of composites, their values might be dependent on fiber volume ratio. We wish to see how sensitive our results are with variations in the critical SIFT values. A parametric study is thus performed and the cases investigated are summarized in Table 4-3. The results from case EFX_1 have already been presented in Figure 4-5 to Figure 4-9, and they represent a good correlation with experimental observation. With respect to the set of critical strain invariant values used in case EFX_1, each of the critical strain invariant values is then increased or decreased up to 25%, or until a significant change in the predicted damage pattern is found.

The damage progression patterns for case EFX_2 to case EFX_4 are given in Figure 4-10 to Figure 4-12. In case EFX_2, there are only significant changes in the damage progression when J_{1Crit} is increased by 19% (Figure 4-10) whereas a decrease of 10% has no effect on the damage prediction. Although the local crushing and the first delamination are predicted correctly when J_{1Crit} is increased, failure

progresses in a vertical direction across layers and the second delamination is not predicted. The damage pattern is therefore rather sensitive to an increase in J_{1Crit}.

For case EFX_3, slight change in damage pattern is observed when ε^{f}_{vmCrit} is decreased by 10%, but no further change is reported when ε^{f}_{vmCrit} is reduced by up to 25% (Figure 4-11). These changes are almost insignificant when compared to case EFX_1. On the other hand, an increase of 20% ε^{f}_{vmCrit} has no effect on damage prediction. Hence, damage prediction is very robust with respect to ε^{f}_{vmCrit}.

Finally for case EFX_4, there is no change in damage prediction when ε^{m}_{vmCrit} is increased by 20% whereas there is slight changes in damage pattern when ε^{m}_{vmCrit} is decreased by 22% (Figure 4-12). Local crushing and the first delamination are predicted, with a slight indication of second delamination. Beyond that, the predicted damage pattern departs considerably from experimental observation as failure in a vertical direction across layers is predicted. Hence, based on the above observations, it may be concluded that damage pattern prediction is reasonably robust within ± 18% of the critical strain invariant values, with the greatest sensitivity due to J_{1Crit}, followed by ε^{m}_{vmCrit} and ε^{f}_{vmCrit}. This is because the changes in the damage pattern are the most significant when J_{1Crit} is increased by 19%, while the least changes are reported when ε^{f}_{vmCrit} is decreased from 10% to 25%.

Table 4-3: Summary of the sensitivity of damage pattern predictions to critical strain invariant values. Changes to the original critical SIFT values are underlined in red.

Case	J_{1Crit}	ε^{f}_{vmCrit}	ε^{m}_{vmCrit}	**Remarks and final damage pattern**
EFX_1	0.0230	0.0182	0.1030	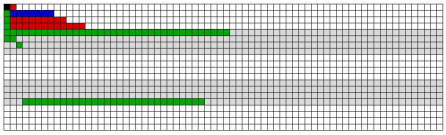 Results are in good agreement with experimental observations.
EFX_2	0.0274	0.0182	0.1030	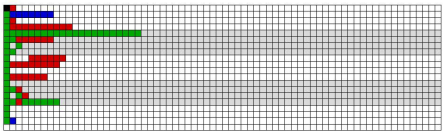 Changes in damage pattern when J_{1Crit} is increased by 19%. There is no change in prediction when J_{1Crit} is decreased by 10%.
EFX_3	0.0230	0.0164	0.1030	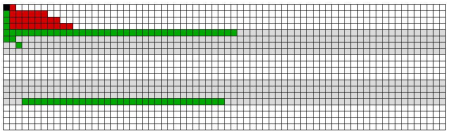 Minor changes in damage pattern when ε^{f}_{vmCrit} is decreased by 10%. There is no change in prediction when ε^{f}_{vmCrit} is increased by 20%.
EFX_4	0.0230	0.0182	0.0800	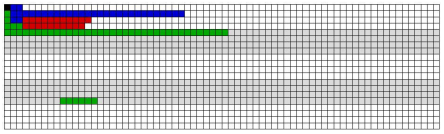 Changes in damage pattern when ε^{m}_{vmCrit} is decreased by 22%. There is no change in prediction when ε^{m}_{vmCrit} is increased by 20%.

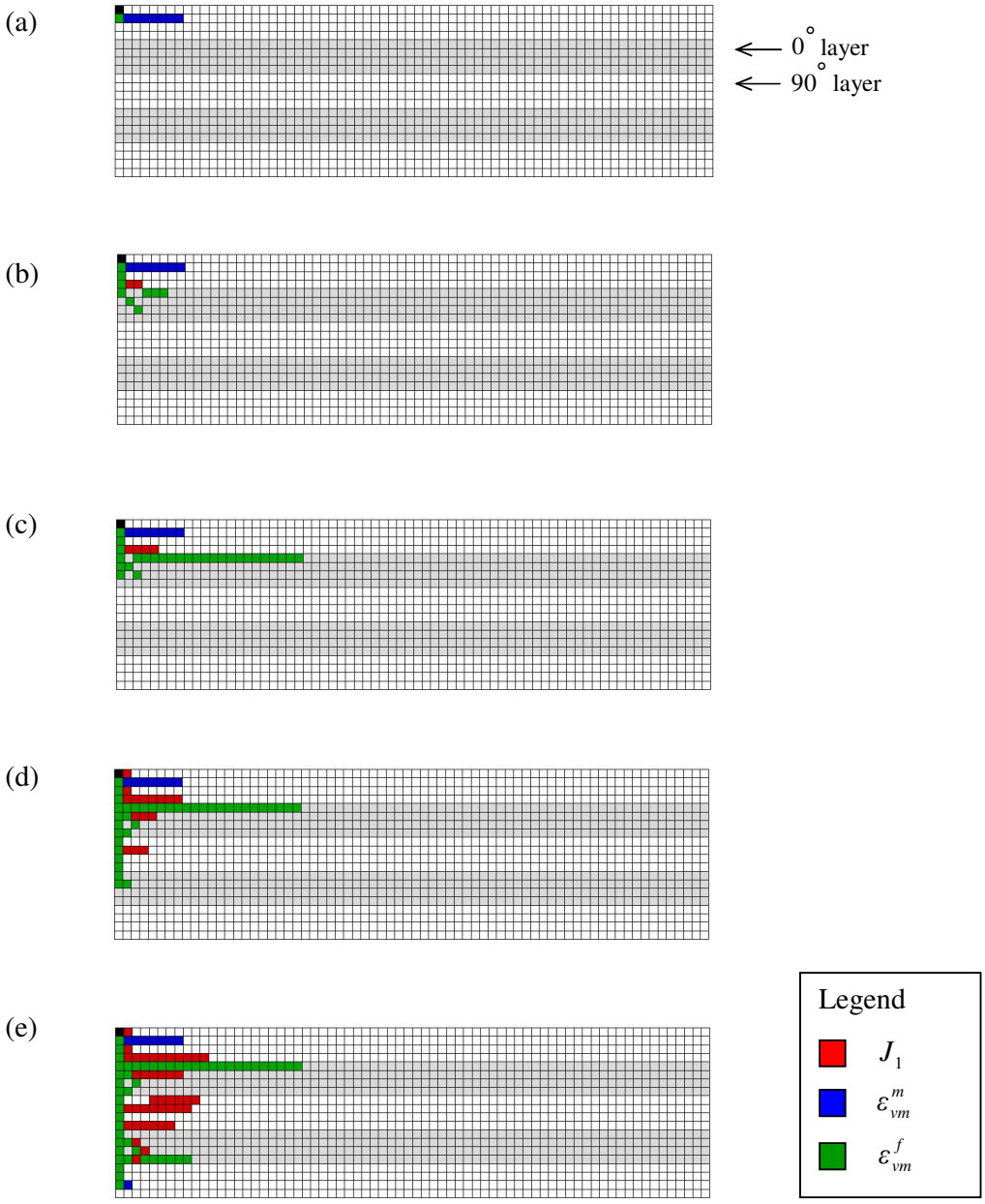

Figure 4-10(a) to (e): Case EFX_2 - Significant change in damage progression pattern when J_{1Crit} is increased by 19 % (J_{1Crit} = 0.0274, ε^f_{vmCrit} =0.0182 and ε^m_{vmCrit} =0.1030).

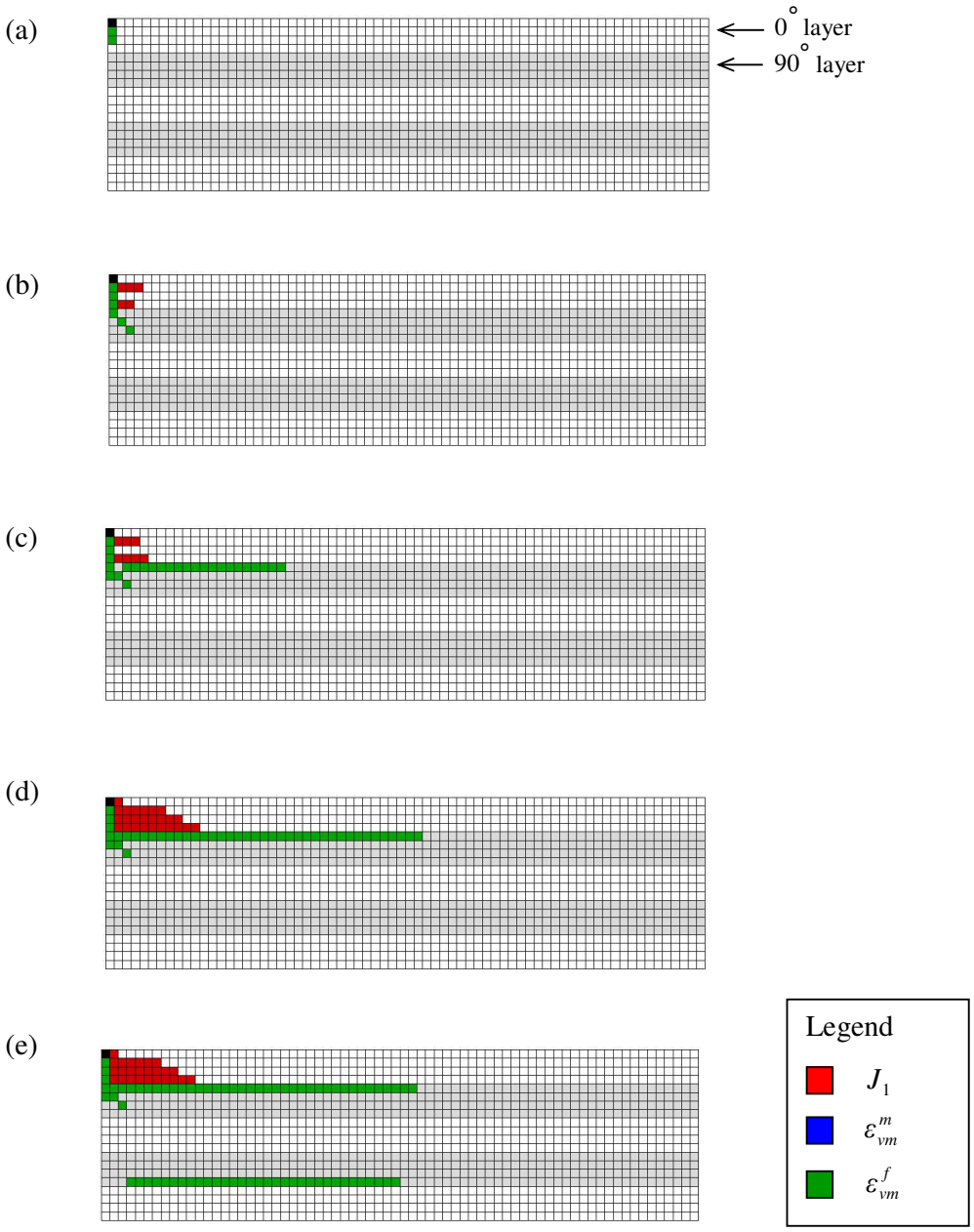

Figure 4-11(a) to (e): Case EFX_3 - Slight change in damage progression pattern when ε^f_{vmCrit} is decreased by 10 % (J_{1Crit} = 0.0230, ε^f_{vmCrit} =0.0164 and ε^m_{vmCrit} =0.1030).

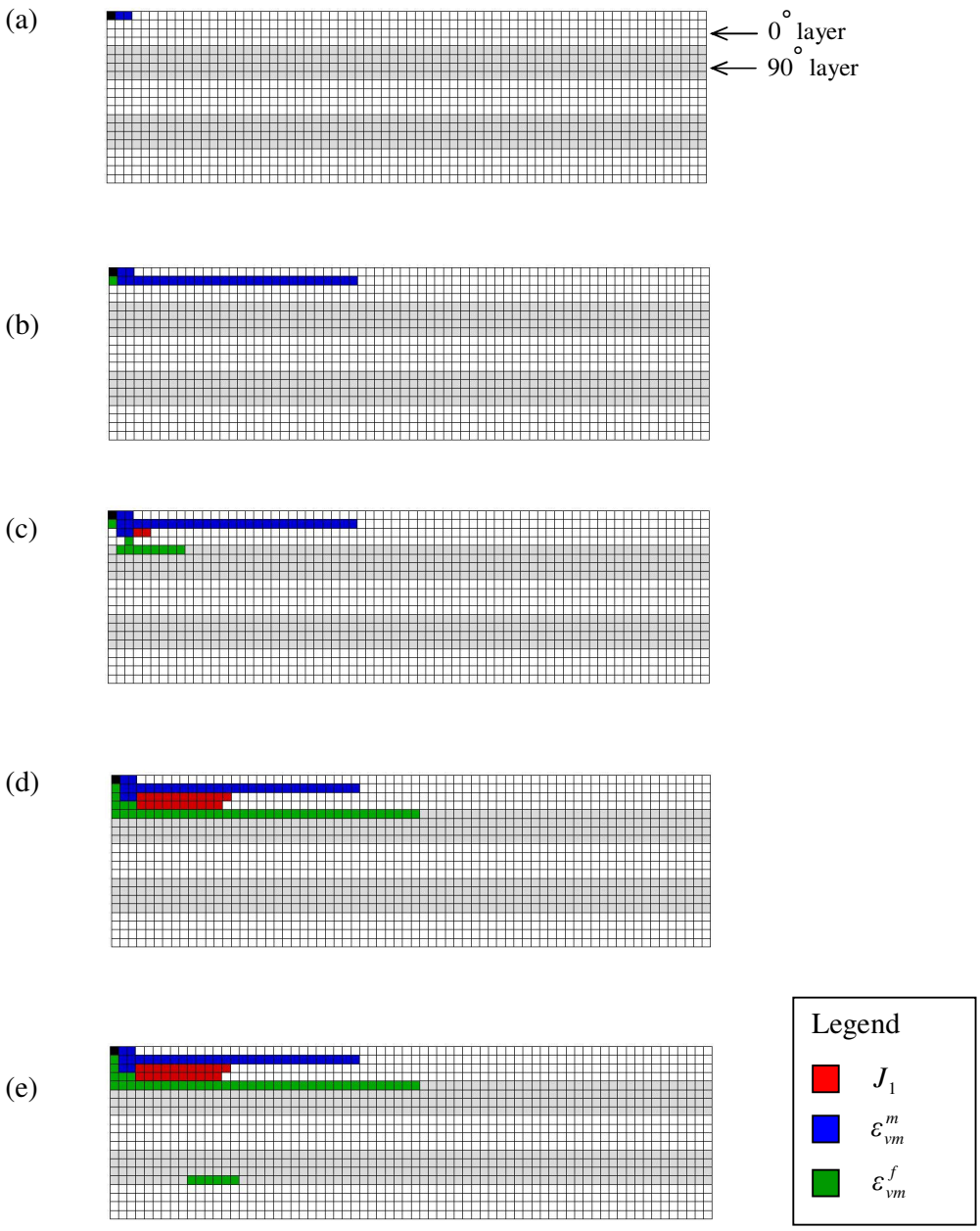

Figure 4-12(a) to (e): Case EFX_4 - Changes in damage progression pattern when ε_{vmCrit}^{m} is decreased by 22 % (J_{1Crit} = 0.0230, ε_{vmCrit}^{f} =0.0182 and ε_{vmCrit}^{m} =0.0800).

4.2.1.5 Conclusions

The damage pattern by EFM and SIFT correlates well with experiment despite the rather simple nodal force reduction scheme used. The interpretations of Figure 4-6 and Figure 4-9 also demonstrate the wealth of information that the use of SIFT can provide on the damage process in the micromechanical level. Although SIFT is a new failure theory, the information it provides on the damage modes for the three-point bend problem studied here does agree with experimental data reasonably well. In addition, the damage patterns in Figure 4-10 to Figure 4-12 from the parametric studies reveal that the damage prediction by SIFT is reasonably robust (± 18% of the critical strain invariant values, with the greatest sensitivity due to J_{1Crit}, followed by ε^{m}_{vmCrit} and ε^{f}_{vmCrit}). This is because the changes in the damage pattern are the most significant when J_{1Crit} is increased by 19%, while the least changes are reported when ε^{f}_{vmCrit} is decreased from 10% to 25%.

4.2.2 Case MPD – Damage Pattern Predicted using MPDM and SIFT

The same critical strain invariant values for Case EFX are used here (i.e. J_{1Crit} = 0.0230, ε^{f}_{vmCrit} =0.0182 and ε^{m}_{vmCrit} =0.1030). Once damage is predicted by SIFT, selected material properties are degraded using various material property degradation schemes in Table 4-2. The subscript *x* of the material properties refer to the global *x*-direction (i.e. spanwise direction). For example, for the 0° ply, E_x, E_y and G_{xy} refer to E_1, E_2 and G_{12} respectively while for the 90° ply, E_x, E_y and G_{xy} refer to E_2, E_3 and G_{23} respectively.

We choose to modify only the x-related component of material properties because the primary load-bearing mechanism for this three-point bend problem is bending, where the bending stresses are mainly oriented in the horizontal or spanwise direction. It is noted that none of the material properties are reduced to zero in order to avoid ill-conditioning of the elemental stiffness matrix of the damaged element.

The damage progression patterns for cases MPD_1 to MPD_3 (Table 4-2) are shown in Figure 4-13 to Figure 4-15 and the results are summarized in Table 4-4. The results employing different degradation schemes in MPDM are different from each other and from the experimental results in Figure 4-2. It is observed that changing certain material properties can affect the results in dramatic ways. For example, comparing the damage patterns of case MPD_1 (Figure 4-13) and case MPD_2 (Figure 4-14), E_y and G_{xy} have negligible influence on damage prediction.

On the other hand, the damage pattern is sensitive to changes in E_x as the damage pattern of case MPD_3 (Figure 4-15) differs drastically from that of MPD_1 (Figure 4-13) and MPD_2 (Figure 4-14). In fact, only case MPD_3 seems to be in a slightly better agreement with experimental observations as the initial damage in the top ($0°$) layer is predicted. This suggests that for the three-point bend problem studied here, E_x does play a major role in the damage progression pattern since E_x needs to be reduced to 1% of its original value (i.e. Figure 4-15) in order to avoid the "triangular-shaped" patterns in Figures 4-13 and 4-14.

However, if we compare the damage patterns obtained with the MPDM (Figures 4-13 to 4-15) to that obtained with the EFM (Figure 4-5), it is observed that there is better qualitative agreement with the experimental damage pattern when the EFM is used. This suggests that for the three-point bend problem studied, the load-bearing capability of the composite beam is most probably compromised in the x-direction only and thus, the degradation scheme of case MPD_3 might be too "strict" as G_{xz} and G_{xy} were modified. This also brings up some questions regarding the degradation schemes of MPDM – What are the "right" material properties to degrade? Is it possible to use the MPDM to yield the same damage pattern prediction obtained with the EFM? We will address these issues in greater details in Chapter 5.

Table 4-4: Summary of final damage patterns predicted by various degradation schemes of MPDM.

Case	**Degradation schemes of MPDM**	**Final damage pattern**
MPD_1	Only E_x is set to 30% of its original value.	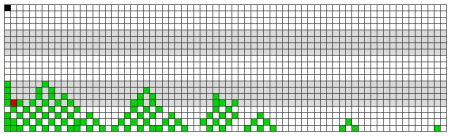
MPD_2	E_x, G_{xy} and G_{xz} set to 30% of their original values	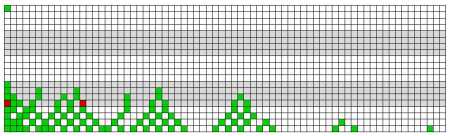
MPD_3	E_x, G_{xy} and G_{xz} are set to 1% of their original values; v_{xy} and v_{xz} reduced to 0.05.	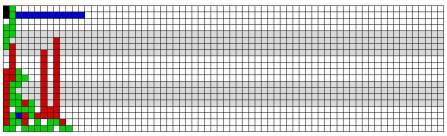

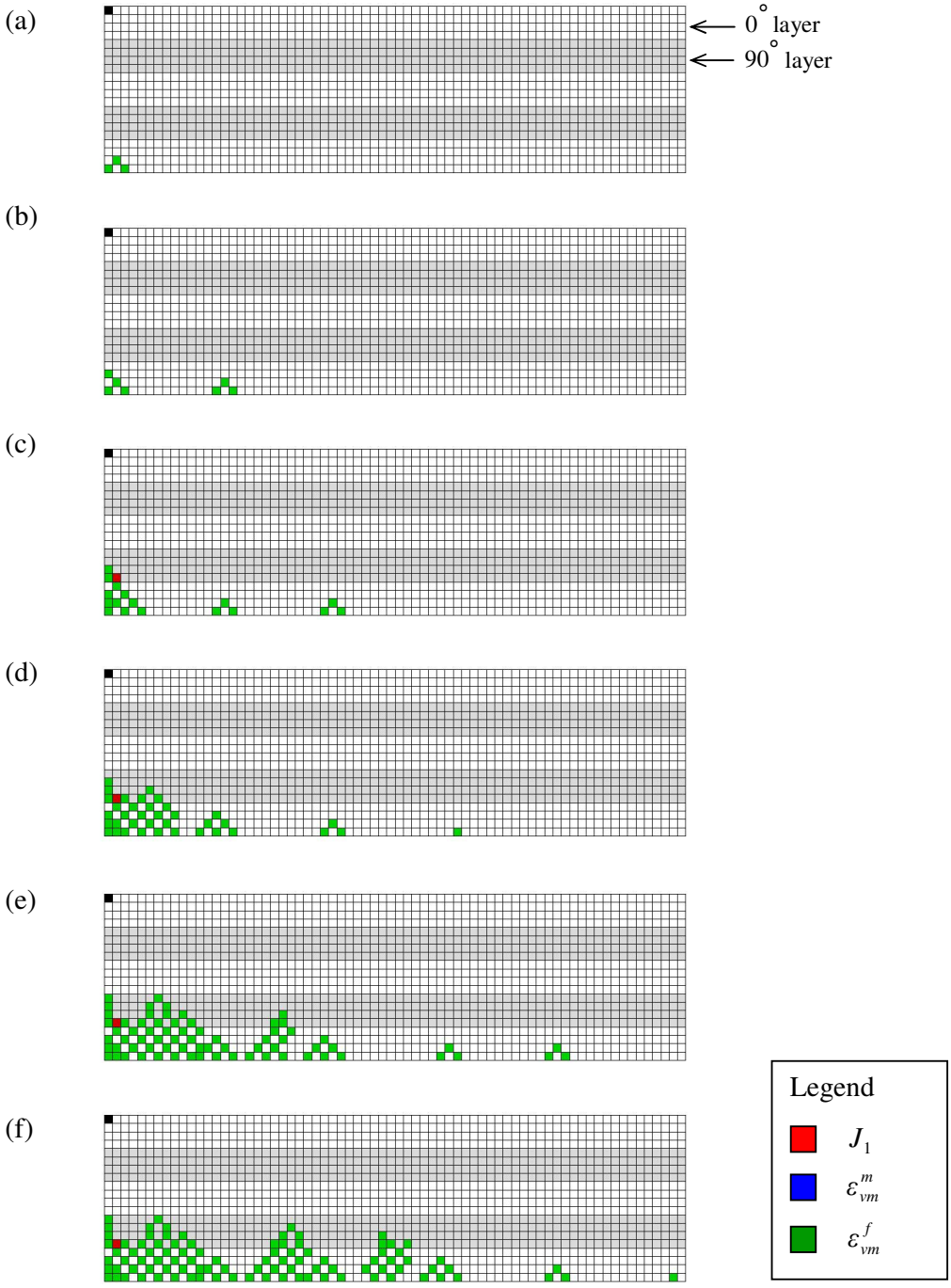

Figure 4-13: Case MPD_1 - MPDM predicted damage progression with only E_x set to 30% of its original value.

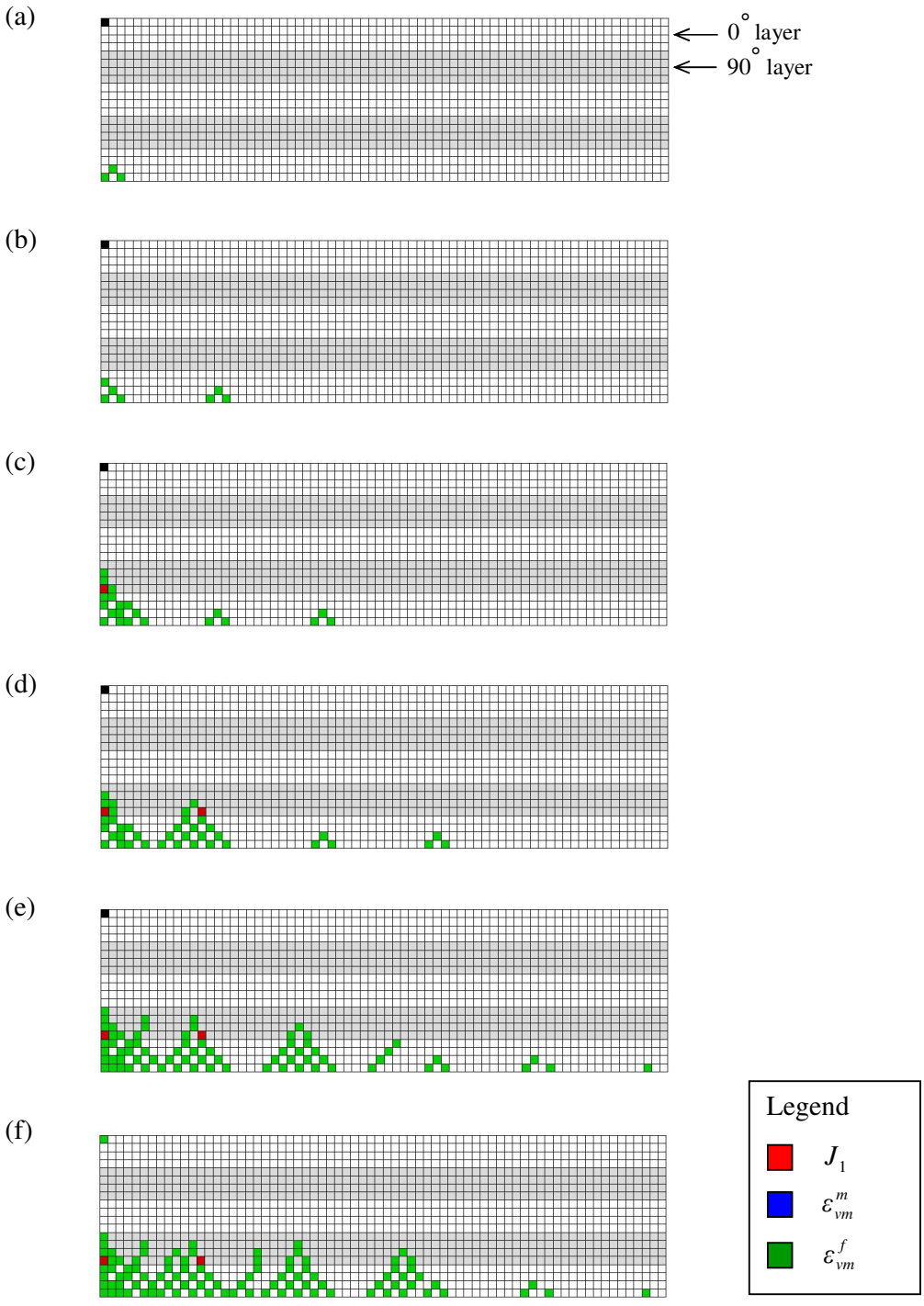

Figure 4-14: Case MPD_2 - MPDM predicted damage progression with E_x, G_{xy} and G_{xz} set to 30% of their original values.

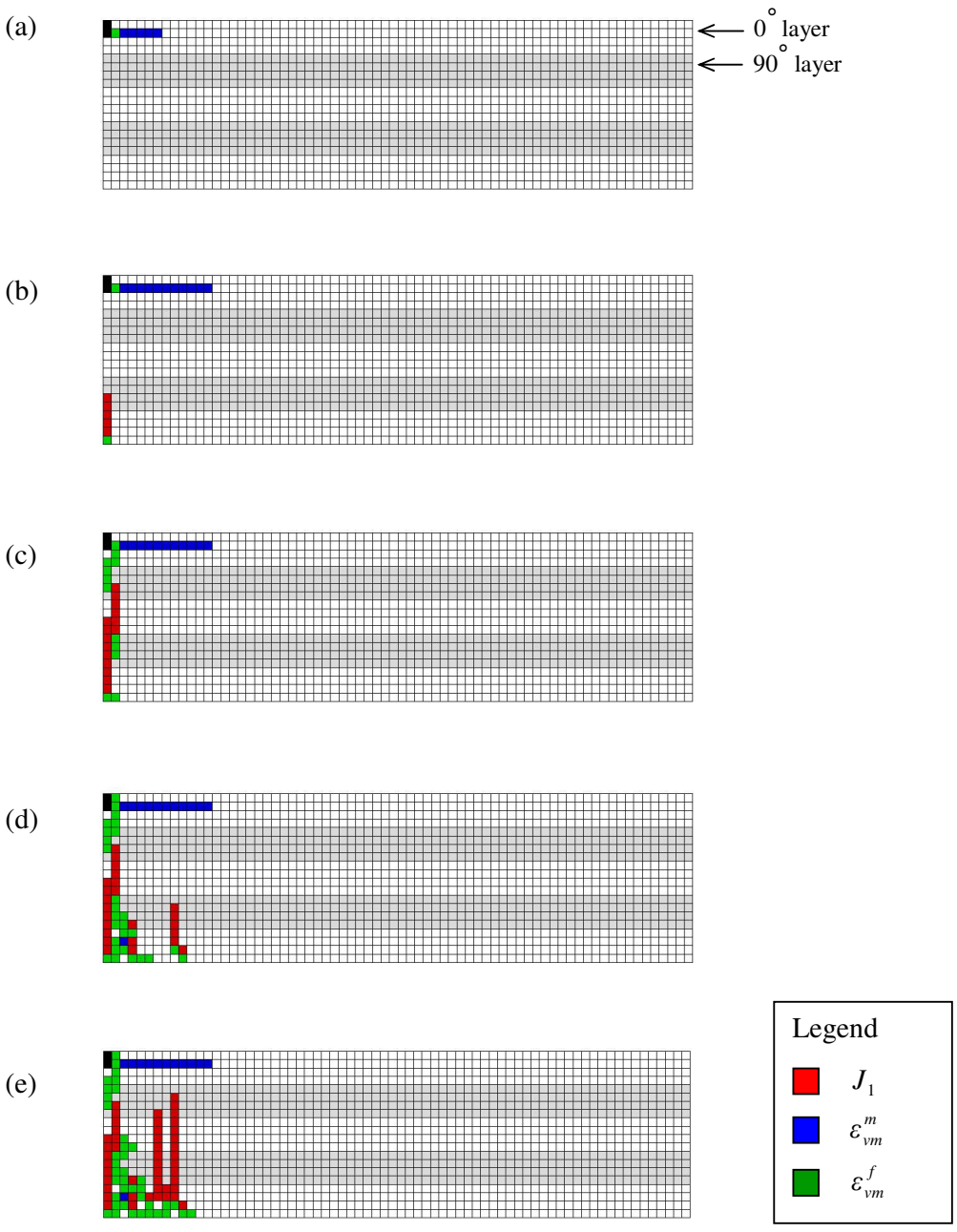

Figure 4-15: Case MPD_3 - MPDM predicted damage progression with E_x, G_{xy} and G_{xz} set to 1% of their original values and v_{xy} and v_{xz} reduced to 0.05.

4.2.3 Case EFX_TW – Damage Pattern Predicted using the EFM with Tsai-Wu Failure Theory

Due to the modular structure of our FE code, the EFM can be used with any other suitable failure theories besides SIFT. In this study, we use the EFM with Tsai-Wu failure theory instead to predict damage progression. The intention is to compare the results using the recently developed SIFT with the well-established Tsai-Wu failure theory.

A 2-D plane stress Tsai-Wu failure theory is used to predict damage. The strengths of composite lamina are taken as X_T=1500 MPa, X_C = -1500 MPa, Y_T=40 MPa, Y_C=-246 MPa and S = 68 MPa. These values are obtained from Chamis [*Chamis, 1987*] based on experimental analysis of coupon tests of unidirectional composite laminae T300/5208 with a fiber volume fraction V_f = 60%. We use the same strength values here although our composite coupons used in this three-point bend problem are not strictly the same composition and have a different fiber ratio (our test coupons are manufactured using Fibredux T800H/924C composite prepreg with a fiber volume fraction of 66%). The same nodal force modification scheme for case EFX (Table 4-2) is used here; the nodal forces in the global x-direction (i.e. spanwise direction) are zeroed once damage is predicted within the element.

The resulting damage progression pattern is shown in Figure 4-16. The damaged elements are shaded grey. It is observed that the damage pattern by EFM and Tsai-Wu failure theory does not correlate well with the experimental pattern in Figure 4-2

as only the initial local crushing of the top 0° layer (Figure 4-16a) is predicted. The Tsai-Wu failure theory, together with the EFM, appears to be unsuitable for this three-point bend problem studied.

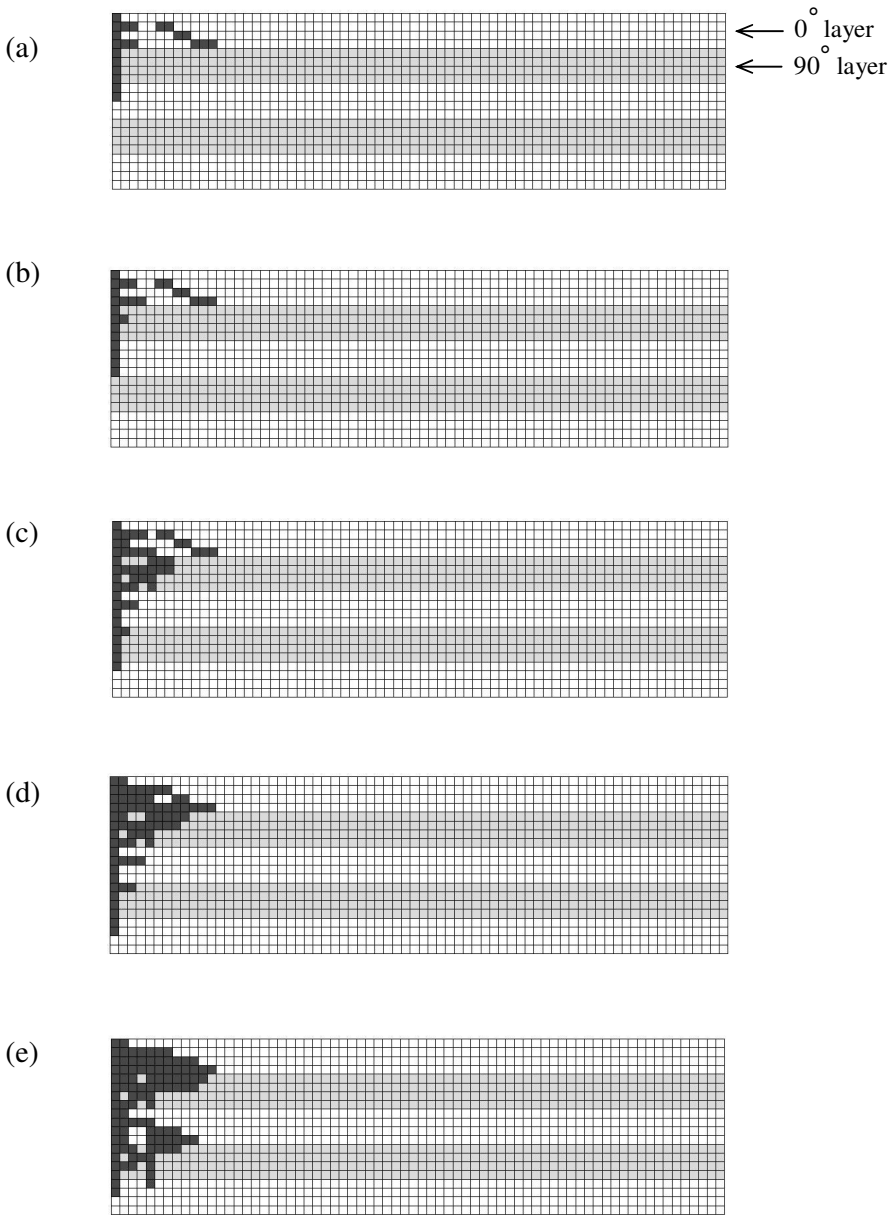

Figure 4-16(a) to (e): Case EFX_TW - Predicted damage progression using EFM and Tsai-Wu failure theory.

4.3 Conclusions

The progressive analysis of $[0_3/90_3/0_3/90_3/0_3]$ laminated composite under a three-point bend load is studied. Experiments are first performed to obtain the damage pattern. Damage progression patterns are later generated using in-house 2D implicit FE code, using different combinations of damage-modeling methods and failure theories. A summary of these damage patterns is given in Table 4-5.

It is observed from Table 4-5 that there is better qualitative agreement with experimental observations when the EFM is used with SIFT (i.e. case EFX). The different degradation schemes in MPDM (i.e. MPD_1, MPD_2 and MPD_3) predict different results from each other and from the experimental results. It also appears that the Tsai-Wu failure theory is unsuitable for this three-point bend problem as the result (i.e. case EFX_TW) does not correlate well with experimental observations.

In summary, for the three-point bend problem studied here, it appears that the use of the EFM with the micromechanics-based SIFT is the most suitable combination for mapping damage initiation and propagation.

Table 4-5: A comparison of experimental damage pattern and the damage patterns predicted using different combinations of damage-modeling methods and failure theories.

Experimental damage pattern

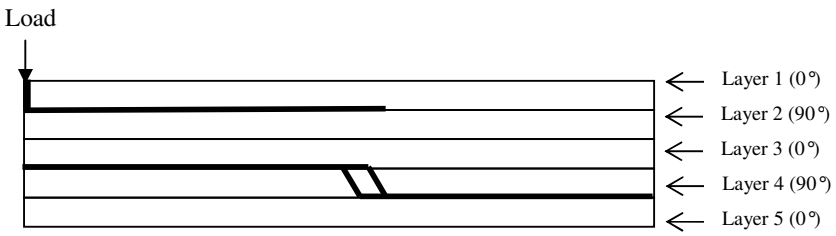

Case	Damage-modeling method	Failure theory	Final damage pattern predictions
EFX*+	Element-failure with *x*-direction nodal forces zeroed	SIFT	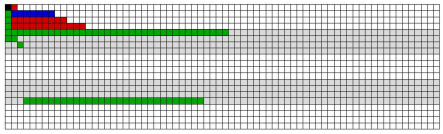
MPD_1*	Material property degradation with E_x reduced to 30% of its original value.	SIFT	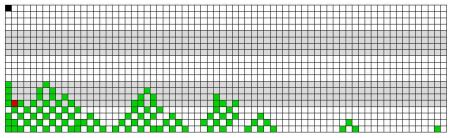
MPD_2*	Material property degradation with E_x, G_{xy} and G_{xz} reduced to 30% of their original values.	SIFT	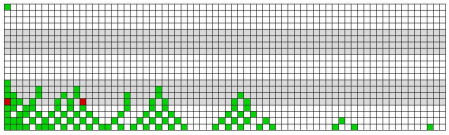
MPD_3*	Material property degradation with E_x, G_{xy} and G_{xz} reduced to 1% of their original values while v_{xy} and v_{xz} are reduced to 0.05.	SIFT	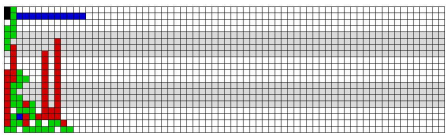
EFX_TW+	EFM where *x*-component of nodal force is reduced to zero	Tsai-Wu	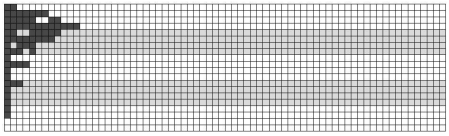

* Cases used to compare damage-modeling methods
\+ Cases used to compare failure theories

5. A Comparative Study of the EFM and the MPDM

In this chapter, we compare the finite element (FE) formulation of the element-failure method (EFM) with the material property degradation method (MPDM). The finite element formulations of the two methods are first re-examined to study the relationship between nodal forces and material stiffness properties. We will demonstrate the limitations of MPDM and show that the EFM is a more general and versatile method than MPDM.

5.1. Relationship between Nodal Forces and Material Stiffness Properties

The force-stiffness relation for a finite element is given by [*Smith and Griffiths, 2004*]:

$$\mathbf{K}\ \mathbf{u} = \mathbf{f} \tag{5-1}$$

where

$$\mathbf{K} = \int_{\Omega} \mathbf{B}^T \mathbf{C} \mathbf{B}\ \partial\Omega \tag{5-2}$$

is the elemental stiffness matrix of undamaged material, integrated over the domain Ω, **B** is the strain operator, **C** is the material stiffness matrix, **u** is the vector of nodal displacements, and **f** is the vector of nodal forces.

For a two-dimensional (2-D) plane stress or plane strain problem, the material stiffness matrix **C** is:

$$\mathbf{C} = \begin{bmatrix} C_{11} & C_{12} & 0 \\ C_{12} & C_{22} & 0 \\ 0 & 0 & C_{66} \end{bmatrix} \tag{5-3}$$

where the material stiffness coefficients C_{ij} are related to engineering constants E_1, E_2, v_{12} and G_{12}. The general three-dimensional (3-D) relationship between C_{ij} and the engineering constants is given in Appendix B. In the case of a unidirectional composite material, subscript 1 of engineering constants refers to the axial fiber direction while subscripts 2 and 3 are the two transverse to fiber directions.

The matrix **B** is defined as:

$$\mathbf{B} = \begin{bmatrix} N_{1,x} & 0 & N_{2,x} & 0 & \cdots & N_{m,x} & 0 \\ 0 & N_{1,y} & 0 & N_{2,y} & \cdots & 0 & N_{m,y} \\ N_{1,y} & N_{1,x} & N_{2,y} & N_{2,x} & \cdots & N_{m,y} & N_{m,x} \end{bmatrix} \tag{5-4}$$

where m is the number of nodes for the element, and $N_{i,x} = \frac{\partial Ni}{\partial x}$ and $N_{i,y} = \frac{\partial Ni}{\partial y}$ are the derivatives of the shape functions N_i with respect to the global x and y coordinates, respectively.

Substituting the expressions of **C** and **B** from equations (5-3) and (5-4) respectively into equation (5-1), the matrix form of force-stiffness relation in equation (5-1) becomes

$$\mathbf{K}\ \mathbf{u} = \mathbf{f}$$

$$\begin{bmatrix} \mathbf{K}_{11} & \mathbf{K}_{12} & \cdots & \cdots & \mathbf{K}_{1m} \\ & \ddots & & & \vdots \\ & & \mathbf{K}_{ij} & \cdots & \mathbf{K}_{im} \\ & & & \ddots & \vdots \\ \text{sym.} & & & & \mathbf{K}_{mm} \end{bmatrix} \begin{Bmatrix} \mathbf{u}_1 \\ \vdots \\ \mathbf{u}_i \\ \vdots \\ \mathbf{u}_m \end{Bmatrix} = \begin{Bmatrix} \mathbf{f}_1 \\ \vdots \\ \mathbf{f}_i \\ \vdots \\ \mathbf{f}_m \end{Bmatrix} \tag{5-5}$$

where $\mathbf{K}_{ij}$ is a (2×2) matrix of the form

$$\mathbf{K}_{ij} = \begin{bmatrix} C_{11}\int_{\Omega} N_{i,x}N_{j,x}\,\partial\Omega + C_{66}\int_{\Omega} N_{i,y}N_{j,y}\,\partial\Omega & C_{12}\int_{\Omega} N_{i,x}N_{j,y}\,\partial\Omega + C_{66}\int_{\Omega} N_{i,y}N_{j,x}\,\partial\Omega \\ C_{12}\int_{\Omega} N_{i,y}N_{j,x}\,\partial\Omega + C_{66}\int_{\Omega} N_{i,x}N_{j,y}\,\partial\Omega & C_{22}\int_{\Omega} N_{i,y}N_{j,y}\,\partial\Omega + C_{66}\int_{\Omega} N_{i,x}N_{j,x}\,\partial\Omega \end{bmatrix},$$

$$\{\mathbf{f}_i\} = \begin{bmatrix} f_{xi} & f_{yi} \end{bmatrix}^T,$$

and

$$\{\mathbf{u}_i\}=\begin{bmatrix} u_{xi} & u_{yi} \end{bmatrix}^T, \text{ for } i,j=1,2,\ldots,m. \tag{5-6}$$

Expanding equation (5-5), the x-component of nodal force at node 1 is

$$\begin{aligned} f_{x1} = & \left(C_{11}\int_{\Omega} N_{1,x}N_{1,x}\,\partial\Omega + C_{66}\int_{\Omega} N_{1,y}N_{1,y}\,\partial\Omega \right) u_{x1} \\ & + \left(C_{12}\int_{\Omega} N_{1,x}N_{1,y}\,\partial\Omega + C_{66}\int_{\Omega} N_{1,y}N_{1,x}\,\partial\Omega \right) u_{y1} \\ & + \left(C_{11}\int_{\Omega} N_{1,x}N_{2,x}\,\partial\Omega + C_{66}\int_{\Omega} N_{1,y}N_{2,y}\,\partial\Omega \right) u_{x2} \\ & + \left(C_{12}\int_{\Omega} N_{1,x}N_{2,y}\,\partial\Omega + C_{66}\int_{\Omega} N_{1,y}N_{2,x}\,\partial\Omega \right) u_{y2} \\ & + \cdots \\ & + \left(C_{11}\int_{\Omega} N_{1,x}N_{m,x}\,\partial\Omega + C_{66}\int_{\Omega} N_{1,y}N_{m,y}\,\partial\Omega \right) u_{xm} \\ & + \left(C_{12}\int_{\Omega} N_{1,x}N_{m,y}\,\partial\Omega + C_{66}\int_{\Omega} N_{1,y}N_{m,x}\,\partial\Omega \right) u_{ym} \end{aligned} \tag{5-7}$$

Grouping the terms according to C_{ij}, equation (5-7) can be rearranged as:

$$\begin{aligned} f_{x1} = & \; C_{11}\int_{\Omega} N_{1,x}\left(\sum_{j}^{m} N_{j,x}u_{xj} \right)\partial\Omega \\ & + C_{12}\int_{\Omega} N_{1,x}\left(\sum_{j}^{m} N_{j,y}u_{yj} \right)\partial\Omega \\ & + C_{66}\int_{\Omega} N_{1,y}\left(\sum_{j}^{m} N_{j,y}u_{xj} + \sum_{j}^{m} N_{j,x}u_{yj} \right)\partial\Omega \end{aligned} \tag{5-8}$$

where $j = 1,2,\ldots,m$.

Similarly, the x-component of nodal force at node 2 is given as:

$$\begin{aligned} f_{x2} = & \; C_{11}\int_{\Omega} N_{2,x}\left(\sum_{j}^{m} N_{j,x}u_{xj}\right)\partial\Omega \\ & + C_{12}\int_{\Omega} N_{2,x}\left(\sum_{j}^{m} N_{j,y}u_{yj}\right)\partial\Omega \\ & + C_{66}\int_{\Omega} N_{2,y}\left(\sum_{j}^{m} N_{j,y}u_{xj} + \sum_{j}^{m} N_{j,x}u_{yj}\right)\partial\Omega \end{aligned} \tag{5-9}$$

where $j = 1,2,\ldots,m$.

Hence, the general expression for f_x at the *ith* node is

$$\begin{aligned} f_{xi} = & \; C_{11}\int_{\Omega} N_{i,x}\left(\sum_{j}^{m} N_{j,x}u_{xj}\right)\partial\Omega \\ & + C_{12}\int_{\Omega} N_{i,x}\left(\sum_{j}^{m} N_{j,y}u_{yj}\right)\partial\Omega \\ & + C_{66}\int_{\Omega} N_{i,y}\left(\sum_{j}^{m} N_{j,y}u_{xj} + \sum_{j}^{m} N_{j,x}u_{yj}\right)\partial\Omega \end{aligned} \tag{5-10}$$

where $i, j = 1,2,\ldots,m$.

Likewise, by expanding equation (5-5), the y-component of nodal force at node 1 is

$$\begin{aligned} f_{y1} = & \left(C_{12}\int_{\Omega} N_{1,y}N_{1,x}\,\partial\Omega + C_{66}\int_{\Omega} N_{1,x}N_{1,y}\,\partial\Omega \right) u_{x1} \\ & + \left(C_{22}\int_{\Omega} N_{1,y}N_{1,y}\,\partial\Omega + C_{66}\int_{\Omega} N_{1,x}N_{1,x}\,\partial\Omega \right) u_{y1} \\ & + \left(C_{12}\int_{\Omega} N_{1,y}N_{2,x}\,\partial\Omega + C_{66}\int_{\Omega} N_{1,x}N_{2,y}\,\partial\Omega \right) u_{x2} \\ & + \left(C_{22}\int_{\Omega} N_{1,y}N_{2,y}\,\partial\Omega + C_{66}\int_{\Omega} N_{1,x}N_{2,x}\,\partial\Omega \right) u_{y2} \\ & + \cdots \\ & + \left(C_{12}\int_{\Omega} N_{1,y}N_{m,x}\,\partial\Omega + C_{66}\int_{\Omega} N_{1,x}N_{m,y}\,\partial\Omega \right) u_{xm} \\ & + \left(C_{22}\int_{\Omega} N_{1,y}N_{m,y}\,\partial\Omega + C_{66}\int_{\Omega} N_{1,x}N_{m,x}\,\partial\Omega \right) u_{ym} \end{aligned} \tag{5-11}$$

Grouping the terms according to C_{ij}, equation (5-11) can be rearranged as:

$$\begin{aligned} f_{y1} = & \; C_{12}\int_{\Omega} N_{1,y}\left(\sum_{j}^{m} N_{j,x}u_{xj} \right)\partial\Omega \\ & + C_{22}\int_{\Omega} N_{1,y}\left(\sum_{j}^{m} N_{j,y}u_{yj} \right)\partial\Omega \\ & + C_{66}\int_{\Omega} N_{1,x}\left(\sum_{j}^{m} N_{j,y}u_{xj} + \sum_{j}^{m} N_{j,x}u_{yj} \right)\partial\Omega \end{aligned} \tag{5-12}$$

where $j = 1,2,\ldots,m$

Similarly, the y-component of nodal force at node 2 is given as:

$$\begin{aligned} f_{y2} = & \; C_{12} \int_{\Omega} N_{2,y} \left(\sum_{j}^{m} N_{j,x} u_{xj} \right) \partial\Omega \\ & + C_{22} \int_{\Omega} N_{2,y} \left(\sum_{j}^{m} N_{j,y} u_{yj} \right) \partial\Omega \\ & + C_{66} \int_{\Omega} N_{2,x} \left(\sum_{j}^{m} N_{j,y} u_{xj} + \sum_{j}^{m} N_{j,x} u_{yj} \right) \partial\Omega \end{aligned} \tag{5-13}$$

where $j = 1,2,\ldots,m$.

Hence, the general expression for f_y at the *ith* node is

$$\begin{aligned} f_{yi} = & \; C_{12} \int_{\Omega} N_{i,y} \left(\sum_{j}^{m} N_{j,x} u_{xj} \right) \partial\Omega \\ & + C_{22} \int_{\Omega} N_{i,y} \left(\sum_{j}^{m} N_{j,y} u_{yj} \right) \partial\Omega \\ & + C_{66} \int_{\Omega} N_{i,x} \left(\sum_{j}^{m} N_{j,y} u_{xj} + \sum_{j}^{m} N_{j,x} u_{yj} \right) \partial\Omega \end{aligned} \tag{5-14}$$

where $i, j = 1,2,\ldots,m$.

Although the nodal force expressions in equations (5-10) and (5-14) are valid for 2-D only, the extension to 3-D is similar and straightforward. Analogous to equations

(5-10) and (5-14), the force-stiffness relation in equation (5-1) can also be expressed in terms of stiffness coefficients C_{ij} as:

$$\mathbf{K}\,\mathbf{u} = \mathbf{f}$$

$$= \mathbf{f}^{C_{11}} + \mathbf{f}^{C_{12}} + \mathbf{f}^{C_{22}} + \mathbf{f}^{C_{66}} \tag{5-15a}$$

Or

$$\mathbf{f} = \mathbf{K}\,\mathbf{u}$$

$$= \mathbf{K}^{C_{11}}\mathbf{u} + \mathbf{K}^{C_{12}}\mathbf{u} + \mathbf{K}^{C_{22}}\mathbf{u} + \mathbf{K}^{C_{66}}\mathbf{u} \tag{5-15b}$$

Comment:

Equations (5-10), (5-14) and (5-15) show the relationship between nodal forces and the material stiffness properties. In the MPDM, the reduction of load-bearing capability of a damaged element is simulated by reducing selected engineering constants or stiffness coefficients C_{ij}. It is evident from the equations (5-10) and (5-14) that in the MPDM, a change in C_{ij} will result in a corresponding change in the nodal forces. On the other hand, in the EFM, a partial loss of load-bearing capability in a failed element is described through the direct manipulation of elemental nodal forces only. This is the main difference between the EFM and MPDM.

5.2. Differences between the EFM and MPDM

The nodal force expressions in equations (5-10) and (5-14) show that a reduction in load-bearing capability (when either C_{ij} or engineering constants are modified) will result in a reduction in the nodal forces f_x and f_y. A closer examination of these expressions reveals the following:

1. It is possible to prescribe a zero f_x without affecting f_y and vice versa with EFM, but not an equivalent with MPDM.

Equation (5-10) shows f_x to be a function of three stiffness coefficients C_{11}, C_{12} and C_{66}. This implies that in MPDM, all the values of C_{11}, C_{12} and C_{66} must be reduced to zero in order to represent a zero f_x state. Similarly, equation (5-14) shows f_y to be a function of C_{12}, C_{22} and C_{66}. This again implies that in MPDM, all the values of C_{12}, C_{22} and C_{66} must be reduced to zero in order to represent a zero f_y state. However, as the expressions of f_x and f_y are both functions of C_{12} and C_{66}, a change to either C_{12} or C_{66} will modify both f_x and f_y. In this case, it is not possible to describe a zero f_x state in MPDM without affecting f_y and vice versa.

In addition, we will show in the following subsection that C_{ij} cannot be reduced to zero in MPDM as this will result in a singular elemental stiffness matrix **K**. This

implies that in MPDM, f_x and/or f_y can never be reduced to zero. Unlike the MPDM, the use of EFM is not governed by C_{ij}. Hence, in EFM, it is possible to prescribe a zero f_x without affecting f_y and vice versa. This advantage of the EFM has been illustrated in Chapter 4 where it is applied to model progressive damage in a laminated composite beam subjected to a three-point bend load.

2. In MPDM, the stiffness coefficients C_{ij} or engineering constants must be reduced to finite values so that matrix **K** stays non-singular.

In the MPDM, a reduction in the load-bearing capability of a damaged element is described by degrading either the element's stiffness coefficients C_{ij} or some of its engineering constants E_1, E_2, E_3, v_{12}, v_{13}, v_{23}, G_{12}, G_{13} and G_{23}. Since the elemental stiffness matrix **K** in equation (5-6) is a function of the stiffness coefficients C_{ij}, we have to ensure that the degraded elemental stiffness matrix $\mathbf{K}^d$ stays non-singular i.e. its determinant remains positive, in order to ensure a solution. Referring to equation (5-2), this in turn requires the degraded material stiffness matrix $\mathbf{C}^d$ to be non-singular.

From equation (5-3), the degraded stiffness matrix $\mathbf{C}^d$ now takes the form:

$$\boldsymbol{C}^d = \begin{bmatrix} C_{11}^d & C_{12}^d & 0 \\ C_{12}^d & C_{22}^d & 0 \\ 0 & 0 & C_{66}^d \end{bmatrix} \tag{5-16}$$

where C_{11}^d, C_{12}^d, C_{22}^d and C_{66}^d are the degraded material stiffness coefficients.

The values of the degraded material stiffness coefficients C_{11}^d, C_{12}^d, C_{22}^d and C_{66}^d must be finite and are bounded by the following equations [*ABAQUS/Standard User's Manual version 6.3*]:

$$C_{11}^d, C_{22}^d, C_{66}^d > 0$$

and

$$\left|C_{12}^d\right| < \sqrt{C_{11}^d C_{22}^d} \tag{5-17}$$

Likewise, since the material stiffness coefficients are functions of engineering constants, the degraded engineering constants E_1^d, E_2^d, E_3^d, ν_{12}^d, ν_{13}^d, ν_{23}^d and G_{12}^d must be finite values which are bounded by the following equations [*ABAQUS/Standard User's Manual version 6.3*]:

$$E_1^d, E_2^d, E_3^d, G_{12}^d, G_{13}^d, G_{23}^d > 0,$$

$$\left|\nu_{12}^d\right| < \sqrt{\frac{E_1^d}{E_2^d}},$$

$$\left|\nu_{13}^{d}\right| < \sqrt{\frac{E_1^d}{E_3^d}} \ ,$$

$$\left|\nu_{23}^{d}\right| < \sqrt{\frac{E_2^d}{E_3^d}} \ ,$$

and

$$1-\nu_{12}^{d}\nu_{21}^{d}-\nu_{13}^{d}\nu_{31}^{d}-\nu_{23}^{d}\nu_{32}^{d}-2\nu_{21}^{d}\nu_{32}^{d}\nu_{13}^{d}>0$$

where

$$\frac{\nu_{kl}}{E_k}=\frac{\nu_{lk}}{E_l} \text{ for } l,k=1,2,3 . \tag{5-18}$$

Equations (5-17) and (5-18) show that the degraded stiffness coefficients C_{ij}^{d} and the degraded engineering constants must be reduced to finite values in order for the degraded elemental stiffness matrix $\mathbf{K}^{d}$ in the MPDM to be non-singular. If these equations are violated, finite element analysis cannot be performed. In addition, these equations implied that in the MPDM, it is not possible to reduce f_x and/or f_y from equations (5-10) and (5-14) to zero as this will require C_{11}^{d}, C_{22}^{d} and C_{66}^{d} to be reduced to zero.

As for the EFM, neither the engineering constants nor the stiffness coefficients C_{ij} are modified. Hence, in the EFM, it is possible to prescribe a zero f_x without affecting f_y and vice versa. In addition, we will show in the next section that the EFM is a more general technique than the MPDM as it is possible to formulate EFM to produce the same results with the MPDM.

3. The convergence of a finite element solution is always guaranteed in the EFM. A solution may not necessarily exist in the use of the MPDM.

Equations (5-17) and (5-18) are essentially the conditions that the use of the MPDM must satisfy in order to ensure that the degraded elemental stiffness matrix $\mathbf{K}^d$ stays non-singular. These equations are also termed "material stability equations" in this chapter as they involve the material properties of the element. If these equations are violated, then finite element analysis is not carried out and hence a solution is not obtained. No such equation exists in the EFM since the material properties are not modified. Hence, the convergence of a solution is always guaranteed in the EFM while a solution may not necessarily exist in the use of the MPDM.

5.3. Formulating the EFM to Produce the Same Results as MPDM

We have seen from the previous section that there are cases where the EFM is used to simulate a particular reduction in load-bearing capability which MPDM is unable to. In this section, we will show that the EFM is a more general technique than MPDM as it can be formulated to reproduce all the results by MPDM while the converse is not true.

Suppose a unique solution by MPDM exists, we now wish to find the vector of nodal forces that must be applied in EFM in order to achieve the same solution of MPDM. In MPDM, the force-stiffness relation of a damaged element is given as

$$\mathbf{K}_{MPDM}\mathbf{u}_{MPDM} = \mathbf{f}_{MPDM} \tag{5-19}$$

where

$\mathbf{K}_{MPDM}$ is the elemental stiffness matrix which is a function of degraded stiffness coefficients C_{ij}^{d}, $\mathbf{u}_{MPDM}$ is the vector of nodal displacements and $\mathbf{f}_{MPDM}$ is the force vector of the damaged element.

In EFM, the stiffness equation of a failed element at force convergence is given by

$$\mathbf{K}_{EFM}\mathbf{u}_{EFM} - \mathbf{f}_{applied} = \mathbf{f}_{EFM} \tag{5-20}$$

where the magnitude of $\mathbf{f}_{EFM}$ is associated with the extent of damage within a failed element and $\mathbf{f}_{applied}$ refers to the vector of external forces that must be applied to the nodes of the failed element in order to achieve convergence to the desired nodal forces in $\mathbf{f}_{EFM}$ (refer to the methodology section on EFM in Chapter 2 for more details).

Assuming a unique solution $\mathbf{u}^*$ exists (i.e. the solution from the use of EFM is identical to that from the use of MPDM), i.e.

$$\mathbf{u}_{EFM} = \mathbf{u}_{MPDM} = \mathbf{u}^* \tag{5-21}$$

and

$$\mathbf{f}_{EFM} = \mathbf{f}_{MPDM} \tag{5-22}$$

Substituting equations (5-21) and (5-22) into equation (5-20), the stiffness equation in EFM becomes

$$\mathbf{K}_{EFM}\mathbf{u} - \mathbf{f}_{applied} = \mathbf{f}_{MPDM} \tag{5-23}$$

Alternatively, equation (5-23) can be partitioned in terms of degraded stiffness coefficients C_{ij}^{d} as follows:

$$\mathbf{K}_{EFM}\mathbf{u}^{*} - \mathbf{f}_{applied} = \mathbf{f}_{MPDM}^{C_{11}^{d}} + \mathbf{f}_{MPDM}^{C_{12}^{d}} + \mathbf{f}_{MPDM}^{C_{22}^{d}} + \mathbf{f}_{MPDM}^{C_{66}^{d}} \tag{5-24}$$

We call **equation (5-24) the reformulated force convergence equation of the EFM**. This equation shows that the EFM can be formulated to produce the same results of MPDM, provided a unique solution $\mathbf{u}^{*}$ exists in MPDM. The proof of a unique solution is given as follows:

Since the stiffness properties in EFM are not modified, the subscript "EFM" in equation (5-20) is dropped and

$$\mathbf{K}_{EFM} = \mathbf{K} \tag{5-25}$$

Using equations (5-19), (5-20) and (5-22), we have

$$\mathbf{K}_{EFM}\mathbf{u}_{EFM} - \mathbf{f}_{applied} = \mathbf{K}_{MPDM}\mathbf{u}_{MPDM} \tag{5-26}$$

Substituting equations (5-21) and (5-25) into equation (5-26), we have

$$\mathbf{f}_{applied} = (\mathbf{K} - \mathbf{K}_{MPDM})\mathbf{u}^{*} \tag{5-27}$$

Equation (5-27) shows that a unique solution by MPDM does exist, provided $\mathbf{K}_{MPDM}$ is not ill-conditioned, i.e. it is non-singular. Used together with equation (5-24), it shows that the EFM can be formulated to obtain the same solution by MPDM. However, the converse is not true (as demonstrated in previous section). Hence, the EFM is a more general and versatile method than the MPDM. This statement is illustrated in the next section through two numerical examples.

5.4. Case Study: The EFM is Formulated to Produce the Results by the MPDM

This section looks at an example problem where the reformulated equation of EFM (i.e. equation (5-24)) is applied to obtain the same results by MPDM. The three-point bend problem described in Chapter 4 and the same set of material properties of the laminated composite beam are used here. Thermal residual strains are assumed to be absent in this problem. SIFT is chosen as the common failure criterion (refer to Chapter 2 for more details about SIFT).

In the MPDM, selected engineering constants of a damaged element are degraded as follows: $E_1^d = 0.1E_1$, $G_{12}^d = 0.5G_{12}$, $G_{23}^d = 0.5G_{23}$ and $G_{13}^d = 0.5G_{13}$. The subscript 1 of the material properties refers to the fiber direction while subscripts 2 and 3 refer to the directions transverse to the fiber. The degraded values are finite in accordance to equation (5-18) in order to keep the degraded elemental stiffness matrix $\mathbf{K}^d$ non-singular. The corresponding nodal force reduction scheme in the EFM is then worked out using equation (5-24).

The damage progression pattern produced by the EFM is the same as that of MPDM (Figure 5-1 and Figure 5-2) where a total number of 100 elements are failed. It is observed that both the sequence of element failure (Figure 5-2) and dominant strain invariant for each failed element (Figure 5-1) have been predicted correctly by the EFM. In addition, the maximum percentage difference between the dominant strain values predicted by the EFM and that of the MPDM is just a mere 0.45% (The strain invariant values of the first four failed elements are shown in Table 5-1). Based on the above observations, the EFM is shown to be able to reproduce results of MPDM by using the reformulated equation (5-24).

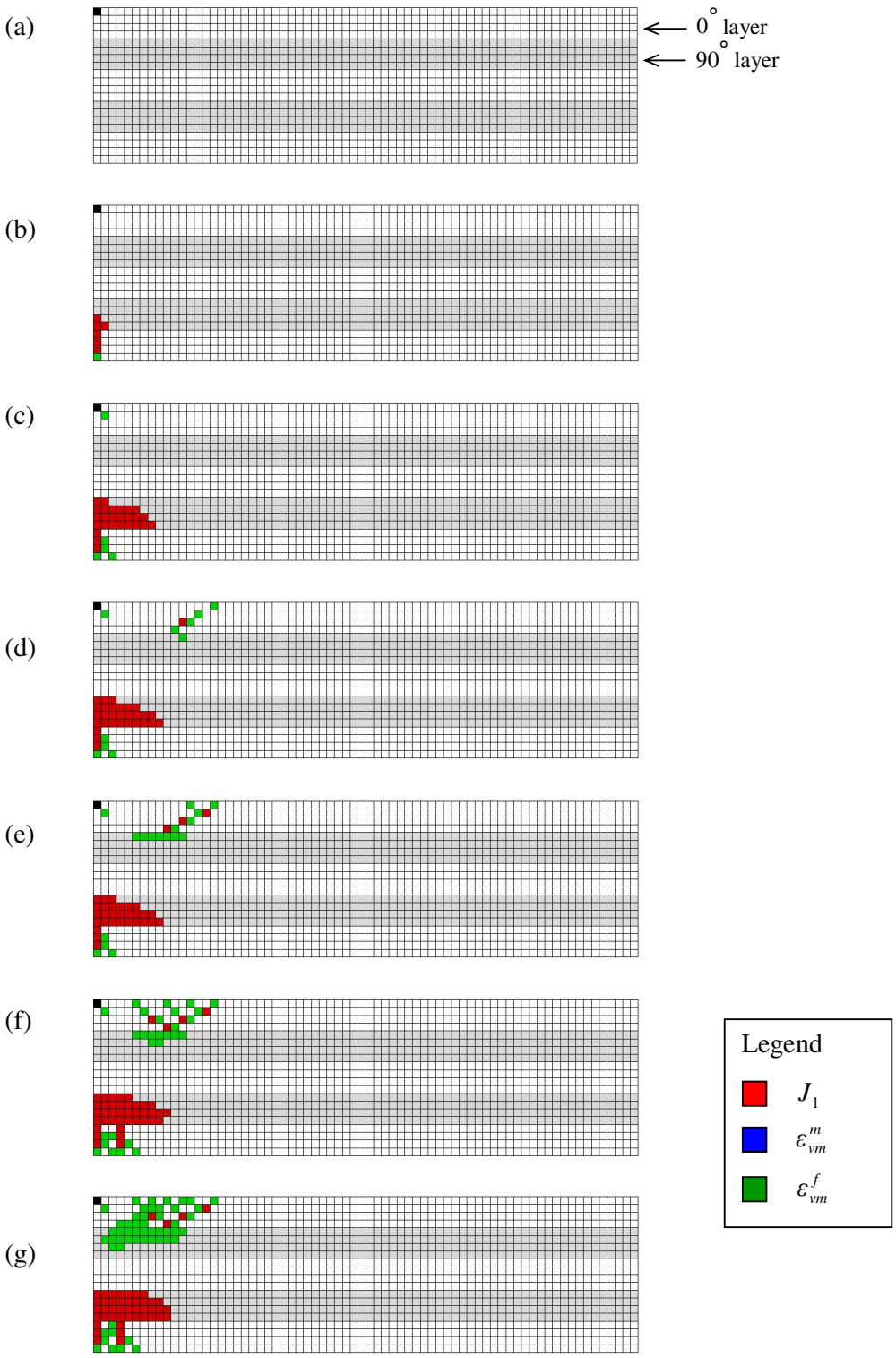

Figure 5-1(a)-(g): MPDM Predicted damage progression with E_1 sets to 10% of its original value and G_{12}, G_{23} and G_{13} set to 50% of their original values.

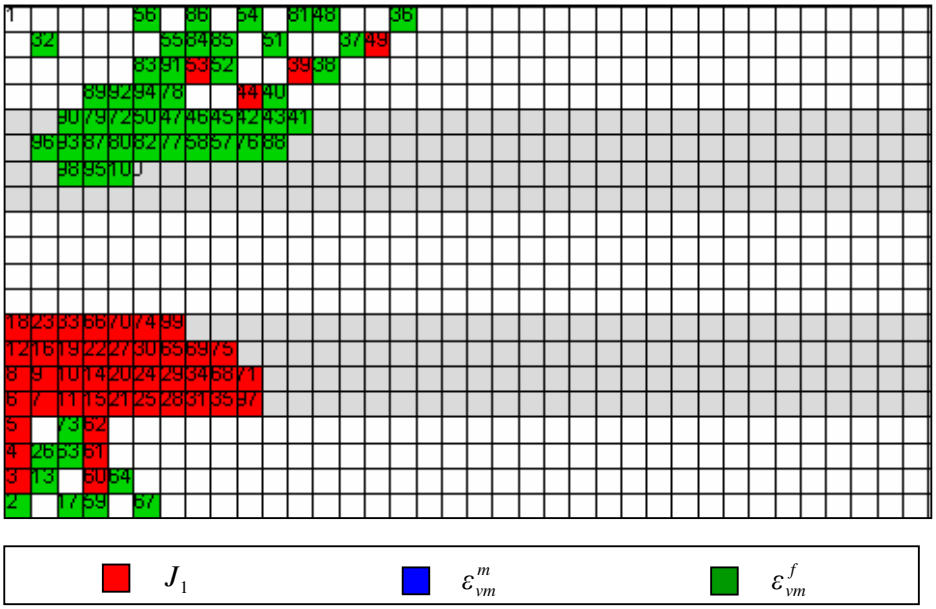

Figure 5-2: Sequence of element failure in MPDM predicted damage progression pattern, with E_1 sets to 10% of its original value and G_{12}, G_{23} and G_{13} set to 50% of their original values. The same element failure sequence is obtained in the damage pattern predicted using the reformulated equation of the EFM.

Table 5-1: Comparison of dominant strain invariant values of selected damaged elements.

Element no.	**Dominant strain invariant**	**MPDM with SIFT**	**EFM with SIFT**	**Percent difference (%)**
2	ε_{vm}^{f}	0.8083	0.8082	0.00
3	J_1	1.0784	1.0736	0.45
4	J_1	1.4435	1.4378	0.39
5	J_1	1.5391	1.5328	0.41

5.5. Conclusions

The basis of the EFM and MPDM is essentially different- the nodal forces are modified in the EFM to reflect the general state of damage and loading of damaged composite material while in the MPDM, the damage effects are reflected by modifying the material properties. The finite element formulations of the EFM and MPDM are re-examined to understand the relationship between nodal forces and material stiffness. From it, we observe the following advantages of the EFM over MPDM:

1. In the MPDM, the stiffness coefficients or engineering constants must be reduced to finite values (not zero) as defined in equations (5-16) to (5-18). This is to avoid ill-conditioning of the stiffness matrix **K** so that a solution to the finite element analysis is assured. As a result, the MPDM can only be used to simulate a limited range of stiffness loss in a damaged element. As the material properties are not modified in the EFM, there is no such limitation in the EFM.

2. The convergence of a finite element solution is always guaranteed in the EFM but a solution may not necessarily exist in the use of the MPDM. The uniqueness of a solution in the MPDM requires that the degradation of material properties satisfy equations (5-16) to (5-18). Since EFM does not modify any material properties, the stiffness matrix **K** in the EFM is always

non-singular and thus, convergence to a finite element solution is always guaranteed.

3. EFM is able to reproduce the results of the MPDM but the converse is not true. Provided $\mathbf{K}_{MPDM}$ is not ill-conditioned, the same solution by MPDM can also always be determined by EFM by using the reformulated force convergence equation of EFM in equation (5-24). On the other hand, there are certain situations in which MPDM is not able to reproduce the results of EFM. This is because the coupling between elemental nodal forces and material properties in the MPDM (i.e. equations (5-10) and (5-14)) show that a change to either C_{12} or C_{66} will affect both f_x and f_y. For example, MPDM cannot describe a zero f_x without affecting f_y and vice versa.

In conclusion, the above advantages of the EFM over MPDM have shown that the EFM is a more general and versatile method than MPDM.

6. Conclusions

The original contributions and major findings of the thesis are summarized in this chapter. This is followed by a list of recommendations for future work.

6.1 Contributions and Major Findings

An element-failure method (EFM) is proposed in this thesis in ***Chapter 2*** to account for local damage in composite materials. It is based on the approach of nodal force modification where nodal forces of a failed element are modified to reflect the general state of damage and loading. It was found that the EFM does not contain any of the drawbacks associated with the traditional material property degradation method (MPDM). For example, unlike the MPDM, the material stiffness properties of a failed element are not altered in the EFM. Thus, there is no ill-conditioning of the stiffness matrix in the EFM which implies that the convergence of a solution is always guaranteed. There is also savings of computational efforts for the EFM since there is no need to reformulate the global stiffness matrix during the damage progression process.

Coupled with a micromechanics-based strain invariant failure theory (SIFT), the EFM is used for the first time in this thesis to predict damage progression process in composite laminates under quasi-static load. A two-dimensional finite element code

implementing the two methods is developed in ***Chapter 3*** and applied in ***Chapter 4*** to predict damage pattern for a $[0_3/90_3/0_3/90_3/0_3]$ composite laminate under a quasi-static three-point bend load. Experiments were performed to obtain actual damage progression patterns and load-displacement curves. It was found that the damage progression pattern obtained with the use of EFM and SIFT agrees well with the experimental observations. Parametric studies on SIFT also showed that the damage prediction by SIFT is reasonably robust to a variation of ± 18% of the critical strain invariant values, where damage prediction is found to be the most sensitivity to the values of J_{1Crit} and least sensitive to the values of ε^f_{vmCrit}.

Using SIFT as the common failure criterion, the results obtained with the EFM are compared with those generated by the traditional MPDM. It was observed that the damage pattern generated from the use of the EFM with SIFT correlate well with experimental observations while those generated from the use of the MPDM with SIFT correlate poorly. Thus, for the three-point bend problem studied herein, the use of the EFM with SIFT is found to be a more suitable combination for mapping damage initiation and propagation in composite laminates.

Finally, in ***Chapter 5***, the major differences between the EFM and the MPDM are addressed further by examining the finite element formulations of the two methods. From the relationship between nodal forces and material stiffness properties, it was found that the EFM is able to reproduce the results obtained with the MPDM, while the converse is not true in general. This, together with the advantages of the EFM

over the traditional MPDM, makes the EFM a more general and versatile method to account for local damage in composite laminates.

6.2 Possible Future Work

The following recommendations are proposed:

1. The FE code developed in this thesis is based on 2-D conditions. This is acceptable because the damage progression pattern for the three-point bend problem studied in this thesis does not vary much in the transverse (third) direction. It is recommended that the code be extended to 3-D conditions to handle problems where the transverse component could be important or to study the effect of delamination in detail.

2. A conservative nodal force modification scheme for the EFM is used in the three-point bend problem studied here whereby the x-component of nodal forces is zeroed. Although the damage prediction obtained agrees well with the experimental results, a more sophisticated nodal force modification scheme for EFM is necessary to address more complicated problems. It is recommended that such a scheme could include the use of damage parameters to quantify the appropriate amount of nodal force to be reduced. The scheme can also include the use of a damage vector to indicate the direction of nodal force to be modified.

3. In the FE code developed in the thesis, the strains of each finite element are evaluated at integration points $(2x2)$ and averaged to represent strains at the centroid of the element. Once the element is failed, all its nodal forces are modified by the EFM by equal proportion. For future work, the amount of nodal force modification to be assigned to individual nodes may be dependent on the integration point that has failed. For example, for an element with strains evaluated at integration points $(2x2)$, only the nodes nearest to the "failed" integration point will be modified by the EFM.

4. For this current project, the nodal forces of all failed element are modified to represent the same state of damage despite new elements being failed as damage progresses. This implies that damage accumulation is not addressed locally within the elements. This is an issue with partially-failed elements.

5. The EFM has been applied to model damage in composite laminates under quasi-static load. For future work, it may be applied to model damage effects in fatigue or dynamic problems

References

1. ABAQUS/Standard User's Manual, version 6.3, 2002. Hibbitt, Karlsson & Sorensen Inc.

2. Allen D H, Harris C E and Groves S E, 1987a. A thermomechanical constitutive theory for elastic composites with distributed damage – I. Theoretical development, *International Journal of Solids and Structures*, vol. 23, no. 9, pp. 1301-1318.

3. Allen D H, Harris C E and Groves S E, 1987b. A thermomechanical constitutive theory for elastic composites with distributed damage – II. Application to matrix cracking in laminated composites, *International Journal of Solids and Structures*, vol. 23, no. 9, pp. 1319-1338.

4. Allen D H, Harris C E, Groves S E and Norvell R G, 1988. Characterization of stiffness loss in crossply laminates with curved matrix cracks, *Journal of Composite Materials*, vol. 22, pp. 71-80.

5. Allen D H and Lo D C, 1991. A model for the progressive failure of laminated composite structural components, In *Enhancing Analysis Techniques for Composite Materials*, ASME-NDE vol. 10, edited by Schwer L, Reddy J N and Mal A, pp. 125.

6. Ambur D R, Jaunky N and Hilburger M W, 2004a. Progressive failure studies of stiffened panels subjected to shear loading, *Composite Structures*, vol. 65, no. 2, pp. 129-142.

7. Ambur D R, Jaunky N, Hilburger M and Davila C G, 2004b. Progressive failure analyses of compression-loaded composite curved panels with and without cutouts, *Composite Structures*, vol. 65, no. 2, pp. 143-155.

8. Atluri S N, 1982. Path-independent integrals in finite elasticity and inelasticity, with body forces, inertia and arbitrary crack-face conditions, *Engineering Fracture and Mechanics*, vol. 16, no. 3, pp. 341-364.

9. Atluri S N, Nishioka T and Nakagaki M, 1984. Incremental path-independent integrals in inelastic and dynamic fracture mechanics, *Engineering Fracture and Mechanics*, vol. 20, no. 2, pp. 209-244.

10. Atlus E, Rotem A and Shmueli M, 1980. Free edge effect in angle ply laminates – a new three dimensional finite difference solution, *Journal of Composite Materials*, vol. 14, pp. 21-30.

11. Averill R C and Reddy J N, 1992. Geometrically nonlinear analysis of laminated composite shells using a macro-micro cumulative damage model, In *Damage Mechanics in Composites*, AMD vol. 150 and AD vol. 32, ASME, edited by Allen D H and Lagoudas D C, pp. 255-273.

12. Bakuckas J G Jr., Lau A C W, Tan T M and Awerbuch J, 1995a. Computational methodology to predict damage growth in unidirectional composites - I. Theoretical formulation and numerical implementation, *Engineering Fracture Mechanics*, vol. 52, no. 5, pp. 937-951.

13. Bakuckas J G Jr., Tan T M, Lau A C W and Awerbuch J, 1995b. Computational methodology to predict damage growth in unidirectional composites – II. Case studies, Engineering *Fracture Mechanics*, vol. 52, no. 5, pp. 953-970.

14. Bathe K J, 1996. Finite element procedures, Prentice-Hall, Englewood Cliffs, New Jersey.

15. Beissel S R, Johnson G R and Popelar C H, 1998. An element-failure algorithm for dynamic crack propagation in general directions, *Engineering Fracture Mechanics*, vol. 61, no. 3-4, pp. 407-425.

16. Butalia T S and Wolfe W E, 2002. A strain-energy based non-linear failure criterion: comparison of numerical predictions and experimental observations for symmetric composite laminates, *Composites Science and Technology*, vol. 62, no. 12-13, pp. 1697-1710.

17. Camanho P P and Matthews F L, 1999. A progressive damage model for mechanically fastened joints in composite laminates, *Journal of Composite Materials*, vol. 33, no. 24, pp. 2248-2280.

18. Chamis C C, 1987. Simplified composite micromechanics equations for mechanical, thermal and moisture-related properties, In *Engineers' Guide to*

Composite Materials, edited by Weeton J W, Peters D M, and Thomas K L, American Society for Metals International, Materials Park, Ohio.

19. Chang F K and Chang K Y, 1987a. Post-failure analysis of bolted composite joints in tension or shear-out mode failure, *Journal of Composite Materials*, vol. 21, pp. 809-833.

20. Chang F K and Chang K Y, 1987b. A progressive damage model for laminated composites containing stress concentrations, *Journal of Composite Materials*, vol. 21, pp. 834-855.

21. Chang F K and Lessard L B, 1991. Damage tolerance of laminated composites containing an open hole and subjected to compressive loadings: Part I – Analysis, *Journal of Composite Materials*, vol. 25, no. 1, pp. 2-43.

22. Chang F K, Scott R A and Springer G S, 1984. Failure strength of nonlinearly elastic composite laminates containing a pin loaded hole, *Journal of Composite Materials*, vol. 18, pp. 464-477.

23. Chen W F and Han D J, 1988. Plasticity for Structural Engineers, Springer-Verlag, New York.

24. Chou S-C, Orringer O and Rainey J H, 1976. Post-failure behaviour of laminates – I. No stress concentration, *Journal of Composite Materials*, vol. 10, pp.371-380.

25. Christensen R M, 1988. Tensor transformations and failure criteria for the analysis of fiber composite materials, *Journal of Composite Materials*, vol. 22, no. 9, pp. 874-897.

26. Coats T W and Harris C E, 1995. Experimental verification of a progressive damage model for IM7/5260 laminates subjected to tension-tension fatigue, *Journal of Composite Materials*, vol. 29, no. 3, pp. 280-305.

27. Coats T W and Harris C E, 1998. A progressive damage methodology for residual strength predictions of notched composite panels, NASA TM-207646.

28. Cook R D, Malkus D S and Plesha M E, 2002. Concepts and applications of finite element analysis, 4th Edition, John Wiley and Sons, New York.

29. Daniel I M and Lee J W, 1990. Damage development in composite laminates under monotonic loading, *Journal of Composites Technology and Research*, vol. 12, pp. 98-102.

30. Feng W W, 1991. A failure criterion for composite materials, *Journal of Composite Materials*, vol. 25, pp. 88-100.

31. Gol'denblat I I and Kopnov V A, 1965. Strength of glass reinforced plastics in the complex stress state, *Mekhanika Polimerov*, vol. 1, pp. 70-78. English translation. *Polymer Mechanics*, vol. 1, pp. 56-60, 1966.

32. Gosse J H, 2002. An overview of the strain invariant failure theory, In *Proceedings of the 10th US-Japan Conference on composite materials,* edited by Chang F K, DEStech Publications, Lancaster, PA, pp. 989-997.

33. Gosse J H and Christensen S, 2001. Strain invariant failure criteria for polymers in composite materials, In *Proceedings of 42nd Structures, Structural Dynamics and Materials Conference,* vol. 1, Paper AIAA-2001-1184, pp. 45-55.

34. Gosse J H, Christensen S, Hart-Smith, J and Wollschlager J A, 2002. Strain invariant failure theory (SIFT) Part I. Damage initiation in composite materials, In *6th Composite Durability Workshop (CDW-6)*, Tokyo, Japan, November 14-15, 2002.

35. Gosse J H, Christensen S, Wollschlager J A and Llanos A S. A strain invariant failure theory (SIFT) for composite materials, *Journal of Composite Materials* (submitted for publication).

36. Hahn H T and Tsai S W, 1973. Nonlinear elastic behavior of unidirectional composite laminates, *Journal of Composite Materials*, vol. 7, pp. 102-110.

37. Hallet S R and Wisnom M R, 2003. Finite element investigation of the effect of progressive damage in notched composites, in *Proceedings of the 14th International Conference on Composite Materials*, ICCM-14, edited by Hahn H T and Martin M, San Diego, US, paper no. 0979.

38. Hart-Smith L J, 1998a. Predictions of the original and truncated maximum-strain failure models for certain fibrous composite laminates, *Composites Science & Technology*, vol. 58, no. 7, pp. 1151-1178.

39. Hart-Smith L J, 1998b. Predictions of a generalized maximum-shear-stress failure criterion for certain fibrous composite laminates, *Composites Science & Technology*, vol. 58, no. 7, pp. 1179-1208.

40. Hashin Z, 1980. Failure criteria for unidirectional fiber composites, *Journal of Applied Mechanics*, vol. 47, pp. 329-334.

41. Hashin Z, 1983. Analysis of composite materials – a survey, *Journal of Applied Mechanics*, vol. 50, pp. 481-505.

42. Hashin Z and Rotem A, 1973. A fatigue failure criterion for fiber-reinforced materials, *Journal of Composite Materials*, vol. 7, pp. 448-464.

43. Herakovich C T, 1998. Mechanics of Fibrous Composites, Wiley, New York.

44. Hill R, 1948. A theory of the yielding and plastic flow of anisotropic materials, In *Proceedings of the Royal Society of London*, Series A, vol. 193, pp. 281-297.

45. Hinton M J, Kaddour A S and Soden P D, 2002a. Evaluation of failure prediction in composite laminates: background to 'part B' of the exercise, *Composites Science and Technology*, vol. 62, pp. 1481-1488.

46. Hinton M J, Kaddour A S and Soden P D, 2002b. A comparison of the predictive capabilities of current failure theories for composite laminates, judged against experimental evidence, *Composites Science and Technology*, vol. 62, pp. 1725-1797.

47. Hinton M J, Kaddour A S and Soden P D, 2004a. Evaluation of failure prediction in composite laminates: background to 'part C' of the exercise, *Composites Science and Technology*, vol. 64, issues 3-4, pp. 321-327.

48. Hinton M J, Kaddour A S and Soden P D, 2004b. A further assessment of the predictive capabilities of current failure theories for composite laminates: comparison with experimental evidence, *Composites Science and Technology*, vol. 64, issues 3-4, pp. 549-588.

49. Hinton M J and Soden P D, 1998. Predicting failure in composite laminates: the background to the exercise, *Composites Science and Technology*, vol. 58, pp. 1001-1010.

50. Hinton M J, Soden P D and Kaddour A S, 1998. Failure criteria in fibre-reinforced-polymer composites, Special issue, *Composites Science and Technology*, vol. 58, Part A.

51. Hoffman O, 1967. The brittle strength of orthotropic materials, *Journal of Composite Materials*, vol. 1, pp. 200-206.

52. Huang H, Springer G S and Christensen R M, 2003. Predicting failure in composite laminates using dissipated energy, *Journal of Composite Materials*, vol. 37, no. 23, pp. 2073-2099.

53. Hung C L and Chang F K, 1996. Bearing failure of bolted composite joints. Part II. Model and verification, *Journal of Composite Materials*, vol. 30, pp. 1359-1400.

54. Hwang W C and Sun C T, 1989. Failure analysis of laminated composites by using iterative three-dimensional finite element method, *Computers and Structures*, vol. 33, no. 1-3, pp. 41-47.

55. Hyer M W and Wolford G F, 2003. Progressive failure analysis of internally pressurized noncircular composite cylinders, in *Proceedings of the 14th International Conference on Composite Materials*, ICCM-14, edited by Hahn H T and Martin M, San Diego, US, paper no. 2085.

56. Jenkins C F, 1920. Report on materials of construction used in aircraft and aircraft engines, *Great Britain Aeronautical Research Committee*.

57. Kachanov M, 1972. Continuum theory of media with cracks, *Mekhanika Tverdogo Tela, ASCE*, vol. 7, pp. 54-59 (in Russian).

58. Kaddour A S, Hinton M J and Soden S D, 2004. A comparison of the predictive capabilities of current failure theories for composite laminates: additional contributions, *Composites Science and Technology*, vol. 64, issues 3-4, pp. 449-476.

59. Knight N F Jr., Rankin C C and Brogan F A, 2002. STAGS computational procedure for progressive failure analysis of laminated composite structures, *International Journal of Non-linear Mechanics*, vol. 37, pp. 833-849.

60. Laws N and Dvorak G J, 1988. Progressive transverse cracking in composite laminates. *Journal of Composite Materials*, vol. 22, pp. 900-916.

61. Lee J D, 1980. Three dimensional finite element analysis of layered fiber-reinforced composite materials, *Computers and Structures*, vol. 12, no. 3, pp. 319-339.

62. Lee J D, 1982. Three dimensional finite element analysis of damage accumulation in composite laminate, *Computers and Structures*, vol. 15, no. 3, pp. 335-350.

63. Lee J W, Allen D H and Harris C E, 1989. Internal state variable approach for predicting stiffness reductions in fibrous laminated composites with matrix cracks, *Journal of Composite Materials*, vol. 23, no. 12, pp. 1273-1291.

64. Lessard L B and Shokrieh M M, 1995. Two-dimensional modeling of composite pinned/bolted joint failure, *Journal of Composite Materials*, vol. 29, no. 5, pp. 671-697.

65. Li R, Kelly D and Crosky A, 2002. An evaluation of failure criteria for matrix induced failure in composite materials, *Composite Structures*, vol. 57, no. 1-4, pp. 385-391.

66. Li R, Kelly D and Ness R, 2003. Application of a first invariant strain criterion for matrix failure in composite materials, *Journal of Composite Materials*, vol. 37, no. 22, pp. 1977-2000.

67. Lim E H and Tay T E, 1994. The effects and evolution of distributed damage on the stiffness characteristics of cross-ply composite laminates, In *Proceedings of Aerospace Technology Seminar 1994: Future Trends In Aerospace Technology*, Air Platform Technology Group, Ministry of Defence, Singapore, pp. 89-95.

68. Lim E H and Tay T E, 1996. Stiffness loss of composite laminates with transverse cracks under Mode I and Mode III loading, *International Journal of Damage Mechanics*, vol. 5, no. 2, pp. 190-215.

69. Lo D C, Coats T W, Harris C E and Allen D H, 1996. Progressive damage analysis of laminated composites (PDALC) – A computational model implemented in the NASA COMET finite element code, NASA TM-4724.

70. Mahishi J M and Adams D F, 1982. Micromechanical predictions of crack initiation, propagation, and crack growth resistance in boron/aluminum composites, *Journal of Composite Materials*, vol. 16, pp. 457-469.

71. Nuismer R J and Tan S C, 1988. Constitutive relations of a cracked composite lamina, *Journal of Composite Materials*, vol. 22, pp. 306-321.

72. Ochoa O O and Reddy J N, 1992. Finite Element Analysis of Composite Laminates, *Solid Mechanics and Its Applications*, vol. 7, Kluwer Academic Publishers, Dordrecht, Boston.

73. Petit P H and Waddoups M E, 1969. A method of predicting the nonlinear behaviour of laminated composites, *Journal of Composite Materials*, vol. 3, pp. 2-19.

74. Puck A and Schneider W, 1969. On failure mechanisms and failure criteria of filament-wound glass-fiber/resin composites, *Plastics and Polymers*, vol. 37, pp. 33-43.

75. Puck A and Schürmann H, 1998. Failure analysis of FRP laminates by means of physically based phenomenological models, *Composites Science and Technology*, vol. 58, no. 7, pp. 1045-1067.

76. Puck A and Schürmann H, 2002. Failure analysis of FRP laminates by means of physically based phenomenological models, *Composites Science and Technology*, vol. 62, no. 12-13, pp. 1633-1662.

77. Rao S S (1999). The finite element method in engineering, 3rd Edition, Butterworth Heinemann, Boston.

78. Reddy J N and Pandey A K, 1987. A first-ply failure analysis of composite laminates, *Computers and Structures*, vol. 25, no. 3, pp. 371-393.

79. Reddy Y S N, Moorthy C M D and Reddy J N, 1995. Non-linear progressive failure analysis of laminated composite plates, *International Journal of Non-linear Mechanics*, vol. 30, no. 5, pp. 629-6493

80. Reddy Y S N and Reddy J N, 1992. Linear and non-linear failure analysis of composite laminates with transverse shear, *Composites Science and Technology*, vol. 44, no. 3, pp. 227-255.

81. Reifsnider K L, 1991. Fatigue of Composite Materials, Composite Material Series, vol. 4, edited by Reifsnider K L, Elsevier Applied Science Publishers.

82. Rotem A, 1998. Prediction of laminate failure with Rotem failure criterion, *Composites Science and Technology*, vol. 58, no. 7, pp. 1083-1094.

83. Rotem A and Hashin Z, 1975. Failure modes of angle ply laminates, *Journal of Composite Materials*, vol. 9, pp. 191-206.

84. Rousseau C Q, 2003. A range of practical failure criteria for laminated composites, In *Composite Materials: Testing and Design*, Fourteenth volume, ASTM STP 1436, edited by Bakis C E, ASTM International, West Conshohocken, PA, pp. 291-319.

85. Rousselier D, 1979. Recent theoretical and experimental results on fast brittle fracture, *International Journal of Fracture*, vol. 12, pp. 799-813.

86. Sandhu R S, 1974. Non-linear behaviour of unidirectional and angle ply laminates, AIAA Journal of Aircraft, vol. 13, pp. 104-111.

87. Sandhu R S, Sendeckyj G P and Gallo R L, 1982. Modeling of the failure process in notched laminates. In *Mechanics of Composite Materials: Recent Advances* (Proceedings of the IUTAM Symposium), edited by Hashin Z and Herakovich C, Pergamon Press, Oxford, pp. 179-189.

88. Shahid I and Chang F-K, 1993a. Nonlinear response of composite laminates due to material nonlinearity and accumulated damage, In *Mechanics of Composite Materials: Nonlinear effects*, ASME-AMD vol. 159, pp. 319-329.

89. Shahid I and Chang F-K, 1993b. Failure and strength of laminated composite plates under multiple in-plane loads, In *38th International SAMPE Symposium*, May 1993, pp. 967-977.

90. Shahid I and Chang F-K, 1995. An accumulative damage model for tensile and shear failures of laminated composite plates, *Journal of Composite Materials*, vol. 29, no. 7, pp. 926-981.

91. Shokrieh M M and Lessard L B, 2000a. Progressive fatigue damage modeling of composite materials, Part I: modeling, *Journal of Composite Materials*, vol. 34, no. 13, pp. 1056-1080.

92. Shokrieh M M and Lessard L B, 2000b. Progressive fatigue damage modeling of composite materials, Part II: material characterization and model verification, *Journal of Composite Materials*, vol. 34, no. 13, pp. 1081-1116.

93. Shokrieh M M, Lessard L B and Poon C, 1996. Three-dimensional progressive failure analysis of pin/bolt loaded composite laminates, In *Agard Conference Proceedings of the 83rd Meeting of the AGARD SMP on 'Bolted Joints in Polymeric Composites*, Florence, Italy, September 2-3, edited by Poon C, RTO/NATO, Neuilly-Sur-Seine, France, pp. 7.1- 7.10.

94. Sleight D W, Knight N F and Wang J T, 1997. Evaluation of a progressive failure analysis methodology for laminated composite structures, *AIAA paper 97-1187, AIAA*.

95. Smith I M and Griffiths D V, 2004. Programming the finite element method, 4th Edition, Wiley, Hoboken, New York.

96. Smithells C J, 1976. Metals reference book, 5th Edition, Butterworth.

97. Soden P D, Hinton M J and Kaddour A S, 1998a. Lamina properties, lay-up configurations and loading conditions for a range of fibre-reinforced composite laminates, *Composites Science and Technology*, vol. 58, no. 7, pp. 1011-1022.

98. Soden P D, Hinton M J and Kaddour A S, 1998b. A comparison of the predictive capabilities of current failure theories for composite laminates, *Composites Science and Technology*, vol. 58, no. 7, pp. 1225-1254.

99. Spilker R L and Chou S C, 1980. Edge effects in symmetric composite laminates: importance of satisfying the traction free edge condition, *Journal of Composite Materials*, vol. 14, pp. 2-20.

100. Strang G and Fix G J, 1973. An analysis of the finite element method, Prentice Hall, Englewood Cliffs, New Jersey.

101. Talreja R, 1985a. Transverse cracking and stiffness reduction in composite laminates, *Journal of Composite Materials*, vol. 19, pp. 355-375.

102. Talreja R, 1985b. A continuum mechanics characterization of damage in composite materials, In *Proceedings of the Royal Society of London*, A399, pp. 195-216.

103. Talreja R, 1986a. Mechanism and models of damage in composite materials, In *Mechanical Characterization of Fibre Composite Materials*, edited by Pyrz R, Aalborg University, Denmark, pp. 40-61.

104. Talreja R, 1986b. Stiffness properties of composite laminates with matrix cracking and interior delamination, *Engineering Fracture Mechanics*, vol. 25, no. 5, pp. 751-762.

105. Talreja R, 1987. Modeling of damage development in composites using internal state variable concepts, In *Damage Mechanics in Composites*, ASME-AD vol. 12, edited by Wang A S D and Haritos G K, pp. 11-16.

106. Talreja R, 1990a. Internal variable damage mechanics of composite materials, In *Yielding, Damage and Failure of Anisotropic Solids*, EGF5, edited by Boehler J P, Mechanical Engineering Publications, London, pp. 509-533.

107. Talreja R, 1990b. Damage mechanics of composite materials based on thermodynamics with internal variables, In *Durability of Polymer Based Composite Systems for Structural Applications*, edited by Cardon A H and Verchery G, Elsevier Applied Science, pp. 65-79.

108. Tan S C, 1988. Effective stress failure models for unnotched and notched multidirectional laminates, *Journal of Composite Materials*, vol. 22, pp. 322-340.

109. Tan S C, 1991. A progressive failure model of composite laminates containing openings, *Journal of Composite Materials*, vol. 25, no. 10, pp. 556-577.

110. Tan S C, 1994. Stress concentrations in laminated composites, Technomic Publishing Company, Lancaster, PA.

111. Tan S C and Nuismer R J, 1989. A theory for progressive matrix cracking in composite laminates, *Journal of Composite Materials*, vol. 23, pp. 1029-1047.

112. Tan S C and Perez J, 1993. Progressive failure of laminated composites with a hole under compressive loading, *Journal of Reinforced Plastics and Composites*, vol. 12, no. 10, pp. 1043-1057.

113. Tay T E and Lim E H, 1993. Analysis of stiffness loss in cross-ply composite laminates, *Composite Structures*, vol. 25, no. 1-4, pp. 419-425.

114. Tay T E and Lim E H, 1996. Analysis of composite laminates with transverse cracks, *Composite Structures*, vol. 34, no. 4, pp. 419-426.

115. Tay T E, Tan V B C and Deng M, 2003. Element-failure concepts for dynamic fracture and delamination in low-velocity impact of composites, *International Journal of Solids and Structures*, vol. 40, no. 3, pp. 555-571.

116. Tolson S and Zabaras N, 1991. Finite element analysis of progressive failure in laminated composite plates, Computers and Structures, vol. 38, no. 3, pp. 361-376.

117. Tsai S W, 1965. Strength characteristics of composite materials, NASA CR-224.

118. Tsai S W, 1968. Strength theories of filamentary structures, In *Fundamental Aspects of Fiber Reinforced Plastic Composites,* edited by Schwartz R T and Schwartz H S, Wiley Interscience, New York, Chapter 1.

119. Tsai S W, 1984. A survey of macroscopic failure criteria for composite materials, *Journal of Reinforced Plastics Composites*, vol. 3, pp. 40-62.

120. Tsai S W, 1992. Theory of Composites Design, Think Composites, Dayton Ohio.

121. Tsai S W and Azzi V D, 1966. Strength of laminated composite materials, *AIAA Journal*, vol. 4, no. 2, pp. 296-301.

122. Tsai S W and Hahn H T, 1975. Failure analysis of composite materials, In *Inelastic Behaviour of Composite Materials,* ASME-AMD vol. 13, edited by Herakovich C T, pp. 73-96.

123. Tsai S W and Hahn H T, 1980. Introduction to Composite Materials, Technomic Publishing Co.

124. Tsai S W and Wu E M, 1971. A general theory of strength for anisotropic materials, *Journal of Composite Materials*, vol. 5, pp. 58-80.

125. Tserpes K I, Labeas G, Papanikos P and Kermanidis T, 2002. Strength prediction of bolted joints in graphite/epoxy composite laminates, *Composites: Part B,* vol. 33, pp. 521-529.

126. Tserpes K I, Papanikos P and Kermanidis T, 2001. A three-dimensional progressive damage model for bolted joints in composite laminates subjected to tensile loading, *Fatigue and Fracture of Engineering Materials and Structures*, vol. 24, no. 10. pp. 663-675.

127. Turvey G J and Osman M Y, 1989. Exact and approximate linear and nonlinear initial failure analysis of laminate Mindlin plates in flexure, In *Composite Structures*, vol. 5, edited by Marshall I H, Elsevier Applied Science, London, Chapter 4, pp. 133-171.

128. Waddoups M E, 1967. Advanced composite material mechanics for the design and stress analyst, *General Dynamics*, Fort Worth Division Report FZM-4763, Fort Worth, TX.

129. Wolfe W E and Butalia T S, 1998. A strain-energy based failure criterion for non-linear analysis of composite laminates subjected to biaxial loading, *Composites Science and Technology*, vol. 58, no. 7, pp. 1107-1124.

130. Wu E M, 1972. Optimal experimental measurements of anisotropic failure tensors, *Journal of Composite Materials*, vol. 6, pp. 472-489.

131. Wu E M, 1974. Phenomenological anisotropic failure criterion, In *Mechanics of Composite Materials*, edited by Sendeckyj G P, Academic Press, New York, vol. 2, pp. 353-431.

132. Yamada S E and Sun C T, 1978. Analysis of laminate strength and its distribution, *Journal of Composite Materials*, vol. 12, pp. 275-284.

133. Zienkiewicz O C and Taylor R L, 2000. The finite element method, 5th Edition, Butterworth Heinemann, Oxford.

Appendix A. Force-displacement Curves of Test Coupons

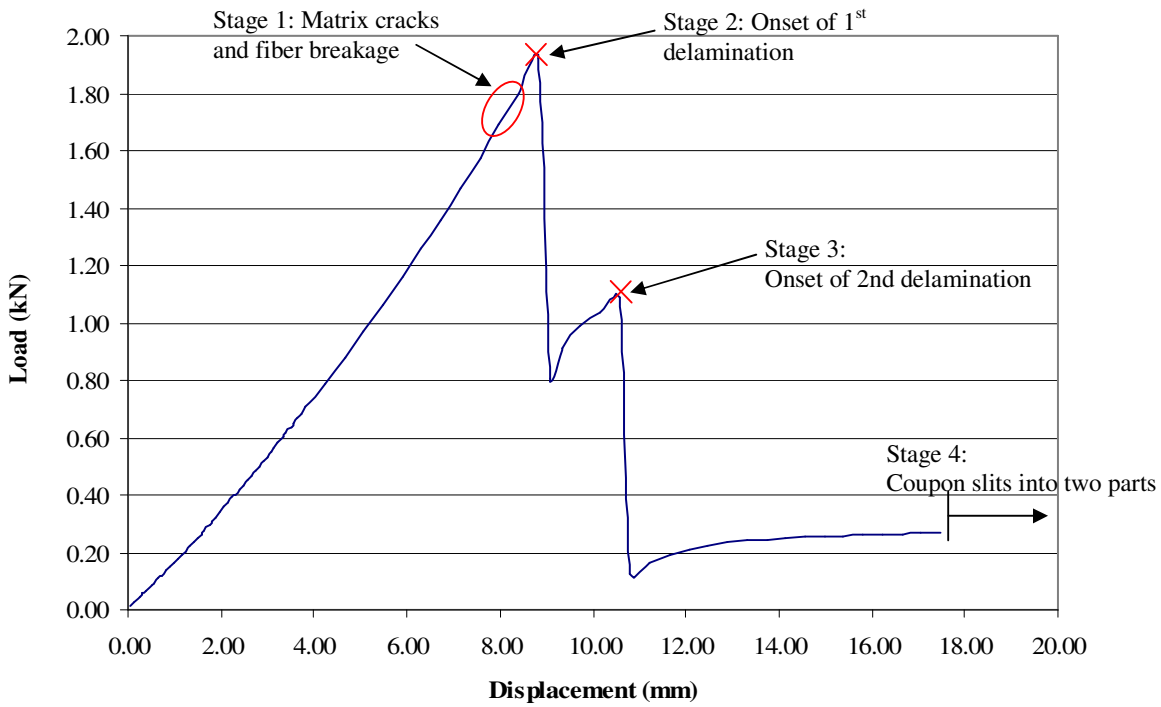

Figure A-1: Force-displacement curve for test coupon no. 1

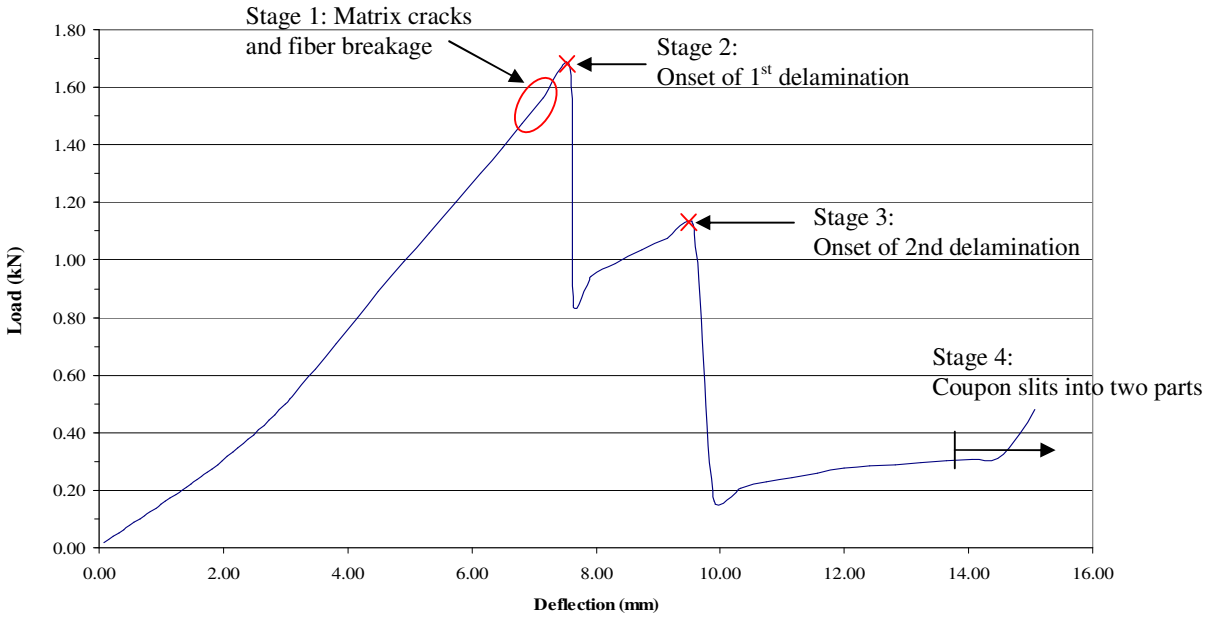

Figure A-2: Force-displacement curve for test coupon no. 2

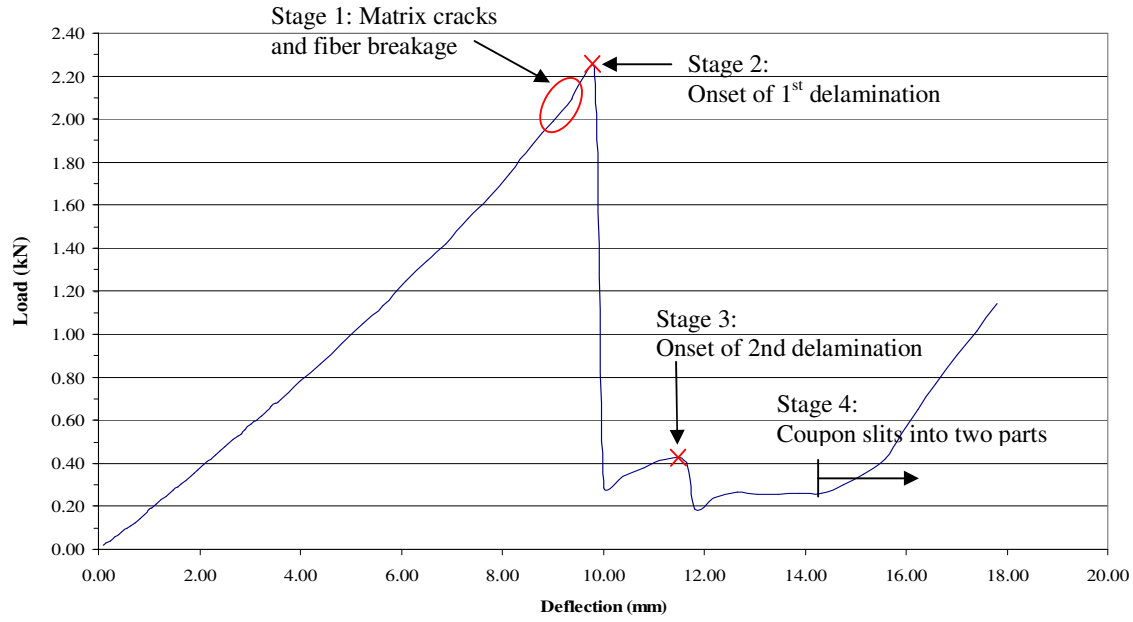

Figure A-3: Force-displacement curve for test coupon no. 3

Appendix B. Constitutive Relations

In a three-dimensional Cartesian coordinate system, the state of deformation can be described by six components of strain and stress, namely, three normal and three shear components. A linear relation between the six components of stresses σ_i and strains ε_j is known as the generalized Hooke's law, and this is given as

$$\sigma_i = C_{ij}\varepsilon_j \quad (k = 1,2,...,6) \tag{B-1}$$

where C_{ij} are known as the stiffness coefficients.

Equation (B-1) can be written in matrix form as

$$\begin{Bmatrix} \sigma_1 \\ \sigma_2 \\ \sigma_3 \\ \sigma_4 \\ \sigma_5 \\ \sigma_6 \end{Bmatrix} = \begin{bmatrix} C_{11} & C_{12} & C_{13} & C_{14} & C_{15} & C_{16} \\ & C_{22} & C_{23} & C_{24} & C_{25} & C_{26} \\ & & C_{33} & C_{34} & C_{35} & C_{36} \\ & & & C_{44} & C_{45} & C_{46} \\ & & & & C_{55} & C_{56} \\ \text{sym.} & & & & & C_{66} \end{bmatrix} \begin{Bmatrix} \varepsilon_1 \\ \varepsilon_2 \\ \varepsilon_3 \\ \varepsilon_4 \\ \varepsilon_5 \\ \varepsilon_6 \end{Bmatrix}$$

where the single subscript notation for stress and strain components is based on the convention

$$\sigma_1 = \sigma_{11},\ \sigma_2 = \sigma_{22},\ \sigma_3 = \sigma_{33},\ \sigma_4 = \tau_{12},\ \sigma_5 = \tau_{13},\ \sigma_6 = \tau_{23}$$

$$\varepsilon_1 = \varepsilon_{11},\ \varepsilon_2 = \varepsilon_{22},\ \varepsilon_3 = \varepsilon_{33},\ \varepsilon_4 = \gamma_{12},\ \varepsilon_5 = \gamma_{13},\ \varepsilon_6 = \gamma_{23} \tag{B-2}$$

In the case of fiber-reinforced composite which is generally orthotropic in nature, the constitutive relation in equation (B-2) reduces to

$$\begin{Bmatrix} \sigma_1 \\ \sigma_2 \\ \sigma_3 \\ \sigma_4 \\ \sigma_5 \\ \sigma_6 \end{Bmatrix} = \begin{bmatrix} C_{11} & C_{12} & C_{13} & 0 & 0 & 0 \\ & C_{22} & C_{23} & 0 & 0 & 0 \\ & & C_{33} & 0 & 0 & 0 \\ & & & C_{44} & 0 & 0 \\ & & & & C_{55} & 0 \\ \text{symm.} & & & & & C_{66} \end{bmatrix} \begin{Bmatrix} \varepsilon_1 \\ \varepsilon_2 \\ \varepsilon_3 \\ \varepsilon_4 \\ \varepsilon_5 \\ \varepsilon_6 \end{Bmatrix}$$

where the stiffness coefficients C_{ij} may be expressed in terms of nine engineering constants E_1, E_2, E_3, v_{12}, v_{13}, v_{23}, G_{12}, G_{13} and G_{23} as [*Herakovich, 1998*]:

$$C_{11} = \frac{1 - v_{23}v_{32}}{E_2 E_3 \Delta},\quad C_{12} = \frac{v_{21} + v_{23}v_{31}}{E_2 E_3 \Delta} = \frac{v_{12} + v_{32}v_{13}}{E_1 E_2 \Delta}$$

$$C_{13} = \frac{v_{31} + v_{23}v_{32}}{E_2 E_3 \Delta} = \frac{v_{13} + v_{23}v_{12}}{E_1 E_2 \Delta},\quad C_{22} = \frac{1 - v_{13}v_{31}}{E_1 E_3 \Delta}$$

$$C_{23} = \frac{v_{32} + v_{12}v_{31}}{E_1 E_3 \Delta} = \frac{v_{23} + v_{21}v_{13}}{E_1 E_2 \Delta},\quad C_{33} = \frac{1 - v_{12}v_{21}}{E_1 E_2 \Delta}$$

$$C_{44} = G_{12}, \qquad C_{55} = G_{13}, \qquad C_{66} = G_{23}$$

$$\Delta = \frac{(1 - v_{12}v_{21} - v_{13}v_{31} - v_{23}v_{32} - 2v_{21}v_{32}v_{13})}{E_1 E_2 E_3} \tag{B-3}$$